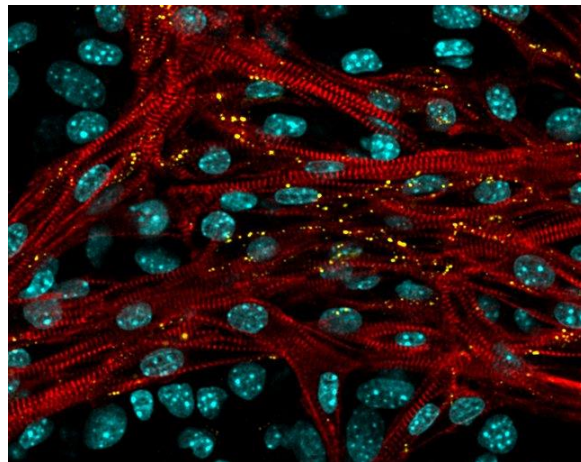**UNIVERSITÀ DI PAVIA**

Dipartimento di Biologia e Biotecnologie "Lazzaro Spallanzani"

Embryonic stem cells and their differentiated cardiomyocytes: a model study of endocrine disruptors toxicity

Cinzia Civello

Dottorato di Ricerca in

Genetica, Biologia Molecolare e Cellulare

Ciclo XXXII – A.A. 2016-2019

UNIVERSITÀ
DI PAVIA

Dipartimento di Biologia e Biotecnologie "Lazzaro Spallanzani"

Embryonic stem cells and their differentiated cardiomyocytes: a model study of endocrine disruptors toxicity

Cinzia Civello

Supervised by Prof. Valeria Merico
Co-supervised by Prof. Silvia Garagna, Dr. Paola Rebuzzini

Dottorato di Ricerca in
Genetica, Biologia Molecolare e Cellulare
Ciclo XXXII – A.A. 2016 -2019

Abstract

Developmental life is a very sensitive time window of the new organism, including our species, during which both maternal and external environment can profoundly influence its fate and long-term health.

At the end of the '80s, the epidemiologist David Barker suggested the hypothesis that several pathologies, that will develop during the adult life, were the consequences of unknown effects exerted by the environment to the development of the foetus.

Among the wide range of environmental stressors that can alter foetal and post-natal development, the endocrine-disruptors (EDs) were recognized by the Endocrine Society and the WHO/UNEP (2012) as a significant global public health challenge. Because of their world-wide distribution in the environment and impact on public health, three EDs deserve special attention: Aroclor 1254, Arsenic trioxide (ATO) and α-Cypermethrin (CYP).

The work I carried out during my PhD was focused on the study of the alterations induced by these three EDs on undifferentiated embryonic stem cells (ESCs) - as an *in vitro* model of the embryonic cells component of the inner cell mass - and on perinatal-like cardiomyocytes obtained after 15 days of ESCs *in vitro* differentiation through the formation of embryoid bodies (EBs).

In *utero* exposure to ATO or Aroclor 1254 is correlated to the onset of cardiac pathologies. However, up to date, their effects on foetal/neonatal cardiomyocytes at cellular and physiological levels are scarcely known.

The main aims of my project were to investigate:

1.   Following ATO exposure, the contractile properties, the sarcomere structure and the expression and localization of connexins of cardiac syncytia;
2.   Following Aroclor 1254 exposure, the calcium-induced calcium-released mechanism (Ca^{2+} toolkit) that finely regulates contraction in cardiomyocytes.

ATO. ESCs-derived cardiomyocytes exposed to 0.1, 0.5 and 1.0 µM ATO for 72h exhibit significant alterations of their contractile properties likely correlated remodelling of the gap junctions, leading to abnormal cardiomyocyte conduction properties, as a consequence of the enhancement of the expression profile of the Cx43 protein and increased size of its immunofluorescence signals. The contractile defects might also be due to changes in cardiomyocyte organisation. The 3D whole mount immunofluorescent localization of α-actinin and troponin T showed the

presence, within the EBs, of cardiomyocytes with regularly organized sarcomeres and cardiomyocytes with disorganized-disoriented sarcomeres. Exploiting bioinformatic tools, mathematical parameters, that describe the level of organization of the sarcomeres, were determined. These parameters were significantly lower in cardiomyocytes with altered striated pattern. They were similar to those of CTR in exposed cardiomyocytes with regularly striated pattern with the exception of sarcomere length and width. Specifically, sarcomeres were shorter in length and higher in width. Altered expression of sarcomeric α-actin and tropomyosin, observed in ATO-exposed samples, may interferes with cardiomyocytes cell shape and consequently, with the volume occupied by cardiac syncytia in the 3D structure of the EBs. As we have shown using a stereology approach, the volume of syncytia exposed to 0.1 and 1 µM ATO is diminished and enhanced, respectively, when compared to the CTR, whereas the volume of syncytia exposed to 0.5 µM ATO remains unchanged. Finally, following a recovery period of 72h, cardiomyocytes did not rescue their normal contractile activity.

Aroclor 1254. Cardiomyocytes, exposed to 1 or 2 µg/ml Aroclor for 24h, were analysed for their kinematics contractile properties and intracellular Ca^{2+} dynamics. Aroclor impaired cardiomyocytes contractile properties by decreasing both amplitude and frequency of spontaneous intracellular Ca^{2+} oscillations. It disrupted intracellular Ca^{2+} homeostasis by reducing the Ca^{2+} content of the sarcoplasmic reticulum and by inhibiting voltage-gated Ca^{2+} entry. Finally, it altered the expression of genes involved in Ca^{2+} toolkit.

Additionally, in the frame of a study aiming at assessing the effects of CYP on terminally differentiated and undifferentiated embryonic cell lines, ESCs were used as model of the inner cell mass, a group of cells transiently present in the pre-implantation mammalian blastocyst, that will give rise to the foetus and to some extra-embryonic tissues. CYP is a planetary used organic pesticide known to induce foetal death and birth defects in many species. In this study, cell growth, cell death, ROS production and the activation of a detoxification response, were analysed in mouse embryonic stem cells (mESCs) and 3T3NIH cells, the latter, a differentiated cell line of embryonal origin, used for comparison. After exposure to their respective LD_{50} doses, R1 undifferentiated mESCs had a negative growth rate until 24h exposure. When the R1 population overcame this phase, its growth rate and population doubling (PD) time were significantly lower compared to

unexposed cells. To the contrary, 3T3NIH cells, soon after 8h exposure, reached the same growth rate and PD time of the CTR population. The reduction of R1 exposed cell population was due to the activation of CYP-induced apoptosis (after 8-24h and at 72h exposure) and cell cycle check points (at 48 and 72h), likely a consequence of an increase of ROS production. In mESCs, ROS increase was accompanied by significant up-regulation of mRNA transcripts of genes coding for the redox-enzymes. Conversely, 3T3NIH, completed apoptosis and reinterred the cell cycle with timing similar to that of CTR, within 48h exposure. CYP also triggered the detoxification endogenous mechanisms. 3T3NIH cells fast induced the transcription of the cytochrome P450 *Cyp1a1* phase I gene, and *Gsta1* and *Ugt1a6* Phase II genes; in R1 cell lines, the expression of phase I *Cyp1a1* gene unexpectedly appeared to be reduced and *cyp1b1* was induced only at 72h exposure.

In summary, the results obtained demonstrated that, on differentiated cardiomyocytes, ATO alters the contractile properties, the sarcomere structure, the expression and localization of connexins of cardiac syncytia. Aroclor 1254 interferes with the calcium-induced calcium-release mechanism (Ca^{2+} toolkit) of cardiomyocytes. On ESCs, α-CYP induces cell death and ROS production, interferes with cell growth and activates Phase II detoxification-response genes.

A further novelty of my work is the adaptation of the whole mount immunofluorescence technique to the organization of EBs. To this very complex cellular organization I applied bioinformatics tools to quantitatively evaluate, for the first time in a 3D context, morphological parameters useful to the understanding of the cellular response to EDs.

The results presented in this thesis set the basis to further unravel the molecular mechanisms of toxicity induced following EDs exposure. Furthermore, they represent a starting point for understanding and deepening the hypothesis of a foetal origin of cardiac disease.

CONTENTS

1 INTRODUCTION

1.1 Ecological Developmental Biology

In the last few years, a quiet revolution has occurred in biology, driven by innovative technologies applied in the fields of developmental biology and ecology. The result is an integrated biology innovative view, in which the environment is seen as a crucial source, not a mere selective filter, of variation capable of influencing and shaping the phenotypes. This new emphasis on the role of the environment in development as given rise to a new discipline, named by Scott Gilbert (2001) Ecological Developmental Biology (Eco-Devo). This new discipline seeks to understand how organisms develop in 'real-world' environments (Gilbert 2001; Sultan 2003). For many years, biologists have ignored the influence exerted by the environment on development due to experimental protocols that impose strictly controlled conditions during animal development; it is still a common belief that, in the laboratory, providing animals with adequate nutrition and temperature is sufficient for the understanding of the complex process of development as it occurs in nature (Bolker, 1995). This belief led to the idea that the genome of the fertilized egg is the only player determining embryonic development. Embryology describes embryogenesis as the process of gene expression, whereby the genes in a zygote's nucleus creates the phenotype. In the new Eco-Devo scenario, developmental biology leaves the well-controlled conditions of the laboratory to study development in more natural contexts, since the developmental trajectories in the laboratory do not always correspond to the developmental trajectories in the wild. The environment can shape developmental trajectories and may be critically important in evolution, conservation biology and medicine (Gilbert, 2016).

The environment can accomplish its specific instructional tasks for the building of a phenotype, during early development, by at least three major routes:

> ➢ **The neuroendocrine system**: the nervous system receives signals from the environment and changes the hormone milieu within the organism. Hormones affect gene expression patterns and control the generation of phenotypes.

> ➢ **Direct induction**: environmental factors may interact directly with cells to activate or turn off pathways that promote gene expression and change cell behavior.

> ➢ **Direct transcriptional modulation**: environmental factors can chemically modify promoter and enhancer regions of specific genes, and these modifications regulate whether these genes are transcribed or repressed (Gilbert, 2005).

Eco-Devo consists of two disciplinary areas. The first area studies the roles of environmental factors in facilitating normal development and includes the field of developmental plasticity and developmental symbiosis. The second area studies the environmental disruption of development and the developmental origin of adult health and diseases (DOAHD), teratology and endocrine disruption.

1.2   Environmental signals for normal development

Environment can act on development through two different mechanisms: developmental plasticity and developmental symbiosis. The first mechanism consists of cues (temperature, photoperiod, presence of predators, population density) that are independent to the developing organism. The second mechanism consists of symbiotic organisms that may or may not be integral to the organism, becoming part of the development signalling system (Gilbert, 2012).

1.2.1   Developmental Plasticity

In 1965, when many geneticists considered developmental variability uninteresting, the gynecologist A.D. Bradshaw coined the term 'phenotypic plasticity' to emphasize that the genotype can shape a repertoire of possible phenotypes, while environment can act differentially and instructively during development (Bradshaw, 2006). Phenotypic plasticity, often called "developmental plasticity", gives to the embryo a better chance to adapt its developmental program to environmental variations and to react to an environmental input with a change in form, state, movement or rate of activity (West-Eberhard, 2003).

Reaction norms and polyphenism are the two main types of developmental plasticity currently recognized (Schmalhausen, 1949; Stearns et al., 1991). Specifically, when developmental plasticity manifests as a continuous spectrum of phenotypes expressed by a single genotype across a range of environmental conditions, this spectrum is called the norm of reaction (or reaction norm) (Schlichting and Pigliucci, 1998; Schmalhausen, 1949; Stearns et al., 1991). In other words, an organism inherits a range of phenotypic potentials, specifically elicited by the environment (Gilbert, 2002). Of all the animals, humans likely have the largest norms of reaction. An example is muscle hypertrophy: people, who exercise, have larger muscles but only within hereditarily defined limits. The size of the muscle depends on environmental conditions and how much load is experienced. Bone density is also regulated by mechanical stress: several genes for osteoblast and osteocyte functions are regulated through the physical load (Nomura and Takano-Yamamoto, 2000; Ogasawara et al., 2001).

The second type of phenotypic plasticity, polyphenism, refers to discontinuous phenotypes elicited by the environment. There are different types of polyphenism based on temperature, nutrition, or the presence of a predator. An example of temperature-induced polyphenism is the phenotype determination of many insects. The butterfly *Bicyclusanynana* changes behaviour and wing pattern to give protection during the cold and hot season (Beldade et al., 2011; Monteiro et al., 2013). In the cold season, the caterpillars metamorphose into butterflies with much reduced eyespots, whose colorations protect them as they crawl in the leaf-litter. At high temperatures, in order to deflect avian predators, the caterpillars develop into a flying butterfly characterized by evident eye-spots (Brakefield et al., 1996; Lyytinen et al., 2004).

1.2.2 Developmental Symbiosis

We may think in terms of "The Age of Reptiles" or "The Age of Mammals", but, as Stephen J. Gould (1996) wrote, we live in "The Age of Bacteria". We not only live in a mutualistic symbiosis with our microbes but also develop in mutual symbiosis with them (developmental symbiosis) (Gilbert, 2012; McFall-Ngai et al., 2012). An interesting symbiosis is that between mammals and the bacteria that reside in the mammalian gut. Bacteria benefit from the nutrient-filled home the host's gut provides, while the host benefits from a range of functional and developmental effects induced by the

bacteria (Bry et al., 1996). In various vertebrates, the gut microbiome, by secreting factors that induce gene expression, is involved in many processes such as: organizing the gut-associated lymphoid tissue, expanding the immune cell repertoire, generating the T17 class of helper-T cell, constructing the gut capillary network, and inducing normal division in the intestinal stem cells (Ardeshir et al., 2014; Olszak et al., 2012; Rawls et al., 2004; Rhee et al., 2004; Stappenbeck et al., 2002; Wesemann et al., 2013).

1.3   Developmental origin of health and disease

Environment can be a source of signal for normal development, to produce the expected phenotype (as in mammal-bacteria developmental symbiosis), to enable an organism to develop an alternate phenotype predicted to be fit for a certain environment (as in polyphenism).

However, environment can exert detrimental effects, disrupting normal development. Developmental life is a very sensitive time window of the new organism, including our species. Both maternal and external environment can profoundly influence human biology and long-term health. The period from conception to early childhood is characterized by high plasticity of the developing organism: it is a time of rapid growth, cellular replication, epigenetic remodelling, differentiation and functional maturation of organ systems. These events, which occur through a tightly controlled and timed processes, may be influenced by variations in the intrauterine milieu, caused by the exposure of pregnant women to environmental factors (Kleinjans et al., 2015). In the past, doctors and biologists believed that the mother's body and the placenta gave protection from the environment during the whole prenatal life (Dally, 1998). In 1941, the Australian ophthalmologist Norma Gregg noticed that women who had contracted rubella during the first trimester of pregnancy had more chances of giving birth to an infant with eye cataracts and heart malformations. This study was one of the first to provide strong evidences that the developing foetus could not be fully protected from the external environment through the maternal body (Gregg, 1991). Over the whole intrauterine period, the placenta plays a crucial role in the growth and survival of the foetus (Burton et al., 2016). One of the first functions of placental cells is to produce substances that suppress the maternal immune response against the foetus, thus avoiding foetal rejection (Nugent and Bale, 2015). In later stages of pregnancy, the placenta guarantees proper foetal

growth, thanks to an important transport function mediating the transfer of oxygen, nutrients, growth factors, and hormones from the mother to the child, and the transfer of carbon dioxide and other waste substances in the opposite direction (Levkovitz et al., 2013). Also, placenta is an important endocrine organ that produces hormones, such as progesterone, human chorionic gonadotrophin (hCG) and human placental lactogen (hPL), fundamental to ensure the continuation of pregnancy and to optimize the development of the foetus (Burton et al., 2016; Nugent and Bale, 2015). Also, placenta can protect the foetus from harmful chemicals present in the mother's blood, at least in part. In fact, *in vitro* perfusion studies demonstrated that such protection is partial and fractions of dangerous chemicals (e.g., metals, polycyclic aromatic and polyhalogenated hydrocarbons, aromatic and aliphatic amines) can enter the foetal blood circulation (Myöhänen and Vähäkangas, 2012). Once entered, environmental toxins come into contact with the developing tissues of the organism, where they may cause alterations. Since developing organisms are extremely sensitive, adverse effects may occur at chemical concentrations far below levels considered harmful in the adult (Newbold et al., 2006). This increased sensitivity could be linked to the immature protective mechanisms (DNA repair mechanisms, immune system, detoxifying enzymes, liver metabolism, the blood/brain barrier) of the foetus or the newborn. In addition, the developing organism has an increased metabolic rate compared to an adult which, in some cases, may result in increased toxicity (Newbold et al., 2007). This implies that the foetus may undergo changes in tissue structure, gene expression patterns and physiological function, which alter its developmental program in ways that make the newborn more susceptible to disease onset later in life (McMullen and Mostyn, 2009a). The aetiology of diseases in adulthood may have a foetal origin and may be attributed to the effects of adverse environmental exposure during the *in utero* life. This causality concept is known as "Barker hypothesis" or "Developmental Origins of Health and Disease" (DOHaD).

1.3.1   The Barker's hypothesis

"The womb may be more important than the home", wrote Professor David Barker in a note about his theory (Barker, 1990). In late 1980, Prof. Barker was the first to recognize the link between foetal growth and the onset of disease in adult life. His theory originally evolved from observations that the regions in England that had the highest rates of infant mortality, in the

early twentieth of the last century, also had the highest rates of mortality for coronary heart disease decades later (Barker and Osmond, 1986). The most commonly registered cause of infant death was low birth weight. These observations led to the hypothesis that low birth weight offspring, who survived infancy and childhood, might have increased risk of coronary heart disease later in life (Barker and Osmond, 1986). This concept stimulated great interest worldwide and it has been confirmed across many studies. Large-scale series of epidemiological studies have shown associations between early growth patterns and an increased risk for hypertension, type 2 diabetes, insulin resistance, obesity and the metabolic syndrome in adult life (McMillen and Robinson, 2005). Non-nutritional early life exposures including maternal diet, lifestyle and infection, as well as exposure to environmental endocrine disruptors, may alter the physiology of the new organism and have consequences on long-term health (Figure 1) (Silveira et al., 2007).
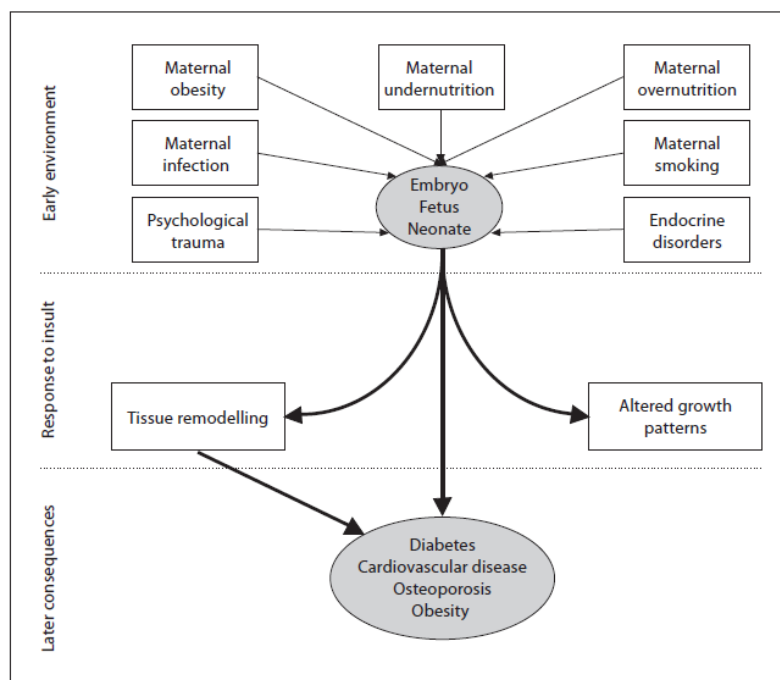
Figure 1. Overview of how adverse environmental cues during the gestational and post-natal windows of development may program pathophysiology and adult disease (Langley-Evans and McMullen, 2010).

There are three key tenets of DOHaD that unfurl the mechanisms by which prenatal and postnatal exposures could be linked to phenotypic changes later in life (Figure 2) (Cota and Allen, 2010):

1. ***plasticity,*** which describes the malleable nature of the human body and its physiology. Plasticity allows the developing organism to adopt a phenotype that best suits the environment. For example, when a foetus receives inadequate blood flow through the placenta, his metabolic pathways adjust to accommodate this environment. Plasticity ends at birth but continues to be moldable at least through early childhood (Sullivan et al., 2008).

2. ***epigenetic modifications***, which play a fundamental role in determining the functional output of the information stored in the genome (Jirtle and Skinner, 2007). During development, the epigenome cycles through a series of precisely timed epigenetic changes designed to guarantee proper development. For instance, epigenetic marks, such as methylation patterns, are laid down during development and are responsible for stem cells differentiation into specific cell types and tissues. The loss and subsequent reestablishment of the epigenetic profile in the developing embryo comprises a critically vulnerable period during which the system is particularly susceptible to environmental influences (Murphy and Jirtle, 2003). Epigenetic aberrations represent a memory of exposure to chemical and/or nutritional factors during early life (Chen and Zhang, 2011).

3. ***programming,*** the programming of adult pathology, due to perinatal insults, is likely the consequence of reduced functional capacity in key organs, a "thrifty" phenotype. This reduced functionality is the consequence of the redistribution of resources to crucial organs at the expense of other organ systems, which become more sensitive to adverse environmental influences in later life (Hales and Barker, 2001). The timing of an insult may be more impactful than the quantity of the harmful exposure, because there are specific time periods during development in which different organs and body systems are more susceptible to the programming of disease (Barker and Thornburg, 2013).

Figure 2. Developmental Origins of Health and Disease theory and its tenets (Thiele and Anderson, 2016).

Recent findings support a "2-hit hypothesis" to explain the adult onset of diseases (Puttabyatappa et al., 2016; Tang and Ho, 2007). The congenital genetic factors, inherited from parents or *de novo* genetic mutations, represent the "first hit", which alone might be insufficient to alter the adult phenotype. Then, the endocrine imbalances resulting from the perinatal insults and/or adverse stressors/exposures during postnatal life may act as a "second-hit," which, through activator effects, might unmask or amplify the underlying defects, culminating in the disease (Puttabyatappa et al., 2016). In this way, the combination of genetic susceptibility with an environmental insult occurring during perinatal life leads to the emergence of an organ disease.

Among the wide range of environmental stressors that can alter the foetal and post-natal developmental trajectory, here after the category of the endocrine disruptors (EDs) is presented, since the prevalence of EDs in our environment and our bodies represents a significant global public health challenge. Recently, organizations such as the Endocrine Society (Diamanti-Kandarakis et al., 2009; Gore et al., 2015) and the WHO/UNEP (Bergman et al., 2013) have published official reports describing the possible health threats posed by EDs. They focused on exposure during critical periods of development and concluded that exposure to EDs is related to many diseases, including impaired reproduction, neurodevelopment, thyroid function, cardiac apparatus and metabolism, as well as increases in hormone-sensitive cancers. EDs show their effects at low doses within the range of human environmental exposure that are assumed to be safe under the current regulations on chemicals. Thus, these reports called for urgent action to regulate EDs.

1.4   Endocrine disruptors

During the last decades, the observation that some exogenous substances could interfere with hormonal and homeostatic systems of an organism (Diamanti-Kandarakis et al., 2009) has led to the identification of the EDs as a new diffused class of toxic agents (Zoeller et al., 2014). According to US Environmental Protection Agency (EPA), an ED is defined as "an exogenous compound that interferes with the synthesis, secretion, transport, binding or elimination of natural hormones in the body that are responsible for the maintenance of homeostasis, reproduction, development and/or behavior" (Kavlock et al., 1996). EDs are highly heterogeneous molecules, but, consistent with their origin, they can be grouped (De Coster and van Larebeke, 2012; Kabir et al., 2015; Lubrano et al., 2013; Monneret, 2017) as follows:

1. industrial (dioxins, polychlorinated biphenyl and alkylphenols);

2. agricultural (pesticides, insecticide, herbicides, phytoestrogens, fungicides);

3. residential (phthalates, polybrominated biphenyls, bisphenol A);

4. pharmaceutical (parabens);

5. heavy metals (cadmium, lead, mercury and arsenic).

There are diverse sources of EDs exposure, widely distributed all over the environment and societies of the world. The use of these substances varies among countries. Some of them have been banned decades ago in some countries, but more recently in others. A characteristic of EDs is their long half-life, an advantageous property for the industries, but quite detrimental to wildlife and humans. These substances do not decay easily, they may not be metabolized or metabolized into more toxic compounds than the founder molecule; even substances that were banned decades ago can persist in high levels in the environment (Calafat and Needham, 2007; Porte et al., 2006). Exposure to EDs may occur through drinking water, breathing air, ingesting food or contacting soil, that are exposed to several pesticides, plasticizers, alkylphenols and flame retardants commonly used in agriculture, industry and household applicants (Diamanti-Kandarakis et al., 2009). Industrialized areas are typically characterized by contamination from a wide range of industrial chemicals that are easily released into the environment for example through

leaching into the soil and water. These are then taken up by microorganisms, algae or plants and then taken by animals. Thus, EDs enter the food chain from the animals to finally reach the human being. Pregnant mothers and children are the most vulnerable populations to be affected by developmental exposures, indeed EDs can be transferred from the pregnant woman to the developing foetus through the placenta and to the newborn through breast milk (Monneret, 2017). EDs were originally thought to exert their actions principally through interaction with hormone receptors, such as estrogen receptors (ERs), androgen receptors (ARs), progesterone receptors, thyroid receptors (TRs) and retinoid receptors. However, many animal studies have demonstrated that the mechanisms which EDs may interrupt the endocrine system and alter hormonal functions are much wider than initially recognized (Diamanti-Kandarakis et al., 2009; National Institute of Environmental Health Sciences, 2015). Specifically, they can:

➢ imitate hormones synthetized in the body like estrogens, androgens, and thyroid hormones, potentially producing overstimulation;

➢ act as antagonists, binding to receptors of endogenous hormones and thereby preventing their binding and the corresponding cell signaling;

➢ interfere with the synthesis, transport, metabolism and elimination of hormones, thereby decreasing the concentration of endogenous hormones.

The mechanism of action of the EDs is not easily predictable due to their chemical differences. EDs like dioxins, PCBs and pesticides may contain halogen substitutions by chlorine and bromine, while some endocrine disruptors are just heavy metals or metalloids, which may have estrogenic activities or act as anti-androgens or thyroid hormone receptor agonists or antagonist (Diamanti-Kandarakis et al., 2009). Because of their world-wide distribution in the environment and impact on public health, three EDs deserve special attention: Cypermethrin, Polychlorinated Biphenyls and Arsenic. They belong to the categories of agricultural, industrial and heavy metal EDs, respectively, and are briefly described below.

1.4.1   A heavy metal ED: Arsenic

Arsenic is a metalloid element with ubiquitous distribution throughout earth's crust, groundwater and biosphere (Sumi et al., 2011). The release of

arsenic into the environment can occur through weathering and mining processes, as well as volcanic activity. Arsenic is also a by-product in smelting processes for many ores including gold, lead, cobalt, nickel, and zinc (Carlin et al., 2016). The World Health Organization (WHO) estimates that over 200 million people worldwide are chronically exposed to arsenic through drinking water at concentrations above the WHO safety standard of 10 µg/l (Naujokas et al., 2013). Contamination of drinking water by Arsenic is considered one of the top global health concerns, given the extent of the population's potential exposure and its association with several diseases, including cancers, type 2 diabetes, cardiovascular diseases, reproductive and developmental alterations (Abernathy et al., 2003; Tapio and Grosche, 2006; Watanabe et al., 2003).

The ability of arsenic to increase disease risk is linked to its ability to produce reactive oxygen species, to alter cell signaling or apoptotic and differentiation responses (Aposhian and Aposhian, 2006; Bode and Dong, 2002; Kitchin, 2001; Rossman, 2003). Also, arsenic is a potent ED, since it alters gene expression through interaction with steroid hormones (Bodwell et al., 2004; Kaltreider et al., 2001).

Epidemiological studies of people exposed to arsenic *via* drinking water in Argentina showed similar exposure levels in the foetus as in the mother, being arsenic able to pass over the placenta to the foetus (Concha et al., 1998). On the contrary, little arsenic is excreted in breast milk because the passage of Arsenic over the mammary gland is limited. Consequently, the newborn is protected against arsenic exposure during the breastfeeding period, whereas formula prepared from the drinking water may cause considerable postnatal arsenic exposure (Concha et al., 1998). Many epidemiological, experimental and mechanistic studies suggest that early-life exposure to arsenic is correlated with health risks later in life (Quansah et al., 2015). Its major adverse health effect detectable in young adulthood is myocardial infarction (Chen and Zhang, 2011; Smith and Steinmaus, 2011), suggesting that exposure during foetal or post-natal life may induce cardiac alterations that will emerge later.

1.4.2   An Industrial ED: Polychlorinated Biphenyls

Polychlorinated biphenyls (PCBs) are man-made organic compounds produced from biphenyls in which some of the hydrogen atoms are replaced by chlorine atoms (Reddy et al., 2019). PCBs were used primarily for

industrial applications (heat transfer, rubber and plastic products, hydraulic machines, dyes, pigments and carbonless copy paper), as they were characterized by insulating properties and non-flammability (Zhu et al., 2011, 2012). They were banned in the 1970s, when, following exposure, adverse effects on human health were identified. However, PCBs are still present in the environment due to their high chemical stability. The most common source of environmental exposure to these substances is through food, such as dairy products, meat and especially fish (Koopman-Esseboom et al., 1994). PCBs can cross the placenta (Kezios et al., 2012), disrupting the endocrine pathways that are important for foetal development, leading to altered foetal growth (Public Health, 2000) or congenital heart defects (Tilson et al., 1990). Moreover, PCBs accumulate in human adipose tissue (Patandin et al., 1998), thus passing to newborns through maternal milk and causing heart functional impairment in the adult (Ross, 2004).

1.4.3 An agriculture ED: Cypermethrin

Pyrethroids are synthetic organic insecticides derived from pyrethrins and used worldwide since the beginning of the '80s, last century, because of their high level of efficiency and low toxicity compared to other insecticides (Yoo et al., 2016). Their insecticidal actions rely in the binding to voltage-gated sodium channels causing the induction of prolonged neuron depolarization (Bradberry et al., 2005; Soderlund, 2012).

Pyrethroids are divided into type I and type II, depending on the structure of the compound and their action and symptoms they cause. α-Cypermethrin (CYP) is a type II pyrethroid pesticide widely employed in crops against pest and insect (Akelma et al., 2019). Humans can be exposed to pesticides *via* different routes: directly from occupational, agricultural and household use, and/or indirectly through diet. Having mostly a lipophilic nature, they have the capability to bind with fats and, consequently, bio-accumulate in the body over time, resulting in substantial health risks (Gilden, 2010). A study revealed that CYP in low dose leads to some metabolic alterations, which can interfere with maternal physiology and foetal metabolism (Hocine et al., 2016). Pesticidal exposure is also linked with cancer development, hormone disruption and reproductive dysfunction (Marettova et al., 2017; Van Maele-Fabry et al., 2010). Foetus and newborns are more vulnerable to pesticides and adversely affected by pesticide exposure in the womb (Huen et al., 2012).

1.5 Developmental origin of cardiac disease

The examples of exposures to EDs described before provide evidences in favour of the DOHaD theory. The reported data show that the environment during the periconception, gestation and lactation periods may predispose or be causative of various adult diseases, such as cardiac diseases, cancer, mental health problems, diabetes mellitus, chronic respiratory disease and musculoskeletal conditions (Tarrade et al., 2015). Among these, heart failure represents the most significant cause of mortality and morbidity in the industrialized countries, with more than 23 million cases worldwide and a survival rate of only 50% within 5 years from diagnosis (Pavesi et al., 2015; Segers and Lee, 2008). That is why it has been defined as a global plague, accounting for 1–3% of all healthcare spending in North America, Western Europe and Latin America (Ponikowski et al., 2014). There are many risk factors that can contribute to the onset of cardiac disease, but many epidemiological and experimental animal studies have demonstrated that adversity in foetal life may make the progeny more susceptible to heart disease and/or heart failure in adult life (Barker et al., 1989, 2010). This happens because the organs and the physiological systems form and start maturation during the life *in utero*. For instance, the heart begins to develop early in gestation but becomes fully mature and complete only after birth. This relatively long gestation and period of postnatal maturation of the hearth lead to prolonged pre- and post-natal exposure to the environment (Monti, 2016).

1.6 Cardiomyogenesis

The heart is the first organ formed in the developing embryo. The decision to commit towards a cardiac cell fate is taken early during mammalian embryogenesis and, in humans, the primordial heart starts to beat at around 22 days after fertilization. The early beating of the heart highlights its crucial function in providing oxygen and nutrients to the various tissues (Später et al., 2014). Cardiomyogenesis starts soon after gastrulation, the morphogenetic process responsible for the formation of the three germ layers (ectoderm, mesoderm, and endoderm), that begins with the appearance of the primitive streak (PS). A subset of epiblast cells moves to the PS and undergoes epithelial-to-mesenchymal transition (EMT), in order to

transitorily forms the mesendoderm (Van Vliet et al., 2012). The heart is derived from the mesoderm and the different populations of cardiac progenitor cells are, for the most part, localized within the anterior PS. They are distributed, in relation to the organizing centre, also called node, in the same anterior-posterior order that they are later found in the tubular heart (Garcia-Martinez and Schoenwolf, 1993). As development proceeds, the precursor population of precardiac mesoderm emigrates on either side of the streak, in an antero-lateral direction, giving rise to the primary heart field (PHF) and the secondary heart field (SHF). The axial distribution is maintained as the PHF migrates to fuse and become the cardiac crescent. At this point, the anterior endoderm seems to have an instructive function in cardiogenesis (Brand, 2003), as it sends cues to cells of the cardiac crescent, which in response to these cues adopt a definitive cardiac fate (Olson, 2001). After cardiac mesoderm has been specified, it moves up to the ventral side of the embryo, where the PHF starts to fuse in order to form a single tube. When the primary cardiac induction is concluded, cells within the SHF are recruited from the lateral plate mesoderm, medial to the PHF (Kelly and Buckingham, 2002). The PHF contributes to form mainly the left ventricle and parts of the atria, whereas the anterior SHF gives rise to the right ventricle and outflow tract. The atrial tissue is formed by the posterior SHF (Meilhac et al., 2014; Paige et al., 2015) (Figure 3). Initially, the heart tube is almost straight, but then the ventricular segment, flipping to the right, bulge ventrally and starts to form a C-shaped heart. Through a series of morphogenetic and looping movements, left-right asymmetry becomes increasingly evident and four-chambered heart finally forms (Christoffels et al., 2000).

Figure 3. Schematic representation of developmental stages during mammalian heart formation (Verma et al., 2013).

1.7 Signalling and gene networks in cardiac development

Cardiac development is a complex process which requires, for its regulation, the networking between major developmental signalling pathways, a higher cardiac-specific array of transcription factors, as well as other transcriptional regulators. There are three main families of extracellular signalling molecules that coordinate the induction of mesoderm formation and its subsequent specification toward a cardiac programme:

1. Wingless integrated (Wnt);
2. Fibroblast Growth Factor (FGF) superfamily ligands;
3. Transforming Growth Factor-beta (TGFβ) superfamily ligands.

These include Wnt3a, bone morphogenetic protein 4 (BMP4), Nodal and activin A (Noseda et al., 2011). These ligands, or their inhibitors, form gradients depending on the spatiotemporal context and send either activating or inhibitory instructive stimuli to finely pattern the developing embryo. This mixture of signalling pathways and downstream transcriptional outcomes guide the expression of cardiac-specific factors in a defined population of

mesodermal cells, the result is the specification of the future cardiac field (Noseda et al., 2011).

Cardiogenesis has been well investigated in the mouse (Arnold and Robertson, 2009; Buckingham et al., 2005; Tam and Loebel, 2007) (Figure 4). Mesoderm induction begins with Nodal signalling in the proximal epiblast on mouse embryonic day 5 (E5.0), which induces Bmp4 expression in the extraembryonic ectoderm nearby the epiblast and, in turn, Bmp4 acts by inducing Wnt3 expression in the proximal epiblast.
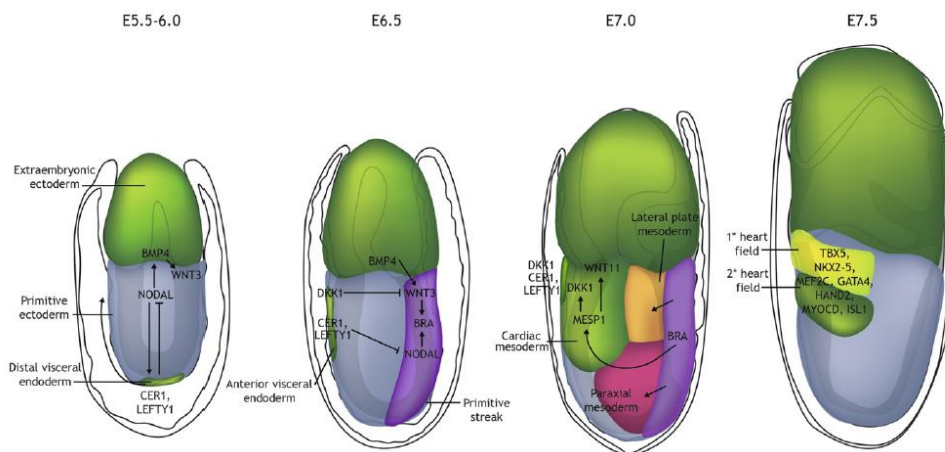
Figure 4. The mouse as a model for human cardiac development: signaling factors involved in cardiac differentiation (Burridge et al., 2012).

Around E5.5, Dkk1 (Wnt antagonist) and Lefty1 and Cer1 (Nodal antagonists) are expressed and moves to the anterior visceral endoderm, confining Nodal and Wnt signalling to the posterior epiblast. At E5.75, Wnt induces the expression of mesoendodermal markers such as T (brachyury) and Eomes. Subsequently, Fgf4 and Fgf8 genes are expressed in the developing PS and are responsible for mesoderm patterning and epithelial-mesenchymal transitions (EMTs). Then, T and Eomes induce the expression of the basic helix–loop–helix (bHLH) transcription factor mesoderm posterior1 (Mesp1) (Costello et al., 2011; David et al., 2011). Mesp1, defined as a "master" regulator of cardiac lineage specification, acts to stimulate cardiac progenitor specification by activating a complex mesh of genes involved in cardiac development, i.e. Gata4, Nkx2.5, Mef2c and Hand2, and indirectly down-regulating the pluripotent genes Nanog, Oct4 and Sox2

16

(Bondue et al., 2008). Cardiac mesodermal cells, under the control of active Bmp4 signalling, start to differentiate in PHF progenitor cells, whereas cardiac mesodermal cells, that are regulated by active Hedgehog (HH) signalling and down-regulation of canonical Wnt signalling, become the progenitor cells of SHF (Dierickx et al., 2012). At this point, Notch induces the expression of Wnt5a, Bmp6 and SFRP1, which altogether increase the proliferation of cardiac progenitor cells (CPCs) (Chen et al., 2008). Also, FGF comes into play with Notch to control proliferation and fate determination of CPCs. When these latter stops proliferating, they begin to differentiate towards immature cardiomyocytes; this process is directed by the down-regulation of both HH and canonical Wnt signalling. The downregulation of canonical Wnt signalling leads to the switching toward non-canonical Wnt signalling, with the induction of Wnt11 (Dierickx et al., 2012). Moreover, BMP signalling is necessary for terminal differentiation, because it maintains the expression of Tbx20 (Shi et al., 2000; Walters et al., 2001). At this stage of differentiation, Nkx2.5 and Tbx5 interact with members of Gata family of zinc finger transcription factors (Gata 4/5/6) and with Serum Response Factor (SRF) to induce the expression of genes involved in the determination of cardiac structural features, such as actin, myosin light chain, myosin heavy chain (MHC), troponins and desmins. Moreover, Tbx5 works together with Nkx2.5 to trigger the expression of atrial natriuretic factor (ANF) and the junctional protein Connexin 40 (Mummery et al., 2012).

1.8 Developmental toxicity assays

The DOHaD has become well accepted within the scientific community, because of convincing animal studies that have accurately defined the outcomes of specific exposures. *In vivo* studies have confirmed that inadequate environments in the womb and during early neonatal life alter development, predisposing the human being to lifelong health problems. The *in vivo* assay, built to evaluate the embryotoxicity of environmental pollutants, used a variety of large (e.g. sheep and pig) and small (e.g. mouse, rat, guinea-pig, more recently zebrafish) animal models, significantly contributing to this research field (McMullen and Mostyn, 2009b; Sukardi et al., 2011). These assays consisted of administering the chemical to the model organism, subsequently evaluating the compound's effects and its possible dramatic effects during the different developmental period and gestational

stages (Chernoff and Kavlock, 1982). There are several advantages using animal models in toxicity testing, such as a defined genetic constitution suitable to controlled exposure, controlled time of exposure, as well as the opportunity of exhaustive examination of all tissues following necropsy (Cunny and Hodgson, 2004). However, despite representing a historically successful system for embryotoxicity evaluation, *in vivo* toxicity test presents several negative aspects. The first aspect is the extent to which animal models reflect human responses. There are many inter-species differences in anatomy, metabolism, physiology and genetics, that could significantly limit the reliability of using animal experimentation to predict human responses to toxicity including reproductive toxicity (Bremer et al., 2005). As Thomas Hartung, pharmacologist and past director of the European Center for the Validation of Alternative Methods (EVCAM), asserted "humans are not 70 kg rats". There are a lot of differences from all laboratory animal species, for example in metabolic rates, food and water intake, pH present in the gut; body temperature, metabolism and elimination routes of xenobiotics, body fat distribution, defence mechanisms and life span" (Hartung, 2008). A second issue is the cost: the maintenance of adequate animal husbandry and the training of qualified staff is extremely expensive, leading to limit the number of replications and repetitions. Finally, ethical concerns have also been raised on using and killing animals (Hartung, 2008; Matthews, 2008; Shanks et al., 2009). Numerous studies revealed that animal physiological and hormonal markers could change because of pain, distress and death experienced by the animals during scientific experiments, even gentle handling (Balcombe et al., 2004). Moreover, Directive 2010/63/EU (Olsson et al., 2016) on the protection of animal used for scientific research restricts the use of laboratory animals. The directive is based on "The Principles of Humane Experimental Technique" published by William Russell and Rex Burch in 1959, in which is described the '3Rs' concept, a solid ethical framework whose purpose is to minimize the use of animals through a systemic evaluation of pain and permanent damage caused to animals during research experiments (Russell and Burch, 1959). These '3Rs' principals consist in reducing the total number of animals used in an experiment, refining experimental procedures to minimize pain and distress and replacing the use of animals with alternative methodologies (Flecknell, 2002). These principles have been universally and unanimously accepted worldwide and, currently, have been introduced into the legislative policies of animal welfare guidelines (Kandárová and Letašiová, 2011). Over the last decades, strong efforts have been made to

18

establish several alternative methods for the prediction of developmental toxicity *in vitro*, in order to reduce and finally replace animal tests. These methods vary from whole embryo cultures of rat (Piersma et al., 2004) or zebrafish (Rubinstein, 2006) and organ cultures (Flint and Orton, 1984) to cell-line-based tests, such as the embryonic stem test (EST) (Genschow et al., 2004). Fast experiments, controlled conditions, subsequent reduction of variability between tests, and relatively accurate results associated with cells of human origin are the advantages associated to the use of these alternative tests (Kandárová and Letašiová, 2011; Ranganatha and Kuppast, 2012). Among a large number of *in vitro* screening methods, the EST is the only method that uses specific cell lines and that does not rely on a continuous source of embryonic tissues or whole embryos from pregnant animals, attracting interest for further development and validation. Moreover, the EST was reviewed by an independent committee and selected for formal validation funded by the ECVAM (Brown et al., 1995).

1.9 Embryonic stem cells as alternative methods for assessing developmental toxicity

More than 20 years ago, Spielmann and colleagues (Spielmann et al., 1997) set up an *in vitro* model for predicting chemical developmental toxicity. The so-called EST takes advantage of the potential of mouse embryonic stem cells (mESCs) to differentiate in culture into a variety of cell types (Hoffman and Merrill, 2007; Keller, 2005; Wobus and Boheler, 2005) and aims to assess three toxicological endpoints following 10 days of chemical exposure:

(i) the morphological analysis of beating cardiomyocytes derived from mESCs differentiation;

(ii) cytotoxic effects on undifferentiated mESCs;

(iii) cytotoxic effects on differentiated 3T3 fibroblasts.

LD_{50}, namely the concentration of a molecule that is required for 50% growth inhibition of a cellular population, is determined from cytotoxicity analysis on mESCs and on 3T3 fibroblast (endpoints ii and iii). Whereas ID_{50}, namely the concentration of a molecule that inhibits cardiomyocytes differentiation in 50% of the population, is calculated from toxicity analysis during mESCs

differentiation into cardiomyocytes (endpoint i). To convert the *in vitro* results into a prediction of the *in vivo* results, a biostatistical based prediction model (validated by EVCAM) is applied to the results obtained by the EST *in vitro*, allowing a classification of chemicals into weak, strong and not embryotoxic chemicals (Genschow et al., 2002; 2004). Currently, the EST standard protocol has been implemented and additional biomarkers are being developed to improve the accuracy of classical EST and assess the endpoints with more objective and informative strategies.

1.10 A stem cell cardiomyocytes-differentiation platform for *in vitro* toxicity tests

The "Laboratory of Developmental Biology", University of Pavia, has further improved the EST, developing an embryonic stem cell differentiation platform which allows to extend the differentiation process up to 15 days, in order to characterize the development of functionally mature cardiomyocytes in its progressive stages and to evaluate how they are affected by the treatment with xenobiotics. We differentiate mESCs into cardiomyocytes in the presence of the xenobiotic molecule of interest either along the whole process of differentiation or at the end of it, on terminally differentiated cells. Using this platform, a variety of assays can be formed to evaluate the *in vitro* toxicity by analysing (Figure 5):

i.   the kinematic parameters of differentiated cardiomyocytes;

ii. the induction or repression of cardiac marker genes;

iii. the structural organization of the sarcomere;

iv. the intracellular calcium homeostasis involved in cardiomyocyte contraction.
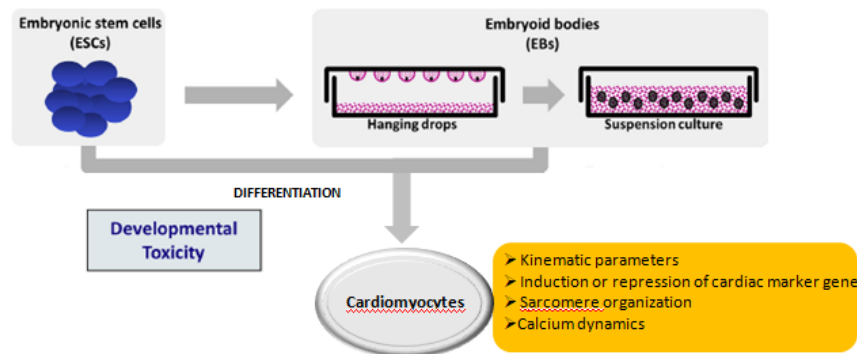
Figure 5. Potential applications of ESCs or embryoid bodies (EBs) for improvement of alternative methods to *in vivo* developmental toxicity testing (adapted from Kim et al., 2019).

Compared with *in vivo* studies, the use of this *in vitro* model of cardiomyocyte differentiation permits a more precise definition of the effects exerted by different chemical molecules on a specific cell type, such as cardiomyocytes, rather than on the entire cardiac developmental process, or alternatively on foetal cardiac cells, obtained at the end of the differentiation process. In the following paragraph, I will briefly describe this embryonic stem cell differentiation platform.

1.11 Cardiac differentiation from mESCs

ESCs are derived from early embryos before implantation in the uterus. They are distinguished by two characteristics: the capacity of self-renewal indefinitely, without ever entering senescence, and pluripotency, that is the unique ability to differentiate into multiple somatic cell types in culture, presumably passing through precursors, when appropriate stimuli are applied (Thomson et al., 1998). The most widely used method for triggering differentiation *in vitro* is the formation of multi-cellular, three dimensional (3D) aggregates formed in a medium that cannot support pluripotency. Due to the similarity of these aggregates to early post-implantation embryos, they were defined embryoid bodies (EBs) (Mummery et al., 2012).Within these aggregates, stochastic events lead to the induction of developmental cues that normally drive embryogenesis, such as differentiation into derivatives of the three germ layers (Itskovitz-Eldor et al., 2000), including spontaneously

contracting cardiomyocytes. There is a wide variety of protocols for EBs formation, but the most suitable method is the "hanging drop" method (Figure 6), that consists of generating single EBs, starting from a defined cell number, in individual droplets of culture medium deprived of LIF (Leukemia Inhibitor Factor), involved in the maintenance of pluripotency (Boheler et al., 2002; Graf et al., 2011; Wobus et al., 1991). After three days of culture in the drop, the EBs generated are cultured in suspension for an additional 2 days and then plated onto multi-well plates, where the differentiation proceeds for other10 days.
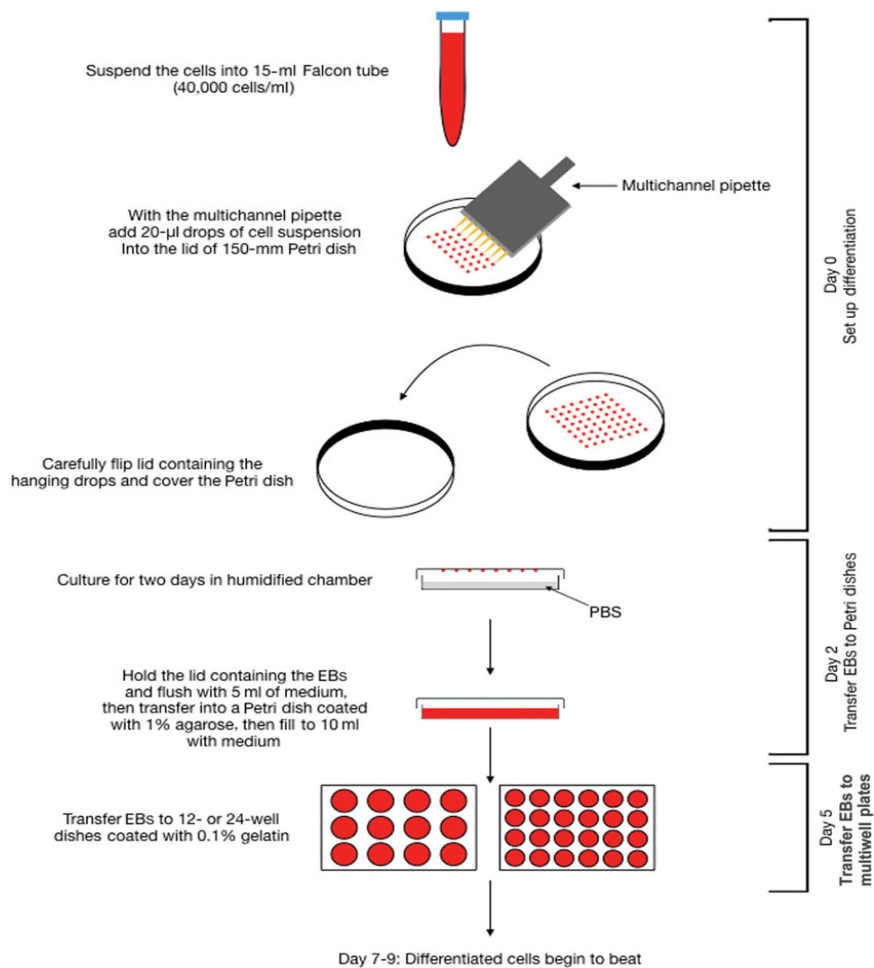
Figure 6. Hanging drop method for mESCs differentiation into cardiomyocytes (Zakariyah et al., 2019).

Within 1 to 4 days after plating, cardiomyocytes contract spontaneously, inducing a regular beating of the EBs. As differentiation proceeds, the number of beating foci increases progressively (Boheler et al., 2002). During differentiation, cardiomyocytes undergo a change in their morphological and functional features. During the early stages of differentiation within EBs, cardiomyocytes are usually small and round, with a variable degree of sarcomeric organization. For example, some nascent myofibrils are organized in sparse and irregular ways, while others contain parallel bundles with starting evidence of A and I bands (Westfall et al., 1997). Upon maturation, cardiomyocytes acquire an elongated shape, present well-developed myofibrils and sarcomeres and connect with adjacent cells through cell-cell junctions, like those observed in the developing heart. During the last stage of differentiation, cardiomyocytes are characterized by well-organized bundles of myofibrils and the sarcomeres present a typical striated structure with I and A bands, Z disks (Fässler et al., 1996), desmosomes and gap junctions (Doetschman et al., 1985) (Figure 7).
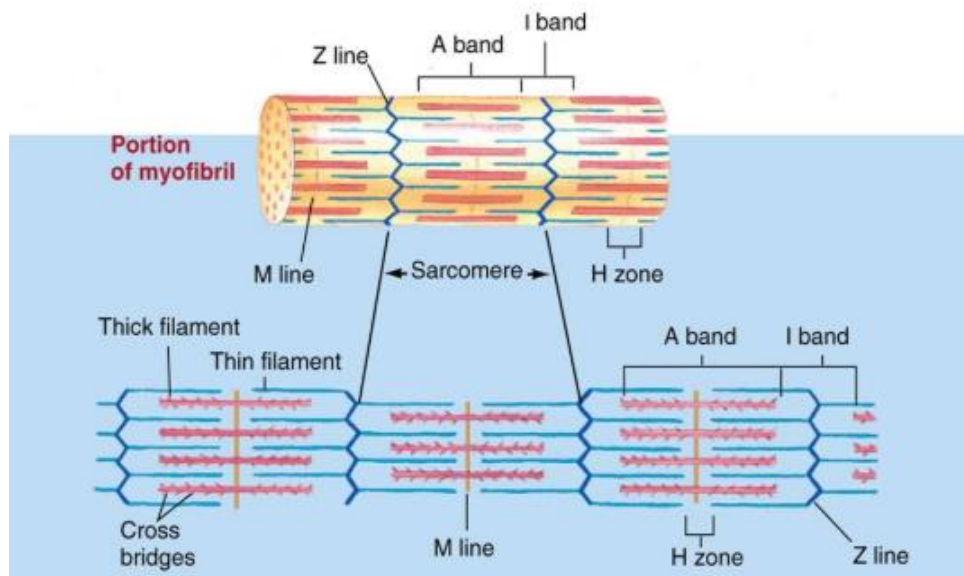
Figure 7. Schematic representation of a portion of myofibril with sarcomeric components (https://www.austincc.edu/apreview/PhysText/Muscle.html).

ESCs-derived cardiomyocytes have cell length, diameter, area, ultrastructure and sarcomere organisation comparable to foetal/neonatal myocytes (Boheler et al., 2002). They express cardiac genes in a developmental controlled manner; for example, the mRNAs encoding Gata-

4 and Nkx2.5 transcription factors appear in EBs before mRNAs encoding the myosin light chain (MLC)-2$_V$, α and βheavy chain of myosin (MHC). From an electrophysiological point of view, early ESCs-derived cardiomyocytes are very similar to primary myocardium cells, while terminally differentiated cardiomyocytes express electrophysiological features that resemble those of foetal/postnatal cardiomyocytes (Hescheler et al., 1997). The differentiation of mouse ESCs through EBs represents a highly regulated culture system in which gene expression, myofibrillar architecture, cellular ultrastructure and electrophysiological functions are controlled similarly to what occurs in cardiac development *in vivo* (Boheler et al., 2002). For this reason, this differentiation procedure represents an ideal platform to test toxic agents (drugs, environmental pollutants etc.) during cardiomyocyte differentiation or at the end of the process.

2   AIM OF THE RESEARCH

Epidemiological studies suggest strong links between EDs exposure and the development of pathologies in young adulthood.

As described in "Introduction", in *utero* exposure to ATO or Aroclor 1254 is correlated to the onset of cardiac pathologies. However, up to date, their effects on foetal/neonatal cardiomyocytes at cellular and physiological levels are scarcely known. Using an ESCs platform of cardiac differentiation to obtain foetal/neonatal-like cardiomyocytes, the main aim of my project was to investigate:

1. the contractile properties, the sarcomere structure and the expression and localization of connexins of cardiac syncytia exposed to ATO;

2. the calcium-induced calcium-release mechanism (Ca^{2+} toolkit) that finely regulates contraction in cardiomyocytes exposed to Aroclor 1254.

Also, undifferentiated ESCs were used as model of the inner cell mass, a group of cells transiently present in the pre-implantation mammalian blastocyst, that will give rise to the foetus and to some extra-embryonic tissues. ESCs were exposed to CYP, a planetary used organic pesticide known to induce foetal death and birth defects in many species, to determine whether and to which extent CYP affects cell growth, determines cell death, reactive oxygen species (ROS) production and which detoxification response it induces.

3   PART 1
STUDY OF THE EFFECTS OF ARSENIC TRIOXIDE ON FOETAL CARDIAC SYNCYTIA DERIVED FROM mESCs

3.1 Background

Arsenic is one of the most toxic metals diffused in the environment (Ratnaike, 2003). More than one hundred million persons worldwide are at risk of arsenic exposure at concentration above 10 µg/l (Naujokas et al., 2013); both the WHO (1993) and the United States Environmental Protection Agency (2001) have reduced the acceptable arsenic concentration in drinking water from 50 to 10 ppb in the past two decades. Arsenic is present in the environment in both inorganic and organic forms, with various oxidation states. The pentavalent (V) and trivalent (III) forms have high cytotoxic potential (Hughes et al., 2011) with the latter having more toxic effects (Cervantes et al., 1994). Arsenic trioxide (ATO) represents the most diffused compound containing inorganic arsenic in the environment.

ATO exposure can induce several different chronic malignancies, highlighting the variety of its cellular targets and its ability to deregulate various cell functions, i.e. cellular energy pathways, DNA replication and repair. Both environmental and occupational exposures have been associated to cardiac toxicity (Alissa and Ferns, 2011) and several studies report that arsenic plays a crucial role in the onset of cardiac disorders (Balakumar and Kaur, 2009; Jomova and Valko, 2011; Tseng, 2008). Cardiac arrhythmia, high rate of cardiomyocytes apoptosis and the induction of calcium overload are the main damages described (Raghu et al., 2009). The same effects have also been reported in clinical reports of patients treated with ATO for the treatment of haematological malignancies (Shen et al., 2004; Wang and Chen, 2008). Chronic exposure to a therapeutic dose of ATO causes ventricular arrhythmia, tachycardia, QT interval prolongation and, occasionally, sudden cardiac death (Drolet et al., 2004; Ducas et al., 2011).

A growing body of evidence indicates that prenatal and early childhood exposure to arsenic can have severe long-term health implications (Concha et al., 1998). In particular, myocardial infarction is its major adverse health effect detectable in young adulthood (Chen and Zhang, 2011; Smith and Steinmaus, 2011). However, up to date, the effects on cardiomyocytes due to ATO exposure during foetal and post-natal life are meagre and yet to be investigated.

26

In this study, cardiomyocytes, obtained from the differentiation of mESCs, were exposed to 0.1, 0.5 and 1.0 µM ATO for 72h. After exposure, we analysed: i) the kinematics contractile properties of the syncytia; ii) the sarcomeric structure; and iii) the connexins expression and localization. All these analyses were conducted preserving the 3D structure of the cardiac syncytia within the EB, in order to maintain its spatial and multi-layered conformation.

3.2 Material and Methods

3.2.1 Embryonic stem cell culture

R1 mESC line was used for the experiments. This cell line was isolated from a 3.5-day post coitum (dpc) F1 blastocyst derived from 129X1/SvJ x 129S1 mating and was kindly provided by Dr. Nagy, Samuel Lunenfeld Research Institute, Mount Sinai Hospital, Toronto (Ontario, Canada). R1 cells were cultured in a complete medium with the following composition: Dulbecco's Modified Eagle's Medium Knockout (KO-DMEM), supplemented with 15% ES Cell Qualified Foetal Bovine Serum, 2 mM L-glutamine, 1X non-essential amino acids solution, 0.5% penicillin-streptomycin (all from Thermo Fisher Scientific), 0.1 mM β-mercaptoethanol (Sigma) and 500 U/ml ESGRO®-leukemia inhibitory factor (ESGRO®-LIF) (Merck). The mESCs were cultivated on 100 x 20 mm Petri dishes (Corning), coated with 0.1% gelatin (Sigma), and regularly passed every 2-3 days, using a 0.05% trypsin-EDTA solution (Thermo Fisher Scientific). Once a week, there were cultured on a feeder layer of STO cells (see below). The cells were maintained in a 37°C incubator, with 5% CO_2.

3.2.2 Feeder layer culture

Mouse STO-SNL2 cell line (STO, American Type Culture Collection CRL-2225), resistant to geneticin by transfection with a plasmid containing the gene encoding for LIF, was used as a feeder layer. STO cells were regularly cultured on 100 x 20 mm Petri dishes (Corning) in a complete medium consisting of low glucose Dulbecco's Modified Eagle's Medium (DMEM), supplemented with 10% foetalbovine serum, 4 mM L-glutamine, 0.5% penicillin-streptomycin (all from Thermo Fisher Scientific), 0.1 mM β-mercaptoethanol (Sigma), 0.2 mg/ml geneticin (GIBCO). STO cells were passed every 2-3 days, using a 0.25% trypsin-EDTA solution (Thermo Fisher Scientific) and were mitotically inactivated with 0.1 µg/ml of mitomycin C (Sigma) for three hours, before using them as a feeder layer.

3.2.3   EBs formation and cardiomyocytes differentiation

mESCs were cultured for three passages on gelatin in order to eliminate the STO feeder layer, before starting differentiation. At day 0 of differentiation, mESCs were detached using 0.05% trypsin-EDTA solution (Thermo Fisher Scientific), collected and centrifuged at 500 rpm for 5 minutes. They were resuspended in complete medium without LIF (called differentiation medium), to induce the differentiation process at the concentration of 50,000 cells/ml. Applying the hanging drop method (Boheler et al., 2002), 10^3 mESCs in a 20 µl drop for a total of 80 EBs were seeded on the cover of a Petri dish and then turned up-side-down in order to allow cell aggregation and EBs formation. On day 3 of culture, EBs were moved on 0.1% agarose-coated 10 mm Petri dish (Corning), to promote their growth in suspension in 10 ml LIF-deprived ECS medium and maintained until day 5. At day 5, 6-7 EBs were transferred onto gelatin-coated 1.9 cm^2 well of a 24 multi-well plate (Corning). Alternatively, about 20 EBs were plated onto gelatin-coated 35 mm glass bottom dish (Greiner Bio-One) for video acquisition (see paragraph 3.2.5) and three dimensional whole-mount immunostaining (see paragraph 3.2.11). All EBs were cultivated until day 15 of differentiation, replacing half medium with fresh every 2-3 days.

3.2.4   ATO preparation and treatment

ATO (As_2O_3 Sigma, cat. N. 11099) was dissolved in 0.1 N NaOH in milliQ water (Merck) to a final concentration of 100 µM. From this solution, the right quantity was added to the differentiation medium to reach a final concentration of 0.1, 0.5 or 1.0 µM. Treatment with ATO was performed at the end of differentiation (day 15), on terminally differentiated cardiomyocytes, for the following 72 hours, up to day 18 of differentiation. In control samples, cardiomyocytes were cultured in the presence of NaOH 0.01 N.

3.2.5   Contraction assay

On day 5 of the differentiation process, about 20 EBs were plated onto 35 mm gelatin-coated glass bottom dish (GreinerBio-One) and on day 15 of differentiation, LIF-deprived ESCs medium was replaced with medium containing ATO at a concentration of 0.1, 0.5 or 1.0 µM or NaOH 0.01 N and

for 72h. After the treatment, the four dishes were individually transferred into the culture chamber of the Nikon BioStation IM at 37°C and with 5% CO_2. The Snagit10 software (Tech Smith corporation, Okemos, Mi, USA) was used to record videos of the beating activity. For each dose, 10 videos of about 40 seconds each were taken. Three independent experiments were performed. Each single video was successively analyzed with the Video Spot Tracker (VST) software, which can track the movement of one or more spots in an AVI video file. In each video, on the first video frame, we have systematically selected 12 markers, based on a defined orthogonal grid. The program records, frame by frame, the spatial-temporal coordinates x, y and t for each marker. The x and y coordinates are expressed in [pixel], while the t coordinate in [s]. The trajectory of the markers was calculated using an algorithm developed by a bioengineering team of our University (Fassina et al., 2011), based on the Matlab programming language (The MathWorks, Inc., Natick, Ma, USA). In order to estimate an ergotropic effect, that is the consumption of energy to originate the contraction movement, the mean kinetic energy of the beating syncytia was evaluated. The mean beat frequency was measured by counting the peaks of the displacement of the vector *s* during the contraction movement and dividing this number by the time. We have also identified and measured the maximum contraction velocities and, consequently, we have calculated the mean contractility of syncytium, based as their mean. Finally, we studied the contraction force of syncytium by the Hamiltonian mechanics, according to which the force is directly related to the kinetic energy.

3.2.6   Recovery

Following for 72h exposure at 0.1, 0.5 or 1.0 μM ATO, the medium was replaced with fresh medium without ATO, every day for 4 days to, evaluate the recovery capacity of cardiac cells. Following this period, the Snagit10 software (Tech Smith corporation, Okemos, Mi, USA) was used to record the videos of the cardiomyocytes beating activity. For each dose, 10 videos of about 40 seconds each were recorded. Three independent experiments were performed. Each single video was successively analysed with the Video Spot Tracker (VST) software (see previous paragraph 3.2.5) to evaluate the kinematics parameters of cardiomyocytes.

3.2.7   RNA extraction and reverse transcription

After 72h ATO exposure, total RNA was extracted, using the GenElute Mammalian Total RNA Kit (Sigma), according to the manufacturer's instruction, from about 250 EBs from CTR and from 0.1, 0.5 or 1.0 μM ATO-treated samples. The total RNA extracted from each sample was retro-transcribed into cDNA using the following mix of reagents, all purchased from Life Technologies (Table 1):

Table 1. PCR mix component for retro-transcription.

Reagents	Final concentration/sample
Buffer 10X	1X
$MgCl_2$ 5 mM	25 mM
dNTP mix 40 mM	16 mM
Random Hexamers	1.875 mM
Oligo d(T)$_{16}$ 50 mM	0.625 mM
MuLV reverse transcriptase 50 U/ μl	50 U
Rnase inhibitor 20 U/μl	20 U

For each sample, about 1 μg of RNA was retrotranscribed, as follows: 25°C for 10 min, 42°C for 15 min, followed by 99°C for 5 min. At the end of the reaction, samples were maintained at 4°C.

3.2.8   Quantitative Real-Time PCR

The cDNA, obtained from reverse-transcription reactions, were diluted adding 80 μl of bi-distilled water. One twentieth of the resulting cDNA was amplified in duplicate by Quantitative Real-Time PCR, using the following PCR mixture (Table 2):

Table 2. PCR mix component for the amplification.

Reagents	Final concentration/sample
Mesa Green qPCR Master Mix Plus SYBR (Eurogentech) 2X	1X
Forward Primer (Diatech) 10 µM	200 nM
Reverse Primer (Diatech) 10 µM	200 nM

For the amplification reaction, a Rotorgene 6000 (Corbett Life Science) was used and the amplification program was set as follows: 95°C for 5 min, followed by 45 cycles at 95°C for 10 sec, 60°C for 15 sec, 72°C for 20 sec. All the primers used for PCR amplification of the target genes were designed using Primer 3 software (Table 3). The β_2-microglobulin gene expression was used for sample normalization (Rebuzzini et al., 2013). The comparative analysis was performed using the Rotorgene 6000 Series Software 1.7. Three independent experiments were performed.

Table 3: Reverse and forward primer sequences used for qRT-PCR.

Gene	Forward Primers	Reverse Primers
Myh6	5' TCACTGCGGAAACTGAAAACG 3'	5' ATGGCCATGTCCTCGATCTTG 3'
Actn2	5' AACCTGGCCATGGAAATAGCA 3'	5' TTCATCGGGTTTGGGAGTGTT 3'
Tnnc1	5' CAGCAAAGGGAAGTCTGAGG 3'	5' TGCAGCATCATCTTCAGCTC 3'
Tnnt2	5' GAAGTTCGACCTGCAGGAAA 3'	5' TTCCCACGAGTTTTGGAGAC 3'
Tnni3	5' GACTTATGCCGACAGCTTCAC 3'	5' GGTCAGATCTGCAATCTCAGTG 3'
Cx40	5' CATACCTCGGAGTGCTGGTG 3'	5' GGCCAAGGACCAAGGATACC 3'
Cx43	5' CTCCTCCTGGGTACAAGCTG 3'	5' AATTCGCCCAGTTTTGCTCG 3'
Cx45	5' TCATCCTGGTTGCAACTCCC 3'	5' CTGCCTTCTTGTCTGCCTCA 3'
β2m	5' GAATTCACCCCCACTGAGACT 3'	5' TGCTTGATCACATGTCTCGAT 3'

3.2.9   Protein extraction

After 72h ATO exposure, EBs were washed two times with PBS 1X, detached and collected in 15 ml tube to be centrifuged at 500 rpm for 5 minutes. The supernatant was discarded, the pellet was resuspended in 1 ml of cold PBS 1X and transferred in 1.5 ml tube (Eppendorf), to be centrifuge at 1300 rpm for 5 minutes. The pellets were frozen in liquid nitrogen and stored at -80°C until proteins extraction. The pellets, still frozen, were lysed in 500 µl of RIPA (Radio Immuno Precipitation Assay) buffer composed of: 50 mM Tris buffer pH 8.0, 150 mM sodium chloride, 1% NP-40, 0.5% sodium deoxycholate (all from SIGMA), 0.1% sodium dodecyl sulphate (FlukaBioChemika) and supplemented with 0.1%phenylmethylsulfonyl fluoride (SIGMA). After 5 minutes, the samples were centrifuged at 1300 rpm at 4°C, the concentration of the proteins was assayed using the Bradford method (Bradford, 1976) with a spectrophotometer (Bio-Rad). The samples were aliquoted and stored at -80°C until usage.

3.2.10 Western Blotting

Five µg of proteins were mixed with Laemmli buffer 1X (2% sodium dodecyl sulphate, 5% β-mercaptoethanol, 10% glycerol, 0.002% bromophenol blue, 60 mM Tris HCl), denatured for 5minutes at 95°C and separated by SDS-PAGE using gels, ranging from 8% to 12% polyacrylamide, in a running buffer composed of 3% Tris base, 14.4% glycine and 1% SDS, for about 5 h. Then, proteins were transfer in the buffer composed of 20% methanol, 0.3% glycine and 0.6% Tris Base onto a nitrocellulose membrane (Hybond-ECL, Amersham Biosciences), at 40V

overnight at 4 °C. After the transfer, the membrane was quickly stained with a non-permanent staining based on 2% Ponceau red and then decolorized with repeat washing with TBS-T (2 mM TRIS-HCl, 13.6 mM NaCl and 0.1% Tween20, pH 7.6) in gently rotation. To minimize non-specific bond, membranes were incubated with specific blocks, before adding the primary antibody solution (Table 4).

Table 4: Primary antibodies and block solutions used for Western Blotting analysis.

Primary Antibody	Block composition/ Incubation time	Antibody dilution/ Incubation time	Source and catalogue number
Mouse anti-heavy chain cardiac myosin	3% BSA in TBS-T/ 30 min room temperature	1:1000 in TBS-T/ 2h at 37°C	Abcam Ab15
Mouse anti-sarcomeric α-actinin	3% BSA in TBS-T/ 30 min room temperature	1:1500 in TBS-T/ 2h at 37°C	SIGMA-ALDRICH A7811
Mouse Anti-sarcomeric actin (Alpha Sr-1)	5% BSA in TBS-T/ 1h room temperature	1:200 in 5%BSA in TBS-T Overnight 4°C	Santa Cruz Biotechnology Sc-58671
Mouse Anti-Troponin T cardiac isoform Ab-1, clone 13-11	3% BSA in TBS-T/ 30 min room temperature	1:1000 in TBS-T/ 2h at 37°C	Thermo Scientific MS-295-P1
Mouse Anti-tropomyosin (F-6)	5% BSA in TBS-T/ Overnight 4°C	1:250 in 5% BSA in TBS-T/ Overnight 4°C	Santa Cruz Biothecnology Sc-74480
Rabbit anti-Connexin 43	5% BSA in TBS-T/ 0.1%Tween-20 1h room temperature	1:1000 in 5% BSA, 0.1% Tween-20 in TBS-T/ Overnight 4°C	Cell Signalling 3512
Rabbit Anti-GAPDH	2% milk in PBS1X/ 30 min room temperature	1:2000 in 1% milk in TBS-T/ 2h at 37°C	GeneTex GTX100118

Membranes were washed three times for 5 minutes with TBS-T before incubating them for 1h at 37°C with the specific secondary antibody (Table 5).

Table 5. Secondary antibodies used for Western Blotting analysis.

Secondary Antibody	Dilution	Source and catalogue number
Goat anti-mouse HRP conjugate	1:20000 in 1% milk in PBS 1X	Molecular Probes F21453
Goat anti-rabbit HRP conjugated	1:25000 in 2%BSA in TBS-T	Sigma A9169

After three washing steps of 5 minutes each, Westar ηC (according to manufacturer's instructions; Cod. XLS100L, CYAGEN) was used for chemiluminescent detection of proteins through ChemiDoc XRS system

(Bio-Rad). Images were acquired with Quantity One software (Bio-Rad) and the quantification of the bands intensities was performed with Image J software. In order to identify the presence of different proteins on the same samples, the membranes were incubated with a stripping-buffer, containing 2% SDS, 62.5 mM Tris HCl pH 6.8 and 0.8% β-mercaptoethanol (SIGMA), for 45 minutes at 50°C in agitation. Then, the membranes were washed in tap water 5 minutes in agitation and then other three times using TBS-T for 10 minutes. At the end of the stripped procedure, the membranes were reused for the detection, as previously described.

3.2.11 Three-dimensional (3D) whole-mount immunofluorescence

A whole-mount immunofluorescence approach was refined by adapting, on our 3D samples, the whole-mount fluorescent immunocytochemistry protocol developed on chick and mouse embryo by Graham and Vermeron (King College London, UK; University of Cambridge, UK; https://www.abcam.com/protocols/whole-mount-staining-protocol). About 15 EBs were plated onto 22 mm gelatin-coated Glass Bottom Dish and cultivated up to 15 days. Then they were exposed for 72h to NaOH and 0.1, 0.5 or 1.0 µM. On day 18, the CTR and ATO-treated cells were washed twice with 1X PBS, fixed in 4% cold paraformaldehyde/1X PBS for 24h and kept at 4°C until usage. The protocol for the 3D whole-mount immunostaining takes 4 days and the samples were processed according to the following steps:

Day 1:

1. Wash with PBS 1X/1% Triton X-100 (SIGMA) 3 times for 30 min

2. Incubate for 1h in block solution consisting of PBS 1X/1% Triton X-100/10% Foetal Bovine Serum (FBS, Life Technologies)/0,2% sodium azide (Carlo Erba)

3. Wash two times with PBS-MT containing PBS 1X/1% milk (FlukaBioChemika)/0.4% Triton X-100.

Cells were incubated for 24h in agitation at 4°C with the primary antibodies:

Table 6. Primary antibodies used for whole-mount immunofluorescence.

Primary Antibody	Antibody dilution	Source and catalogue number
Mouse anti-sarcomeric α-actinin	1:800 in PBS-MT	SIGMA-ALDRICH A7811
Mouse Anti-Troponin T cardiac isoform Ab-1, clone 13-11	1:200 in PBS-MT	Thermo Scientific MS-295-P1
Rabbit anti-Connexin 43	1:150 in PBS-MT	Cell Signalling 3512

Day 2 and 3:

1. Wash with PBS 1X/1% Triton X-100/10% FBS, 3 times for 45 min.

2. Wash with PBS 1X/1% Triton X-100, 3 times for 10 min.

3. Wash with PBS 1X/1% Triton X-100/10% FBS/0,2% sodium azide, 3 times for 45 min.

4. Wash with PBS 1X/1%Triton X-100, 3 times for 10 min.

Incubate for 40h, on a gentle rotation device, at 4°C with secondary antibodies (Table 7):

Table 7. Secondary antibodies used for whole-mount immunofluorescence.

Secondary Antibody	Antibody dilution	Source and catalogue number
Alexa Flour 488 conjugated anti-mouse	1: 500 PBS 1X/1% Triton X-100/10% FBS/0.2% sodium azide	Molecular Probes F21453
Anti-rabbit TRITC	1: 150 PBS 1X/1% Triton X-100/10% FBS/0.2% sodium azide	Sigma Aldrich A9169

Day 4:

1. Wash in PBS 1X/1% Triton X-100, 3 times for 10 min.

2. Stain the nuclei with 0,2 µg/ml DAPI for 2h.

3. Wash with PBS 1X, 3 times for 30 min.

4. Mount with VECTASHIELD Mountain Medium (Vector Labs)

Antibody immunofluorescence localization was detected with a Leica TCS SP8 confocal microscope, equipped with a white light laser and a 405 nm laser. The images were acquired using 40X and 63X plus 1.5 digital zoom objectives. Stacks were obtained with axial distances of 0.5 μm. Three independent experiments were performed.

3.2.12 Analysis of the volume occupied by the cardiac syncytia

Given the complexity of the 3D cellular structure of the EBs, the 3D confocal images were analyzed using a stereology approach, that is based on the 3D interpretation of 2 dimensional (2D) planar sections of a tissue. The images were obtained from at least 20 coring for each single experiment, setting the limit of acquisition on the nuclei staining (from the top to the bottom of the entire coring). The software Image*J* (https://imagej.nih.gov/ij/) was used to analyze the images acquired with a 40X oil immersion objective. An Image*J* tool, called SUM, able to sum the pixel intensities of all slices along the Z direction, was applied to each stack of a coring. On the obtained image, the Integrated Density (IntDen), that is the integral of the fluorescence intensity on the area, was calculated (this integral is useful to analyze an image characterized by a non-homogeneous spatial distribution of fluorescence intensity). Then, using an area in which cardiomyocytes were absent, the mean background value was evaluated with the same approach. Finally, the Corrected Total Fluorescence (CTF) was determined applying the following formula:

$$CTF = (IntDen\ of\ EB\ coring\ SUM) - n \times mean\ (IntDen\ background)$$

where n is the number of slices specific for each single coring and IntDen is the integral of the fluorescence intensity on the selected area.
This approach allowed to derive quantitative information from 2D measurements applicable to the 3D contest.

### 3.2.13 SarcOmere Texture Analysis (SOTA)

The algorithm developed by Sutcliffe and colleagues (2018) was employed to determine the texture quality of the sarcomeres. Images of cardiac syncytia were acquired with 63X oil immersion objective plus 1.5 digital zoom with a Leica TCS SP8 confocal microscope. Specific "regions

of interest" (ROI) were designed on specific portions of cardiac sarcomeres of CTR or ATO-exposed samples and analyzed with SOTA algorithm. Using the Matlab software (The MathWorks, Inc.), Fourier, Gabor and Organization score, together with sarcomere length and width, were measured.

3.3 Results

3.3.1 Kinematics and dynamics properties

The kinematics and dynamics features of cardiac syncytia of CTR, 0.1, 0.5 or 1.0 µM ATO-exposed samples for 72h were determined, analyzing the recorded AVI videos. Specifically, chronotropic (beat frequency [Hz]), inotropic (contraction force [pixel/s2] and contractility [pixel/s]) and ergotropic (consumption of ATP for kinetic energy [pixel2/s2]) features were mathematically calculated from the movements of the beating syncytia, using an algorithm developed by Fassina and collaborators (Fassina et al., 2011). The results are summarised in Figure 8.
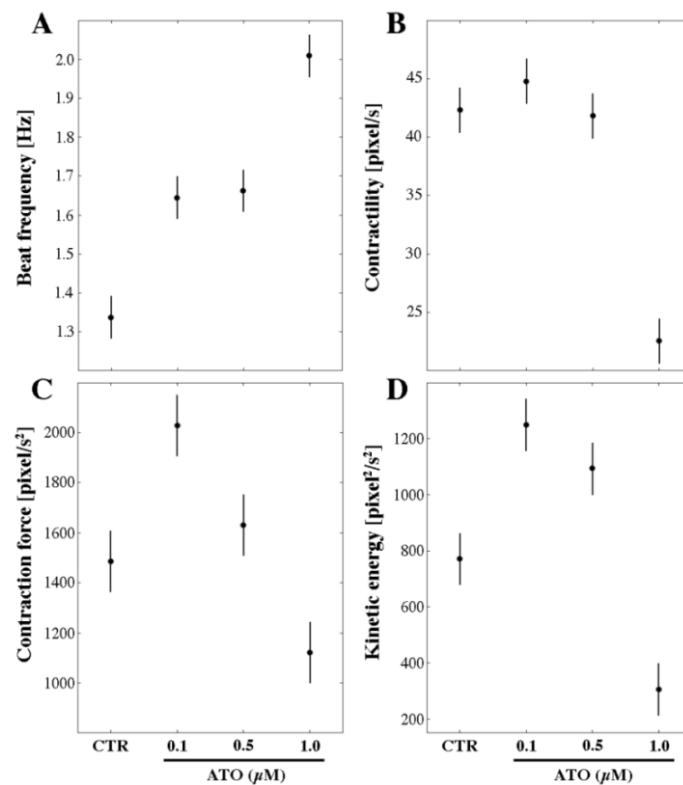
Figure 8. Contractile properties of cardiac syncytia of CTR and 0.1, 0.5 or 1.0 µM ATO-exposed samples for 72 hours. (A) Beat frequency [Hz]; (B) contraction force [pixel/s^2]; (C) contractility [pixel/s]; (D) kinetic energy [pixel^2/s^2]. The vertical bars represent 95% confidence intervals for the difference between averages according to the "Least Significant Difference" statistical test.

The analysis showed a significant increase ($p<0.05$) of the beat frequency at all ATO doses, whereas the contractility resulted significantly diminished ($p<0.05$) only for cardiomyocytes exposed to 1 µM ATO. Contraction force was unchanged ($p>0.05$) at 0.5 µM ATO, while it was higher ($p<0.05$) at 0.1 µM ATO and lower ($p<0.05$) at 1.0 µM ATO. Cardiomyocyte kinetic energy was significant altered ($p<0.05$) at all the three ATO doses. Fold-changes, calculated setting CTR values at 1, are reported in Table 8.

Table 8. Fold-changes of the kinematic parameters of cardiomyocytes exposed to ATO, relative to CTR set at 1. *$p<0.05$.

Parameters	*0.1 µM*	*0.5 µM*	*1.0 µM*
Beat frequency	1.2*	1.3*	1.5*
Contractility	1.07	0.99	0.5*
Contraction force	1.3*	1.06	0.7*
Kinetic energy	1.6*	1.05*	0.4*

To understand whether the observed contractility alterations might reflect changes in cardiomyocyte organisation, sarcomere structure and gap junction expression and localization were examined.

3.3.2 Whole-mount 3D immunolocalization of α-actinin and troponin sarcomeric proteins

To investigate the organization of the sarcomere, a whole-mount immunofluorescence technique was applied. The classical immunofluorescence approach requires the isolation of single cells, obtained using an enzymatic/mechanic disaggregation protocol that destroys the entire structure of the EBs (Rebuzzini et al., 2013; 2015). This method, although still the most commonly used, it is harsh and the possibility that it might contribute to differentially alter the sarcomeric apparatus in CTR and treated samples cannot be excluded. Thus, to avoid this problem, the analysis of cardiac syncytia was done by adapting a whole-mount protocol, previously developed by Graham (Kings College, London) and Vermor (University of

Cambridge) for the characterization of chick and mouse embryos. This protocol allows to preserve the 3D structure of the entire EBs. At day 18 of differentiation, CTR and 0.1, 0.5 or 1.0 µM ATO-treated EBs were used to immunolocalise α-actinin and troponin T, two fundamental proteins of the sarcomere contractile apparatus. After immunostaining, confocal optical sections from the top to the bottom of the EBs thickness were acquired to localise the fluorescent signals corresponding to the two proteins. On CTR cardiomyocytes, both α-actinin and troponin T displayed the sarcomere-specific striated pattern (Figure 9A and 10A). To the contrary, cardiomyocytes cultured in the presence of ATO showed both regularly organized sarcomere striated pattern, and alteration of the myofibrillar components with absence of the striated configuration and disorganized-disoriented sarcomeres (Figure 9B and 10B).
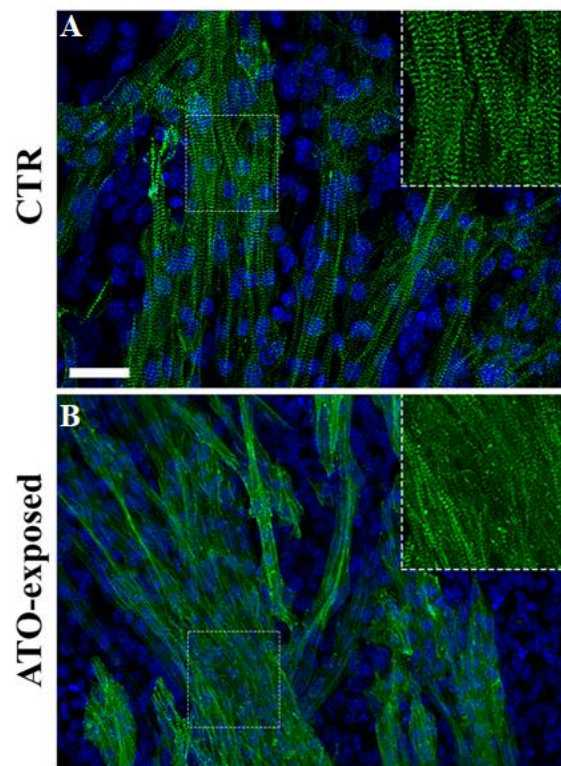
Figure 9. Whole mount immunofluorescence localization of cardiac α-actinin (green) protein in (A) CTR cardiomyocytes with correct sarcomere striated pattern (magnification in the inset) or (B) 1.0 µM ATO-treated cardiomyocytes presenting regions characterized by disorganized sarcomeric structures (magnification in the inset). Nuclei are stained with DAPI (blue). Bar: 20 µm.
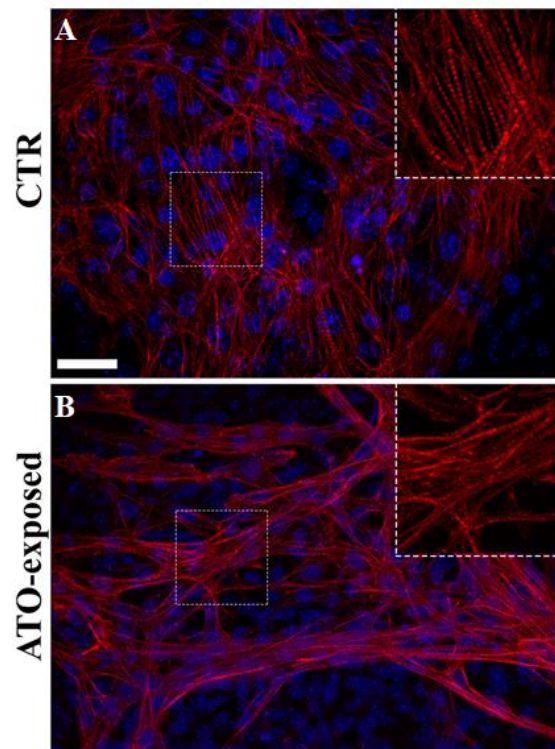
Figure 10. Whole mount Immunofluorescence localization of Troponin T (red) protein in (A) CTR cardiomyocytes with correct sarcomere striated pattern (magnification in the inset) or (B) 1.0 µM ATO-treated cardiomyocytes presenting regions characterized by disorganized sarcomeric structures (magnification in the inset). Nuclei are stained with DAPI (blue). Bar: 20 µm.

We have not been able to quantify the frequency of the disorganized compared to the organized regions within the EBs, since no appropriate bioinformatics tools, able to extract this information from the high complexity of a 3D structure, are currently available. In the future, we are planning a collaboration with bioinformatics engineers to address this complex issue. Instead, we used a specifically developed algorithm to compare the sarcomere texture of CTR and treated cardiomyocytes, as described in the following paragraph.

### 3.3.3 Analysis of the Sarcomere Texture Analysis

To characterize the texture quality of the sarcomeres in ATO-exposed samples compared to CTR, the algorithm published by Sutcliffe and collaborator (Sutcliffe et al., 2018) was applied. This algorithm, named

SarcOmere Texture Analysis (SOTA) and developed for the analysis of 2D isolated cardiac cell, is a pixel-based image analysis for assessing sarcomere structure. The SOTA algorithm automatically segments cardiomyocytes derived from immunofluorescence images analyzing their sarcomere morphology and structure. Several parameters that describe the regularity of the sarcomere texture can be obtained. Among them, three parameters were chosen:

- the Haralick correlation (also named Organization score);
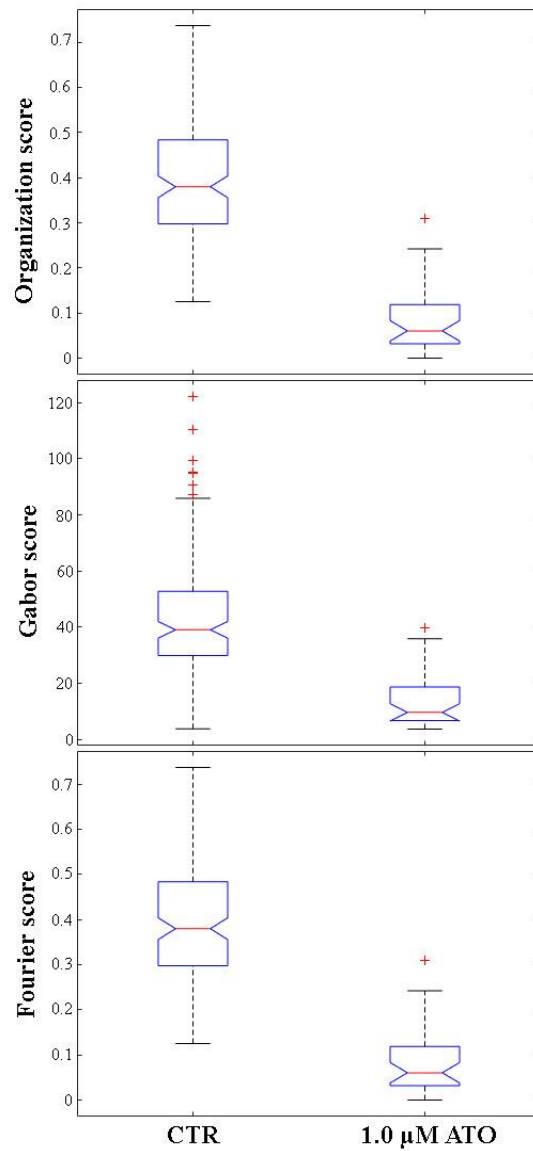
- the Gabor score;

- the Fourier score.

These three parameters describe the structural characteristics of the sarcomeres marked with fluorescence α-actinin signals, providing a measurable score of the level of their organization (for the mathematics, see Sufcliffe et al., 2018). To obtain reliable results on the 3D samples, we choose α-actinin positive areas, defined as "region of interest" (ROI) (Figure 11), within single confocal Z-slices; the ROIs were analyzed through the SOTA algorithm. The sarcomere organization values, obtained for CTR samples, agreed with those obtained from the analysis of the sarcomeres of 2D cardiomyocytes reported in the original paper (Sufcliffe et al., 2018), indicating that the procedure adopted for the analysis of the sarcomeres of cardiomyocytes within the 3D EBs structure was reliable. After the validation of the procedure, two different comparisons were performed:

1. ROIs of organized sarcomeres of CTR samples (Figure 11A, white ROIs 1 and 2) were compared to ROIs of sarcomeres without striated configuration or with disoriented sarcomeres of 1.0 µM ATO-exposed sample (Figure 11 B, red ROIs 4 and 5);

2. ROIs of organized sarcomeres of CTR samples (Figure 11A, white ROIs 1 and 2) were compared to ROIs of organized sarcomeres of 1.0 µM ATO-exposed samples (Figure 11B, white ROI 3).
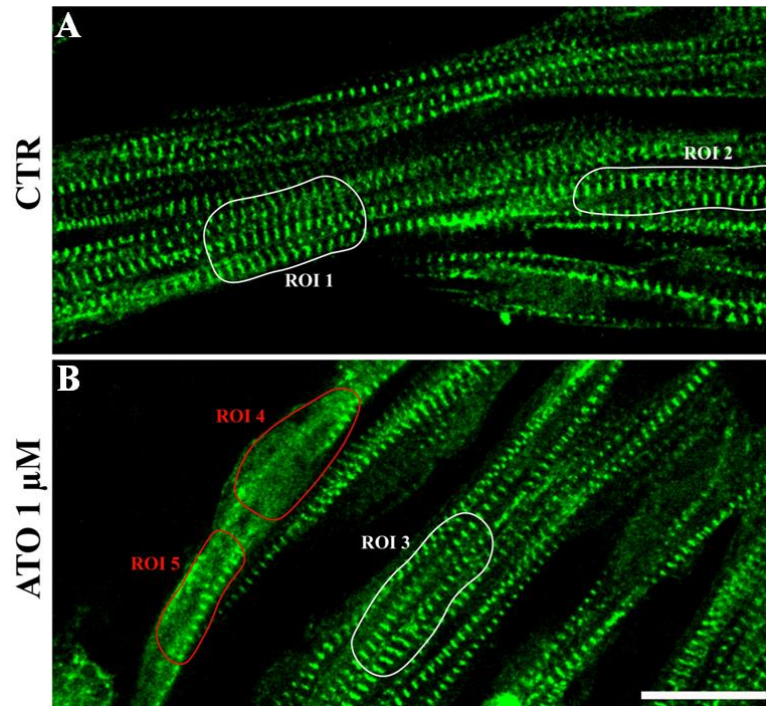
Figure 11. Examples of regions of interest (ROI) in CTR (A) and ATO-exposed samples (B). In (B), ROI 3 shows regular striated signals, whereas ROIs 4 and 5 show altered α-actinin signals. Bar, 15 μm.

The results obtained from comparison 1) were summarized in Figure 12. In 1.0 µM ATO-exposed samples all three parameters were significantly ($p<0.001$), different compared to CTR samples, confirming the irregular and disorganized α-actinin pattern observed when compared to the pattern observed in CTR samples.

Figure 12. The Organization, Gabor and Fourier scores mathematically describe the organization quality of repeated patterns. The graphs illustrate the comparison between organized ROIs in CTR and ROIs in the ATO-exposed sample. The red lines in the graph are the median, whereas the blue lines below and above the red lines are the 25th percentile and 75th percentile, respectively. The red marks are out-layer values.

In the second comparison, the three scores were not significantly different ($p>0.05$) in the comparison between CTR and 1.0 µM ATO-exposed samples (Figure 13), suggesting well-organized sarcomeric structures (Sutcliffe et al., 2018).
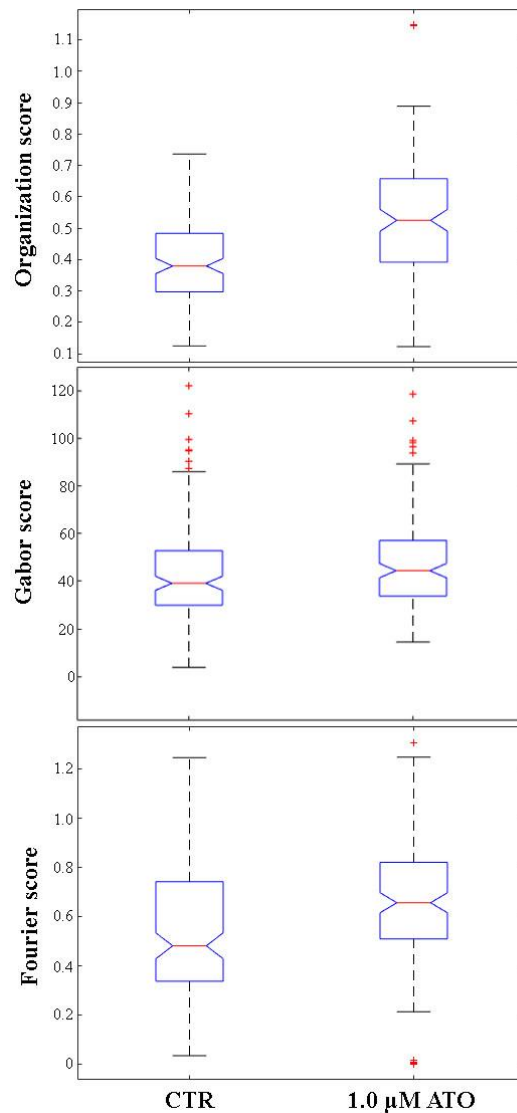
Figure 13. Organization, Gabor and Fourier scores were compared considering only regions characterized by regular striated sarcomere patterns in both CTR and 1.0 µM ATO-exposed cardiomyocytes. The red lines in the graph are the median, whereas the blue lines below and above the red lines are the 25th percentile and 75th percentile, respectively. The red marks are the out-layer values.

SOTA algorithm, on the same ROIs with organized striated pattern, can also provide information on sarcomere organization, such as its length (the distance between two Z bands) and width (Z bands width) (Figure 14).
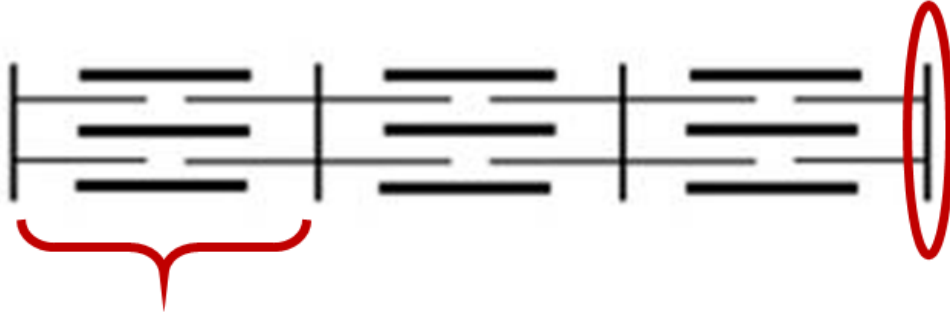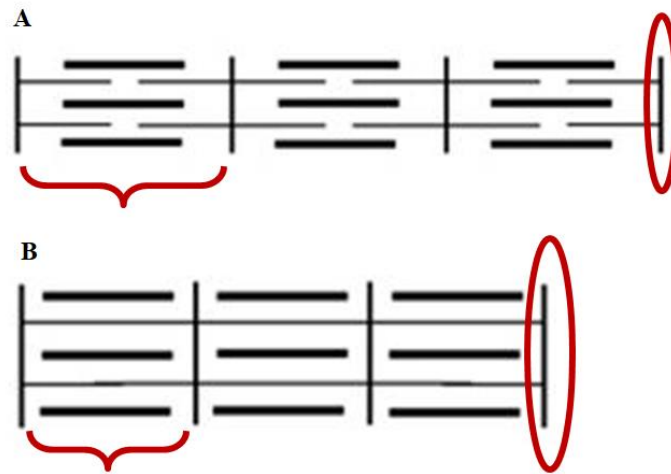

Figure 14. Schematic representation of sarcomeres in which the curly bracket indicates the length and the circle indicates the width.

Results are summarized in Figure 15. In ATO-exposed samples, sarcomere length is significantly shorter (*i.e* the distance between two Z-bands is decreased) ($p<0.001$), whereas sarcomere width appears to be significantly ($p<0.001$) higher (Figure 15), indicating that the portion where thin and thick filaments overlap is wider compared to CTR samples (Figure 16).
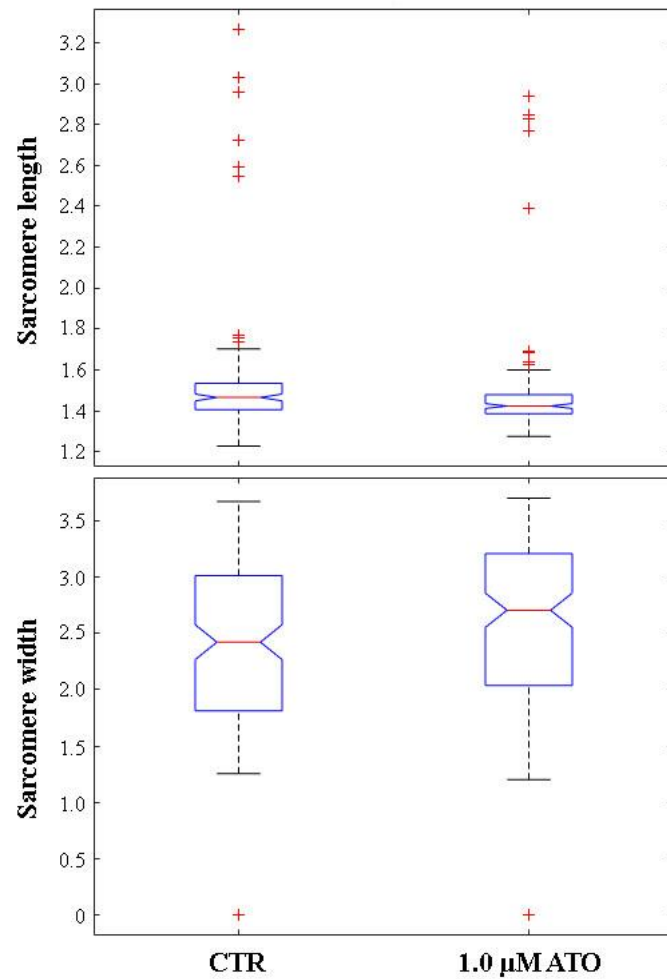
Figure 15. Length and width of sarcomeres with organized striated pattern of both CTR and 1.0 µM ATO-exposed samples. The red lines in the graph are the median, whereas the blue lines below and above the red lines are the 25th percentile and 75th percentile, respectively. The red marks are the out-layer values.

49

Figure 16. Schematic representation of sarcomere organization in CTR (A) and ATO-exposed (B) cardiomyocytes in which the curly bracket indicates sarcomere length and the circle indicates the width.

Then, we asked whether the alteration of sarcomere organization was correlated with alteration of sarcomere protein expression.

3.3.4 Expression profiles of sarcomeric genes and proteins

Since a skewed ratio of sarcomeric protein components is known to correlate with the disruption of sarcomere organization (Neri et al., 2011; Rebuzzini et al., 2015), the expression profiles of α-actinin (*actn2*), myosin (*Myh6)* and Troponin T (*tnnc1*, *tnnt2* and t*nnt3* subunits)genes (Figure17) and of myosin, α-actinin, troponin T, tropomyosin and sarcomeric α-actin proteins (Figure 18) were analysed. No differences (*p*>0.05) in the expression profiles of the genes studied were detected (Figure 17). Myh6 gene presents an high standard deviation that can mask a possible significativity. To this purpose we have planned to increase the number of biological replicates.
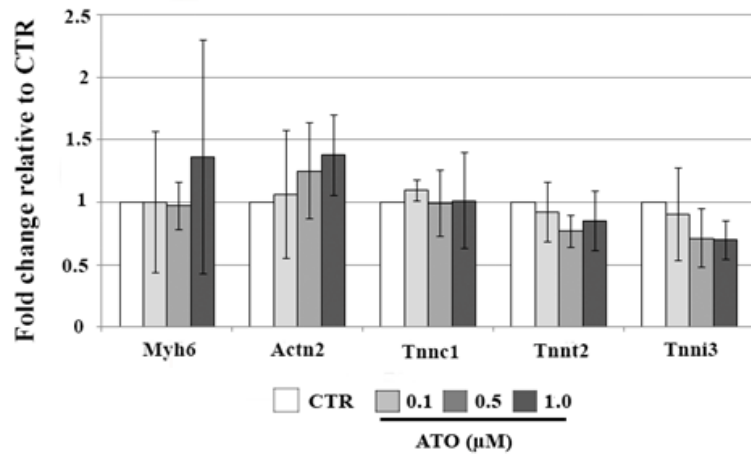
Figure 17. Expression profile of genes of sarcomeric components. No significative (*p*>0.05) differences were recorded in ATO-exposed cardiomyocytes when compared to CTR.

When compared to CTR, the expression of myosin, α-actinin and troponin proteins was not altered, whereas, the expression of sarcomeric α-actin was significantly down-regulated (*p*<0.05 and *p*<0.001)in treated samples at all ATO doses (Figure 18A); specifically, 0.47-, 0.53-, 0.49-fold reduction was observed in 0.1, 0.5 and 1.0 µM ATO-exposed syncytia, respectively (Figure 18B). Tropomyosin protein resulted significantly up-regulated (2.3-fold) only in 1.0 µM ATO-exposed EBs, when compared to CTR.
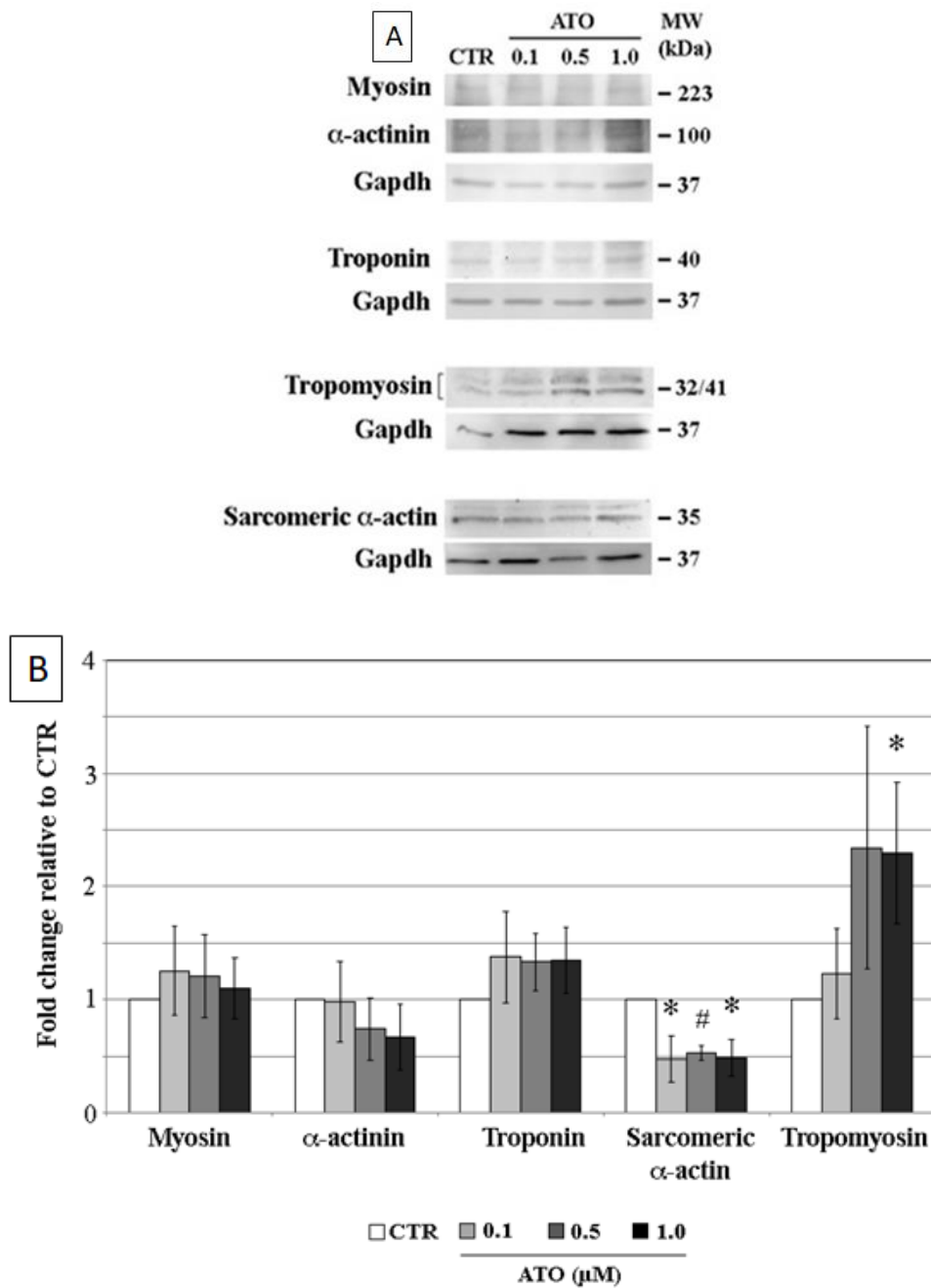
Figure 18. (A) Western blotting analysis of myosin, α-actinin, troponin, tropomyosin and α-actin sarcomeric proteins on terminally differentiated cardiac syncytia, after exposure to 0.1, 0.5 and 1.0 μM ATO; (B) Quantification of

sarcomeric proteins expression, relative to CTR, set at 1*p<0.05; #p<0.001*. Three independent experiments were performed.

The ratio of troponin T, myosin, α-actinin, tropomyosin and α-actin was 1:1.5:3:1:7, respectively, in CTR samples, ratio consistent with that of foetal cardiomyocytes (Potter, 1974; Rebuzzini et al., 2015) (Table 9). In cardiac syncytia exposed to ATO, irregular stoichiometry of sarcomeric proteins was observed with a skewed ratio for Tropomyosin at 1.0 µM and α-actin at all the three doses (Table 9).

**Table 9.** Ratio among the five sarcomeric proteins studied (Troponin set at 1) of foetal, control and exposed cardiomyocytes.

Sample	Troponin	α-actinin	Myosin	Tropomyosin	α-actin
Foetal cardiomyocytes	1.0	2.9	1.5	1.0	7.0
CTR	1.0	2.9	1.5	1.0	7.0
0.1 µM	1.0	2.9	1.5	1.0	3.3
0.5 µM	1.0	2.9	1.5	1.0	3.6
1.0 µM	1.0	2.9	1.5	2.3	3.3

To understand whether the alteration of the sarcomeric proteins induced by ATO exposure may determine a change in the shape of cardiomyocytes, the volume occupied by cardiac syncytia in the 3D structure of the EBs was evaluated.

3.3.5 Cardiac syncytia volume within the 3D EBs

To evaluate the volume occupied by cardiac syncytia in the 3D structure of the EBs, a stereology method was applied quantifying the α-actinin fluorescence intensity of a 2D image, generated through the overlap of all the planar focal planes present in a coring (for details see "Material and Methods"). Figure 19 shows a 3D view of the localization of the nuclei of all the cell types present in a specific coring (Figure 19A and C) and the 3D distribution of the cardiac component (Figure 19B and D).
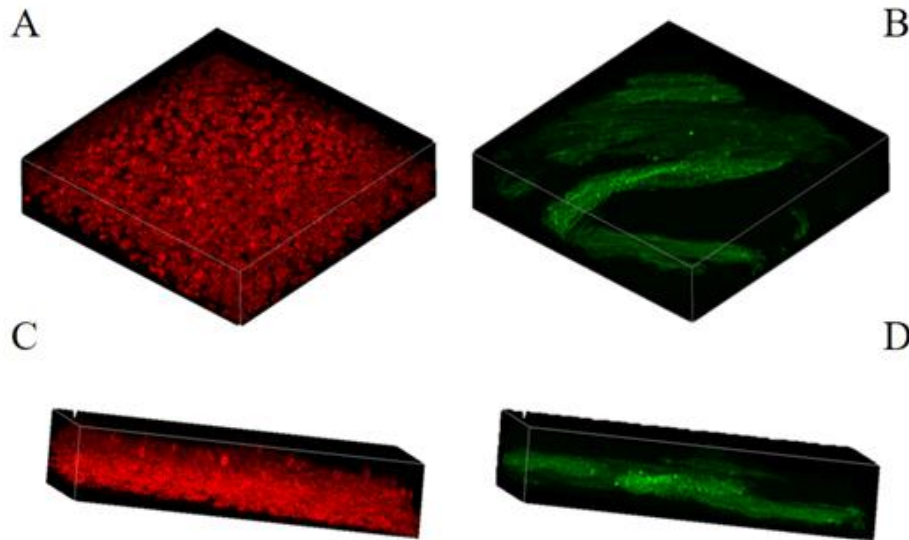
Figure 19. 3D representation of the distribution of nuclei (red) of the different cell types forming an EB and the distribution of cardiomyocytes marked with α-actinin antibodies. A) frontal, C) lateral view of nuclei irrespectively of the cell type; B) frontal, D) lateral view of cardiomyocytes.

The results obtained are summarized in Figure 20. Cardiac cells exposed to 0.1 µM ATO had a Corrected Total Fluorescence (CTF) value significantly decreased (0.3 fold; p=0.0205) compared to CTR, suggesting a smaller volume occupied by cardiomyocytes within the EBs. On the contrary, in 1.0 µM ATO-exposed, the CTF value is significantly higher (1.3 fold*; p*=0.0129) compared to control samples, suggesting that cardiomyocytes occupy bigger volume within the EBS. The CTF value of samples exposed to 0.5 µM ATO remained unaltered (p=0,1352), compared to that of the CTR.
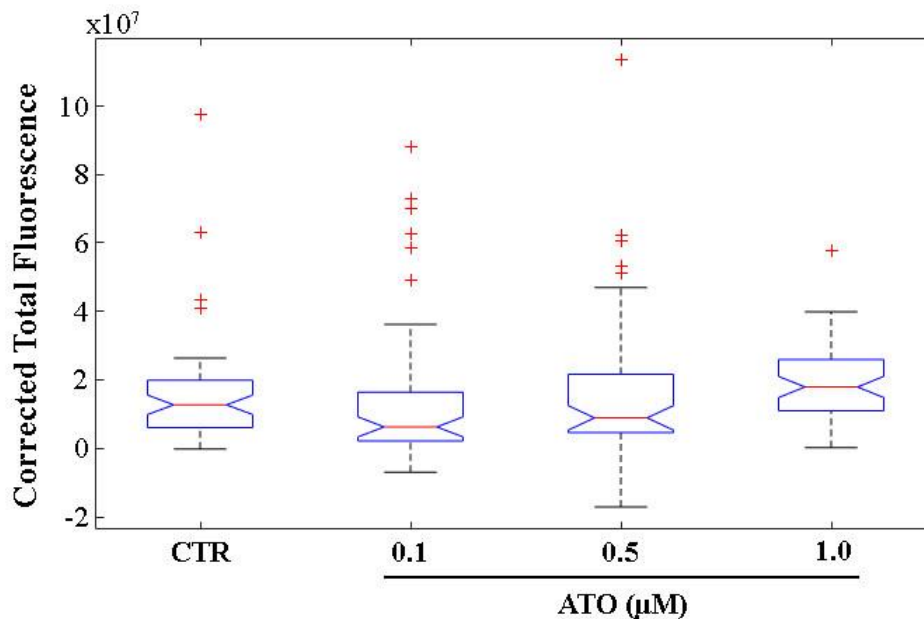
Figure 20. Corrected Total Fluorescence values of areas randomly sampled from CTR and ATO exposed EBs. About 15 EBs for each sample were analyzed. The red lines in the graph are the median, whereas the blue lines below and above the red lines are the 25th percentile and 75th percentile, respectively. The red cross above the graphs are out-layer values.

Next, to understand whether changes in the kinematics and dynamics properties of exposed samples might correlate with alterations of the gap junctions, that regulate the electrical potential from cell-to-cell to trigger the contractile signal, we determined gene expression profiles of Connexins *Cx40, Cx43, Cx45* and protein expression profiles and the localization of Cx43.

3.3.6 Gene and protein expression profiles of Cx40, Cx43, Cx45

In the presence of 0.1 μM ATO, gene transcript quantification of Cx40 did not show significant ($p>0.01$) differences; however, the high standard deviation suggests to increase the number of biological replicates to confirm or refute the results.Whereas the expression of Cx43 and Cx45 was significantly higher ($p<0.05$) compared to CTR (1.7- and 1.8-fold, respectively) (Figure 21). Conversely, cardiomyocytes treated with 0.5 μM

ATO and 1.0 μM ATO showed significant induction of the number of transcripts of all genes analysed ($p<0.001$; $p<0.05$) (Figure 21). Specifically, in cardiomyocytes exposed to 0.5 μM ATO, Cx40, Cx43 and Cx45 transcripts were 1.6-, 2.3- and 1.9-fold up-regulated respectively, compared to CTR cardiac cells. Similarly, in cardiomyocytes treated with the highest ATO dose Cx40, Cx43 and Cx45 transcripts showed 1.6-, 1.8 and 2.2-fold change increase, respectively (Figure 21).
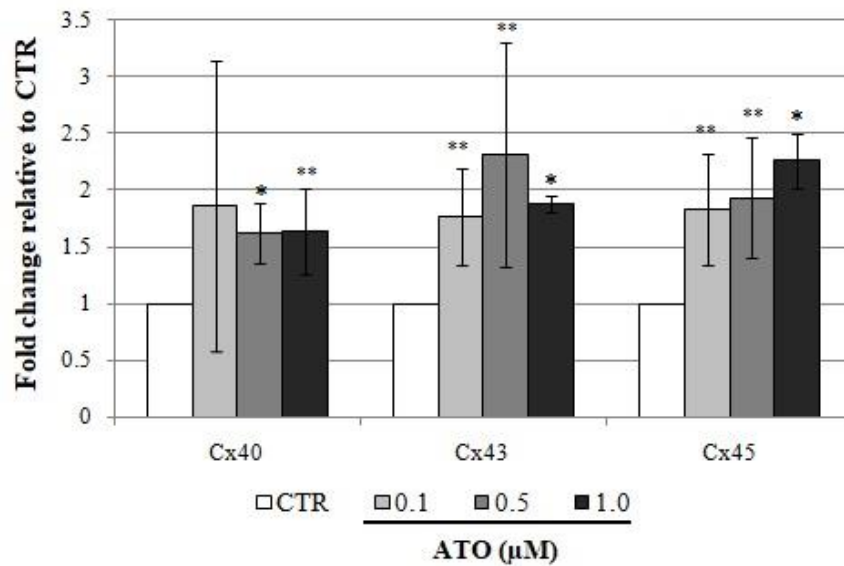
Figure 21. Expression profile of genes that mark the major connexin isotypes in CTR and ATO-exposed cardiomyocytes. Values are expressed as mean ± standard deviation. Three independent experiments were performed. *$p<0.001$, **$p<0.05$.

Then, the expression of Cx43, the most abundant connexin of the heart, was determined by Western blotting. When compared to CTR, cardiomyocytes exposed to all the three doses of ATO displayed a substantial increase ($p<0.001$) of Cx43 protein expression (1.8-, 1.7- and 1.9-fold) (Figure 22).
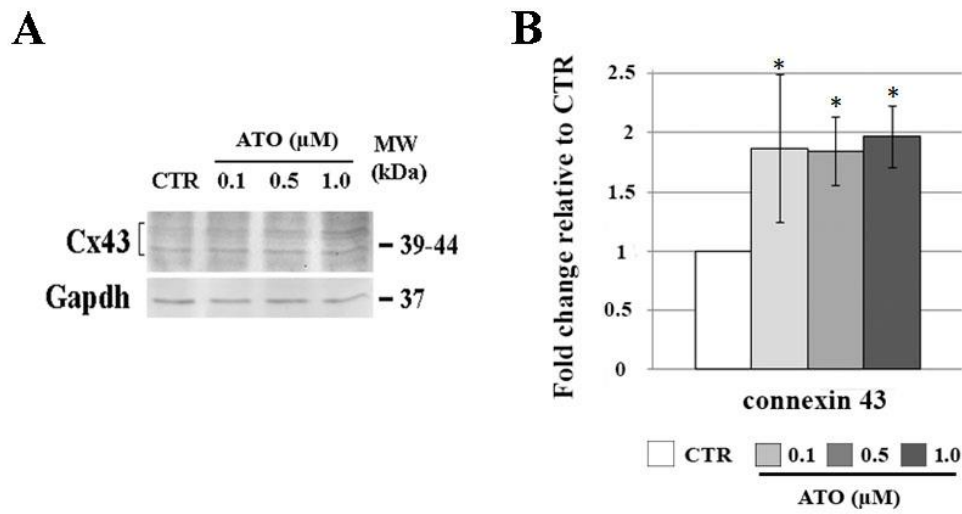
Figure 22. (A) Western blotting analysis of Cx43 protein obtained from CTR or ATO-exposed cardiomyocytes. (B) Quantification of Cx43 expression, relative to CTR, set at 1. *p<0.001.*

3.3.7 3D immunofluorescence localization of Connexin 43

Whole-mount immunofluorescence using Cx43 and α-actinin antibodies were used for the identification of gap-junctions and cardiac cells, respectively. Compared to CTR, cardiomyocytes exposed to the three ATO doses showed bigger, irregularly, distributed foci (Figure 23).
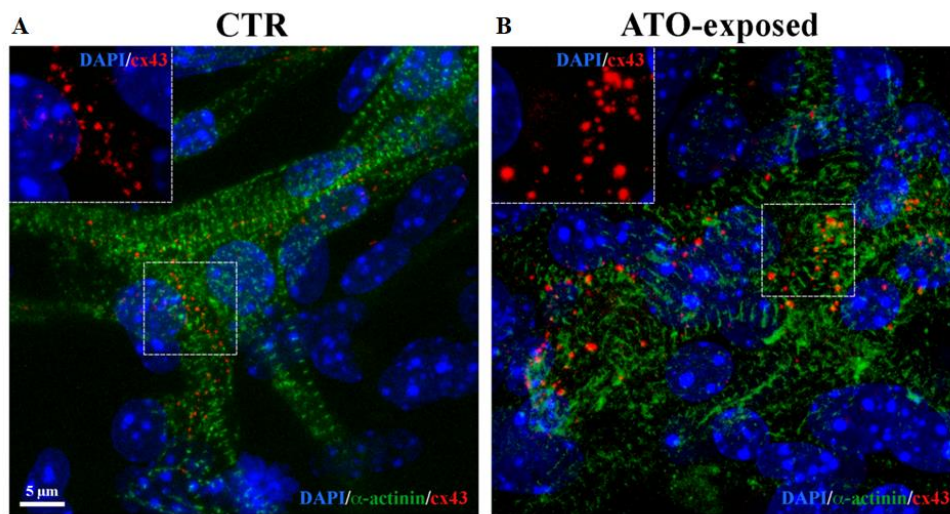
Figure 23. Whole mount Immunofluorescence localization of cardiac α-actinin (green) and Connexin 43 (red) proteins in (A) CTR cardiomyocytes (magnification in the inset) or (B) 1.0 µM ATO-treated (magnification in the insert). Nuclei are stained with DAPI (blue). Bar: 5 µm.

3.3.8 Recovery of cardiomyocytes kinematics and dynamics properties after ATO removal

We asked whether cardiomyocytes may rescue their normal kinematics and dynamics properties when ATO is removed from the culture medium. Since the turnover of the myofibrillar proteins is highly variable [ranging from 3.5 days for Troponin T to 10.3 days for actin (Martin, 1981)], a recovery period of 96h, compatible with the viability of EBs in culture, was applied (Figure 24).
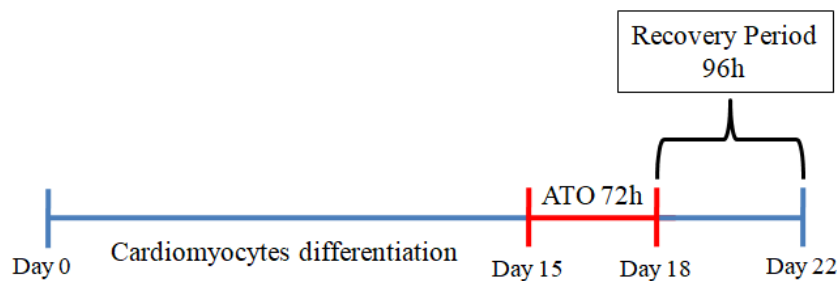
Figure 24. Cardiomyocytes differentiation and recovery period following ATO treatment.

Cardiomyocytes exposed to the three ATO doses display a dramatic fall of almost all parameters at the end of the recovery period (Figure 25), suggesting the cellular damage induced by ATO exposure was still present after 96h recovery.
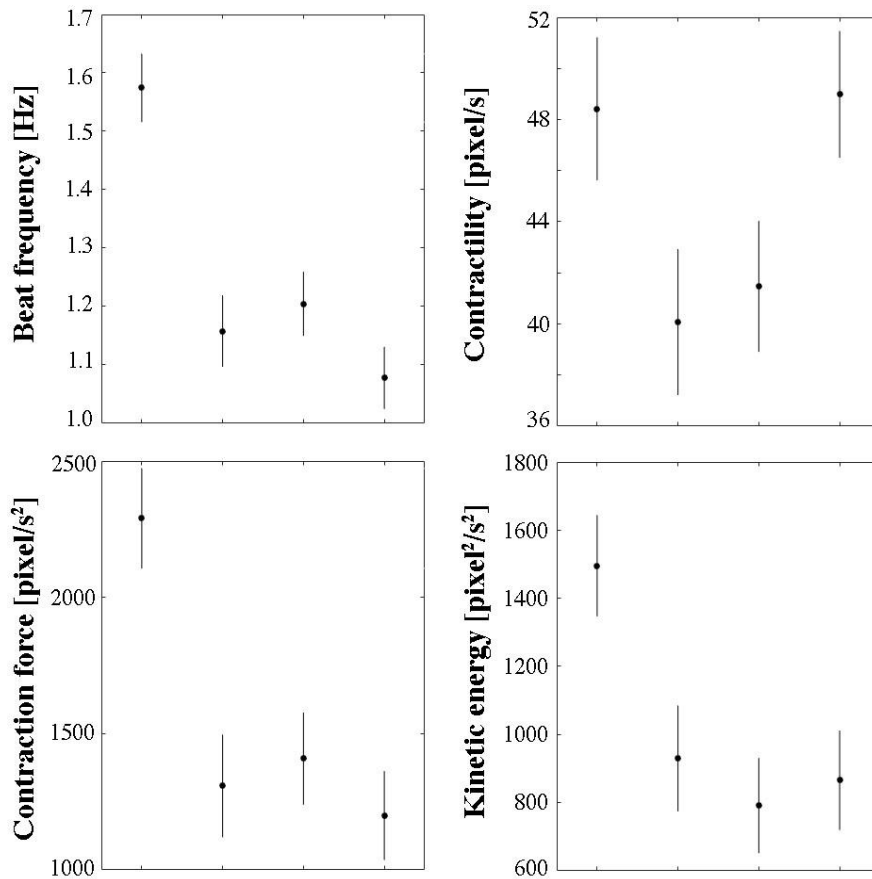
Figure 25. Contractile properties of cardiac syncytia following a recovery period of 96h of CTR and samples exposed for 72 hours to 0.1, 0.5 or 1.0 μM ATO. (A) Beat frequency [Hz]; (B) contraction force [pixel/s^2]; (C) contractility [pixel/s]; (D) kinetic energy [pixel^2/s^2]. The vertical bars represent 95% confidence intervals for the difference between averages according to the "Least Significant Difference" statistical test.

Specifically, cardiomyocytes showed significant decline ($p<0.05$) of all the parameters evaluated, except for contractility, which remained unaltered at 1 μM ATO (Table 10).

59

Table 10. Fold changes of kinematics parameters, after the recovery period of 96h, of cardiomyocytes exposed to 0.1, 0.5 and 1 µM ATO for 72h. *p<0.05.*

Parameters	0.1 µM	0.5 µM	1.0 µM
Beat frequency	0.8*	0.7*	0.7*
Contractility	0.6*	0.5*	1.0
Contraction force	0.6*	0.6*	0.5*
Kinetic energy	0.8*	0.9*	0.6*

3.4 Discussion

Here, we investigated the effects that ATO exerts on perinatal-like cardiomyocytes obtained from mESCs, an *in vitro* cell model that recapitulates the molecular events and the functional features of cardiomyocyte differentiation from mesoderm to specialised cardiac cells (Boheler et al., 2002; Wobus and Boheler, 2005).

We showed that cardiomyocytes exposed for 72h to 0.1, 0.5 or 1.0 μM ATO [doses in the range of the inorganic arsenic present in contaminated water (Halem et al., 2009; States et al., 2011)] are able to contract but with impaired kinematic parameters. The exposure to 0.1 μM ATO does not affect cardiomyocytes contractility, whereas significantly increases their beat frequency, contraction force and kinetic energy, compared to CTR samples. Cardiomyocytes exposed to 0.5 μM of ATO maintained unaltered the contraction force and contractility but showed a significant increase of the other two parameters. A more detrimental effect was recorded for syncytia exposedto1.0 μM of ATO which show significant increase in the beat frequency and, on the contrary, a significant decrease of all the other parameters analysed.

The alteration of the kinematics parameters might be the result of impaired cell-to-cell transmission of the contractile signal. To this regard, significant enhancement of the expression profiles of *Cx40*, *Cx43* and *Cx45* connexin genes and of Cx43 protein, paralleled by increased size of the Cx43 immunofluorescence signals, might contribute to the remodelling of gap junctions leading to abnormal cardiomyocyte conduction properties. In support of our hypothesis, structural model studies showed that arsenic can directly bind to Cx43 channels potentially causing conformational changes in their structure (Hussain et al., 2018).

Sarcomere structural changes can also contribute to abnormal cardiomyocyte kinematics and dynamics properties. The 3D analysis of cardiac syncytia exposed to all ATO doses revealed the presence of two different populations of cardiomyocytes: 1) cardiomyocytes with regular striated pattern and 2) cardiomyocytes with disorganized and/or disoriented sarcomeres, with partial or complete loss of the regular striated pattern. When the sarcomere texture was evaluated using SOTA algorithm (Sutcliffe et al., 2018), organized sarcomeres of ATO-exposed cells had the same parameters as those of CTR cardiac cells, except for sarcomere length and width.

Specifically, sarcomeres were shorter in length and higher in width, a condition that is associated to cardiomyocytes with impaired contraction ability (Kuo et al., 2012).

ATO does not influence theexpression level of *actn2*, *myh6*, *tnnc1*, *tnnt2* and *tnni3* genes. Instead, it alters the expression of sarcomeric α-actin and tropomyosin proteins, but not of myosin, α-actinin and troponin. Similar results were obtained by Kopljar and collaborators (Kopljar et al., 2017) which demonstrated that cardiomyocytes, derived from human-induced pluripotent stem cells exposed to 1, 3 and 10 μM arsenic for 72h, showed altered profiles of sarcomeric proteins.We propose that the skewed protein ratio of two (in our experimental conditions) proteins of those making up the sarcomeres is enough to disrupt their organisation (Neri et al., 2011; Rebuzzini et al., 2015; Thompson and Metzger, 2014). We hypothesize that ATO might interfere with the translation of some sarcomeric proteins, their turnover, or cause their post-translational modifications. To this regard, ATO, through the production of ROS and reactive nitrogen species (RNS) in exposed cells (Flora, 2009; Zhao et al., 2008b), can indirectly provoke oxidation or nitrosylation of the sarcomeric proteins, causing their structural change (Steinberg, 2013).These alterations might severely impair the stability of the proteins present in the sarcomeric apparatus, damaging those interactions necessary to guarantee the maintenance of the proper sarcomere structure. In addition, it has been shown that ATO can alter structural cytoskeleton elements, including structural actin (Izdebska et al., 2014).

The imbalanced ratio among sarcomeric proteins, including actin, observed in our ATO-exposed samples may interferes with cardiomyocytes cell shape and consequently, with the volume occupied by cardiac syncytia in the 3D structure of the EBs, as we have shown using a stereology approach. In fact, the volume of syncytia exposed to 0.1 and 1.0 μM ATO is diminished and enhanced, respectively, when compared to the CTR, whereas the volume of syncytia exposed to 0.5 μM ATO remains unchanged.

Finally, following a recovery period of 72 h, cardiomyocytes did not rescue their normal contractile activity after ATO exposure, as shown by the analysis of kinematics and dynamics parameters. Cardiomyocytes might undergo irreversible cellular damage caused by arsenic exposure. Several are the potential cardiotoxicity mechanisms behind this damage, including oxidative stress, DNA fragmentation, apoptosis and functional changes of the ion channels involved in the heart physiology (Chang et al., 2007; Muthumani and Prabu, 2014; Zhao et al., 2008a, 2008b).

Further studies are necessary to understand the intracellular Ca^{2+} dynamics in exposed samples showing altered beating parameters and to unravel the epigenetic changes that might be involved in the inability to recover cardiomyocyte contractile activity.

4 PART 2

POLYCHLORINATED BIPHENYLS REDUCE THE KINEMATICS CONTRACTILE PROPERTIES OF EMBRYONIC STEM CELLS-DERIVED CARDIOMYOCYTES BY DISRUPTING THEIR INTRACELLULAR CA^{2+} DYNAMICS

The results of this work have been reported in a full paper published in Scientific Reports (2018 Dec 17;8(1):17909. doi: 10.1038/s41598-018-36333-z.), attached at the end of this thesis. Below, a brief Background, a summary of the Results obtained, and of the Discussion are reported.

4.1 Background

PCBs are a class of industrial chemicals that were mass-produced worldwide since the late 1920, until their commercial production was banned, initially by the Toxic Substances Control Act (TSCA) in the United States in 1979, as a reaction to the concern over adverse human health effects(Grimm et al., 2015). Being fat-soluble, PCBs accumulate in fat tissues and are passed to newborn through maternal milk (Agudo et al., 2009), increasing the myocardial wall thickness and inducing cardiac hypertrophy, thus impairing the heart functionality in the adult (La Merrill et al., 2016). Whilst the detrimental effects on the perinatal heart anatomy are evident, unknown are the PCBs effects at the cellular and molecular levels.

Our study aimed at dissecting the key physiological processes behind the observed heart contraction defects, by analysing in ESCs-derived cardiomyocytes the calcium-induced calcium-release mechanism (Ca^{2+} toolkit) that finely regulates contraction. Cardiomyocytes, obtained from *in vitro* differentiation of mESCs, were exposed for 24 h to Aroclor 1254 (Aroclor), a mixture of more than 80 PCBs, at doses in the range of environmental contamination (1 and 2 µg/ml). Their kinematics contractile properties and intracellular Ca^{2+} homeostasis were evaluated.

4.2   Results

4.2.1   Contractile properties after Aroclor exposure

The effects of Aroclor on the contractile properties of beating syncytia were evaluated by analysing the kinematics and dynamics features of cardiomyocytes, exposed to 1 or 2 µg/ml Aroclor for 24h. After exposure to 1 µg/ml Aroclor, both beat frequency and kinetic energy showed significant decrease when compared to CTR. More adverse effects were observed when syncytia were exposed to 2 µg/ml, since all four parameters (beat frequency, kinetic energy, contractility and contraction force) were significantly reduced.

4.2.2   Analysis of spontaneous intracellular Ca^{2+} oscillations

In Aroclor-exposed samples, the analysis of the intracellular Ca^{2+}machinery, which regulates cardiomyocyte contraction, showed reduction of both amplitude and frequency of spontaneous intracellular Ca^{2+} oscillations, suggesting that Aroclor might interfere with the intracellular Ca^{2+} handling machinery in beating syncytia.

4.2.3   Analysis of molecular machinery underlying spontaneous Ca^{2+} activity

In CTR cardiac syncytia, the use of tetracaine, inhibitor of the ryanodine receptors (RyR), induces a prompt inhibition of the intracellular Ca^{2+} spikes, suggesting the crucial role of RyR receptor in shaping Ca^{2+} signal. Also, the removal of external Ca^{2+}resulted in the progressive decline in the amplitude of the Ca^{2+} transients, ended up with a complete arrest of Ca^{2+} activity and the blockade of Inositol trisphosphate receptor (InsP$_3$Rs) with 2-APB failed to affect the ongoing Ca^{2+} transients. Overall, these findings confirm that RyR2-dependent rhythmical Ca^{2+} release underlies the onset of the spontaneous Ca^{2+} oscillations, whereas voltage-dependent Ca^{2+} entry maintains them over time. The same results were obtained when the beating syncytia were exposed to 1 or 2 µg/ml Aroclor. The application of angiotensin II, which stimulate InsP3-induced Ca^{2+} release from the SR (Sedan et al., 2010), during ongoing oscillations caused in CTR syncytia transient

enlargement of the first Ca^{2+} spike, followed by a short-lasting reduction in the amplitude of the subsequent Ca^{2+} oscillations. Conversely, when beating syncytia were exposed to 1 or 2 µg/ml Aroclor, angiotensin II caused a large Ca^{2+} spike whose decay to the baseline was overlapped by RyR2-dependent spontaneous Ca^{2+} oscillations. These observations suggest that the InsP3-sensitive Ca^{2+} pool is increased in the presence of Aroclor.

Next, we investigated the single components of the Ca^{2+} toolkit, i.e., RyR2 and L-type voltage-gated Ca^{2+} channels (VGCCs).

4.2.4 Analysis of sarcoplasmic reticulum (SR) Ca^{2+} content

The acute addition of Aroclor in the $0Ca^{2+}$medium did not induce any detectable variation in $[Ca^{2+}]i$ at both 1 or 2µg/ml. Instead, 24 h exposure to Aroclor caused a significant ($p<0.05$) reduction in basal $[Ca^{2+}]i$. Caffeine (20 mM), a selective RyR agonist, triggered a Ca^{2+} response in CTR samples, while it failed in the presence of Aroclor at both concentrations. SR Ca^{2+} content was evaluated using cyclopiazonic acid (CPA) SERCA inhibitor. Exposure to Aroclor caused a significant reduction in CPA-induced Ca^{2+} release under $0Ca^{2+}$ conditions, which hints at a remarkable reduction in SR Ca^{2+} levels. Finally, cardiomyocytes were depolarized with high-KCl solution to monitor voltage-dependent Ca^{2+} entry. We observed that high-KCl-induced Ca^{2+} entry was significantly reduced in the presence of each dose of Aroclor. Overall, these data strongly suggest that Aroclor reduces the SR Ca^{2+} content, decreases the resting $[Ca^{2+}]i$ and inhibits voltage-dependent Ca^{2+} inflow in cardiomyocytes. Consequently, the spontaneous Ca^{2+} oscillations that drive cardiac contraction are inhibited, which contributes to explain Aroclor-dependent cardiac functional alterations. Also, Aroclor modifies the expression of genes involved in the Ca^{2+} toolkit.

4.2.5 Expression analysis of genes involved in Ca^{2+} toolkit

The exposure to both Aroclor concentrations did not significantly alter the quantitative expression of *Atp2a2* gene (coding for SERCA2A, cardiac isoform of the Ca^{2+}-ATPase that sequesters Ca^{2+} back into the SR). Conversely, the expression of *Ryr2* (cardiac muscle SR RyR isoform), and *Itpr2* (cardiac muscle SR InsP3R isoform) significantly increased, whereas

the expression of *Cacna1c* (α subunit of L-type VGCCs) significantly decreased only in syncytia exposed to 2 μg/ml.

4.3 Discussion

Our study demonstrates that Aroclor exerts its detrimental effects on the beating properties of ESCs-derived cardiomyocytes, acting on the intracellular Ca^{2+} machinery. The spontaneous intracellular Ca^{2+} oscillations represent the main source of Ca^{2+} for the contractile machinery during cardiac development (Fu et al., 2006; Yang et al., 2002). These spontaneous Ca^{2+} spikes are generated by rhythmic Ca^{2+} release from SR through RyR2, which in turn evokes a $Na+/Ca^{2+}$ exchanger-mediated membrane depolarization and activates VGCCs (Viatchenko-Karpinski et al., 1999; Yang et al., 2002).

In accordance with earlier observations on other PCBs (Kodavanti, 2006; Pessah et al., 2010), Aroclor heavily impaired spontaneous intracellular Ca^{2+} oscillations of cardiomyocytes, affecting both their frequency and amplitude. The signalling machinery underlying the rhythmic Ca^{2+} signal was not affected by the treatment, as, both in the absence or in the presence of Aroclor1254, the intracellular $Ca2^{+}$ oscillations were mainly driven by RyRs and supported by extracellular Ca^{2+} entry. These data indicate that RyRs and VGCCs work to shape the spontaneous Ca^{2+} oscillations also in Aroclor-exposed syncytia.

Thus, we moved our attention to single components of the Ca^{2+} toolkit involved in the oscillatory signal to evaluate whether and how Aroclor interferes with them. We determined that Aroclor exposure induced significant reduction in basal $[Ca^{2+}]i$ and SR Ca^{2+} levels in cardiomyocytes, which is reflected in a dramatic decrease in the caffeine-releasable Ca^{2+} pool. Additionally, Aroclor heavily inhibited voltage-dependent Ca^{2+} entry, as measured in response to high-KCl extracellular solution. Similar results were obtained in neuronal cells, in which it was demonstrated that Aroclor 1254 induced a depletion of SR Ca^{2+} store through the activation of InsP3Rs (Inglefield et al., 2001; Kang et al., 2004). The acute exposure to Aroclor did not trigger any detectable increase in $[Ca^{2+}]i$, suggesting that Aroclor causes massive and rapid release of intra-luminally stored Ca^{2+} which is the most intuitive mechanism to explain the depletion of the SR Ca^{2+} pool underpinning the rhythmic Ca^{2+} release. This result differs compared to that observed in rodent neurons (Lesiak et al., 2014; Wayman et al., 2012) and PC12 cells (Wong et al., 2001), in which PCB-95 and Aroclor 1254 stimulate RyRs-dependent intracellular Ca^{2+} release.

It has been demonstrated that PCB congeners sensitize RyRs by binding to one or more components of the RyR macromolecular complex (Chelu et al., 2004; Samsó et al., 2009). We speculated that Aroclor fails to increase $[Ca^{2+}]i$ because they physiologically resemble to perinatal cardiomyocyte, which are characterized by an immature SR (Nakanishi et al., 1988; Pegg and Michalak, 1987), lack of expression of components of the adult RyR macromolecular complex. The effects observed after 24h-exposure could be explained by an interference with the Ca^{2+} handling machinery.

Gene expression analysis demonstrated that both 1 or 2µg/ml Aroclor induced significant increase of the expression of *Ryr2*, as also reported in rat cerebellum cells(Yang et al., 2009). The upregulation of *Ryr2* transcript expression is predicted to increase, rather than decrease, the release of $Ca^{2+}$from SR to the cytoplasm, thus increasing the spiking activity of beating syncytia. We hypothesize that Aroclor might be able to interfere with SERCA-mediated Ca^{2+} sequestration, causing the fall in SR Ca^{2+} levels. However, the mechanism whereby Aroclor inhibits SERCA activity is yet to be elucidated (Kodavanti et al., 1998; Sharma et al., 2000), since our data demonstrate that the transcript levels of *Atp2a2* gene, that codes for SERCA2A, are not altered after 24h Aroclor exposure. Real Time PCR disclosed that only 2 µg/ml Aroclor 1254 decreased the expression of *Cacna1c*, which encodes for the α subunit of L-type VGCCs. While this mechanism is likely to play a major role in reducing voltage-dependent Ca^{2+}entry at the higher dose, it does not explain the inhibitory effect observed at 1 µg/ml. However, earlier reports clearly demonstrate that PCB congeners, including Aroclor 1254, have the potential to modulate plasma membrane channels(Mundy et al., 1999; Voie and Fonnum, 1998). We hypothesize that, besides reducing *Cacna1c* expression, Aroclor 1254 inhibits L-type VGCCs through a non-yet identified mechanism in cardiomyocytes.

In conclusion, for the first time, we demonstrate that perinatal cardiac syncytia exposed to Aroclor 1254 undergo a dramatic functional alteration of the kinematics contractile properties, due to the disruption of the intracellular Ca^{2+} machinery. These findings contribute to the understanding of the molecular mechanisms underpinning the PCBs-induced cardiovascular alterations, which are emerging as an additional life-threatening hurdle associated to PCB pollution.

5   PART 3
CYPERMETHRIN-INDUCED TOXICITY IN MOUSE EMBRYONIC STEM CELLS

5.1   Background

Synthetic pyrethroids are the most worldwide diffused pesticides, largely used since the '80s in households and in agriculture (Feo et al., 2011) because of their effectiveness and low toxicity compared to other insecticides, such as organophosphorus and carbamic ester compounds (Tang et al., 2018; Yoo et al., 2016). As a result of their diffusion and uncontrolled use, pyrethroids, contaminating water and soil, have entered the food chain (Bhattacharjee et al., 2012; Choudhury et al., 2013; Debbab et al., 2014; Gilden, 2010; Tang et al., 2018), becoming a human health hazard (Saillenfait et al., 2015).

Cypermethrin (CYP) is the most used pyrethroid, employed on a wide scale against a broad range of insects (Manfo et al., 2012; Nantia Akono et al., 2019). It is a type II pyrethroid insecticide, classified by the World Health Organization as moderately hazardous (class II). CYP detrimental effects have been described on adults and during embryonic development of several vertebrate species. Specifically, earlier studies demonstrated that CYP generates oxidative stress and apoptosis in fish liver (Jin et al., 2011a, 2011b; Uner et al., 2001), retina (Paravani et al., 2018), kidney (Uner et al., 2001) and gill (Paravani et al., 2019) cells and also in mouse macrophages (Huang et al., 2016), rat brain and liver (Giray et al., 2001) cells. In the mouse, by impairing endometrial receptivity, CYP severely reduces embryo implantation (Zhou et al., 2018). Unknown remains whether CYP has effects during pre-implantation, a developmental window with three main critical moments. The first occurs at the time of embryonic genome activation (2-cell and 4-cell stage in mouse and human, respectively) (Jukam et al., 2017) the second when the embryo reaches the morula stage (Jukam et al., 2017), followed by the most critical at the blastocyst stage, when, in our species, the great majority of embryos fails to implant and is lost (Koot et al., 2012). Lack of implantation is either a consequence of a functional damage to the endometrium or to the cell lines that make up the blastocyst, i.e., the

trophectoderm or the inner cell mass (ICM), which will contribute, respectively, to the extra-embryonic tissue (e.g., placenta) or to the foetus. The damage to the ICM cells, when not selective against the embryo, could, however, cause serious damage to the foetus or appear much later in development, childhood or adulthood. Despite the blastocyst being one of the most vulnerable moment in the life of a new individual, studies to access the embryo-toxicity of test substances, performed on model animals, are complicated by the required experimental setting and the restricted number of blastocysts that may be obtained, either *in vivo* or *in vitro*, for each single experiment. To this regard, ESCs are an *in vitro* model study that overcomes these limitations, as for each experiment millions of pluripotent cells are available to the analysis of the test substance. ESCs, derived from the ICM of preimplantation blastocysts, maintain the same pluripotency characteristics and differentiation capacity (Evans and Kaufman, 1981; Martin, 1981; Thomson et al., 1998).

In this work, using mESCs as an *in vitro* model that resembles the characteristics of the blastocyst's ICM, we studied CYP-induced alterations previously described in adult somatic cells and in the developing embryo. Specifically, cell growth, cell death, ROS production and the activation of a detoxification response, were analysed in mESCs and 3T3NIH cells, the latter, a differentiated cell line of embryonal origin, used for comparison.

5.2 Materials and Methods

5.2.1 Cells and cell cultures

R1 mESC line was cultivated as reported in paragraph 4.1. The 3T3NIH cell line (generous gift by Prof. Giulotto, Department of Biology and Biotechnology, University of Pavia) was cultured in DMEM (Sigma) supplemented with 10% FBS, 4 mM L-glutamine, 1X non-essential amino acids, 0.5% penicillin/streptomycin (all from Life Technology) and 0.1 mM β-mercaptoethanol (Sigma). Cells were routinely passaged with 0.25% trypsin every 2-3 days.

5.2.2 Cypermethrin preparation

α-cypermethrin [α-Cyano-(3-phenoxyphenyl)-methyl 3-(2,2-dichlorovinyl)-2,2-dimethyl cyclopropane carboxylate] (Abcam) was dissolved to a final concentration of 100 mM in dimethyl sulfoxide (DMSO). The solution was maintained at -20°C and renewed every 7 days, to ensure the stability of the molecule, according to manufacturer instructions.

5.2.3 Determination of LD$_{50}$ dose of CYP for 3T3NIH and R1 cell lines

CYP toxicity was carried out by measuring the alteration of growth of a massive cell culture, as described by Rebuzzini and colleagues (Rebuzzini et al., 2007). Briefly, 3×10^4 R1 and 3T3NIH cells were seeded in 6 cm Petri dish (Corning) and exposed to increasing concentrations of CYP (0.01, 0.05, 0.1, 0.2, 0.4, 0.6, 0.8 to 1 mM) or to 0.01% DMSO (Control, CTR) or without the vehicle. After 72 h, the cells were collected in PBS 1X, pelleted at 1200 rpm for 8 min, lysed in 0.1 M NaOH and incubated at 50°C in the water bath for 30 min. The number of cells was estimated by measuring the absorbance of the lysate at 260 nm.

5.2.4 Determination of cell growth curve

3T3NIH and R1 cells were seeded at a density of 8×10^4 and 5×10^4, respectively, and incubated with the relative RD$_{50}$ concentration of CYP

for72 h. The cells were harvested after 8, 24, 48 and 72 h, and counted using a Bürker chamber. The number of cells at different time points was normalized to the initial seeded number of cells. Since the cell doubling is a base-2 exponential phenomenon, a way to linearize the Cartesian representation of the cell growth curves is to apply the base-2 logarithm function to the cell number, that is: log2 (cell number). In such linear representation, the growth curves are lines with positive slope if the cell number increases or, on the contrary, with negative slope if the cell number decreases. More specifically, the linearization permits to use the linear regression of the experimental data (via Matlab programming language, The MathWorks, Inc.), by which we calculated the 'best' slopes and intercepts using at least a triplicate measure of the cell number at each time point. Finally, the slopes of two lines were considered different when $p<0.05$ with 95% confidence bounds (Fisher, 1921).

5.2.5 Apoptosis Annexin V assay

The ApopNexin^{TM} FITC and propidium iodide (PI) kit assay (Merck Millipore) was used to detect apoptosis after CYP treatment. Briefly, 3T3NIH (1.5×10^4 cells) and R1 (10^5 cells) were seeded in 6 cm Petri dishes and exposed to 0.6 mM and 0.3 mM CYP, respectively, for 8 (only 3T3NIH), 12 (only R1), 24, 48 and 72h. Cells were harvested according to the manufacturer instructions and analysed, after staining, by bivariate flow cytometry (FITC band in FL1 and PI band in the FL3 channel). The analyses of the samples were performed using a flow cytometer FACS Lyric BD (BD Biosciences). A minimum of 50000 events were acquired for each sample. Data were processed, plotted and analysed using the BD FACSuite^{TM} flow cytometer software.

5.2.6 Reactive oxygen species quantification

The cell-permeant 2',7'-dichlorodihydrofluorescein diacetate (H_2DCFDA) fluorescent probe (Thermo Fisher Scientific) was used to evaluate the intracellular levels of reactive oxygen species. Fibroblast 3T3NIH (2×10^5 cells) and R1 (10^5 cells) were seeded in 10 cm Petri dishes and exposed to 0.6 mM or 0.3 mM CYP, respectively, for 8 (only 3T3NIH), 12 (only R1), 24, 48 and 72h (both cell lines). Then, cells were collected,

73

centrifuged at 500 rpm for 5 min and resuspended in PBS 1X solution containing 10 µM H_2DCFDA. The mixture was incubated 37ºC for 30 min under dark condition. The analyses of the samples were performed using a flow cytometer FACS Lyric BD (BD Biosciences). A minimum of 50000 events were acquired for each sample. Data were processed, plotted and analysed using the BD FACSuite[TM] flow cytometer software.

5.2.7   Cell cycle analysis

Fibroblast 3T3NIH (2×10^5 cells) and R1 (10^5 cells) were seeded in 10 cm Petri dishes and exposed to 0.6 mM and 0.3 mM CYP, respectively. After 8 (3T3NIH), 12 (R1), 24, 48 and 72h, the cells were harvested, washed in PBS 1X and stained with 1.5 ml of 50 µg/ml propidium iodide (PI), containing 100 U/ml of RNase and 0.05% Igepal (Sigma). The analyses of the samples were performed using a flow cytometer FACS Lyric BD (BD Biosciences). A minimum of 50000 events were acquired for each sample. Data were processed, plotted and analysed using the BD FACSuite[TM] flow cytometer software.

5.2.8   RNA extraction, reverse transcription and Real-Time PCR

Total RNA was extracted from 3T3NIH (2×10^5 cells) and R1 (10^5 cells) cells after 8 (3T3NIH), 12 (R1), 24, 48 and 72h of CYP exposure using GenElute Mammalian Total RNA kit (Sigma) according to the manufacturer's instructions (For details see paragraph.4.7). One twentieth of the resulting cDNA was amplified in duplicate by Real-Time PCR in 20 µl reaction mixture with 200nM of each primer (designed with Primer 3 software, see Table 11) and MESA GREEN qPCR Master Mix Plus for SYBR assay no ROX sample (Eurogentec) at 1X as final concentration (For details see paragraph 4.8).

**Table 11**. Primers sequences used for gene expression analysis

Gene	Forward	Reverse
Cat	5' TCATCAGGGATGCCATATTGT 3'	5'ACTCCAGAAGTCCCAGACCAT3'
Gpx1	5'CTACACCGAGATGAACGATCTG3'	5' CTTGCCATTCTCCTGGTGTC 3'
Gpx4	5'TGTGGAAATGGATGAAAGTCC 3'	5' ACGCAGCCGTTCTTATCAAT 3'
Sod1	5' TGTCCATTGAAGATCGTGTGA 3'	5' TTGCCCAAGTCATCTTGTTTC 3'
Sod2	5' CTTACAGATTGCTGCCTGCTC 3'	5'GTAGTAAGCGTGCTCCCACAC 3'
Sod3	5'CTGAACTTCACCAGAGGGAAA 3'	5'CCAGTAGCAAGCCGTAGAACA 3'
Cyp1a1	5' CTGCCTAACTCTTCCCTGGAT 3'	5'ATGTGGCCCTTCTCAAATGTC 3'
Cyp1b1	5' CCAGGTGCAAACTTGAGACA3'	5' TGTCTGCACTAAGGCTGGTG 3'
Nqo1	5' TTCTCTGGCCGATTCAGAGT 3'	5' TCTGGTTGTCAGCTGGAATG 3'
Gsta1	5' CTTCTGACCCCTTTCCCTCT 3'	5' GCCAGTATCTGTGGCTCCAT 3'
Ugt1a6	5' ATTGCCTCAGACCTCCTCAA 3'	5' GAGACCATGGATCCCAAAGA 3'
β2m	5' GAATTCACCCCCACTGAGACT 3'	5'TGCTTGATCACATGTCTCGAT 3'

5.2.9   Statistical analysis

The results were analysed using SigmaStat software. Data, expressed as mean ± SD, were analysed by the one-way ANOVA and by the post hoc LSD test.

5.3 Results

We first determined at 0.3 mM and 0.6 mM, for mouse R1 ESCs (R1) and 3T3NIH respectively, the dose of CYP that reduces growth of 50% (LD_{50}) (Figure 26), and, based on these results, all the experiments described below were performed at these specific LD_{50}. The presence of the vehicle did not significantly alter cell growth of both cell lines ($p>0.05$) (data not shown).
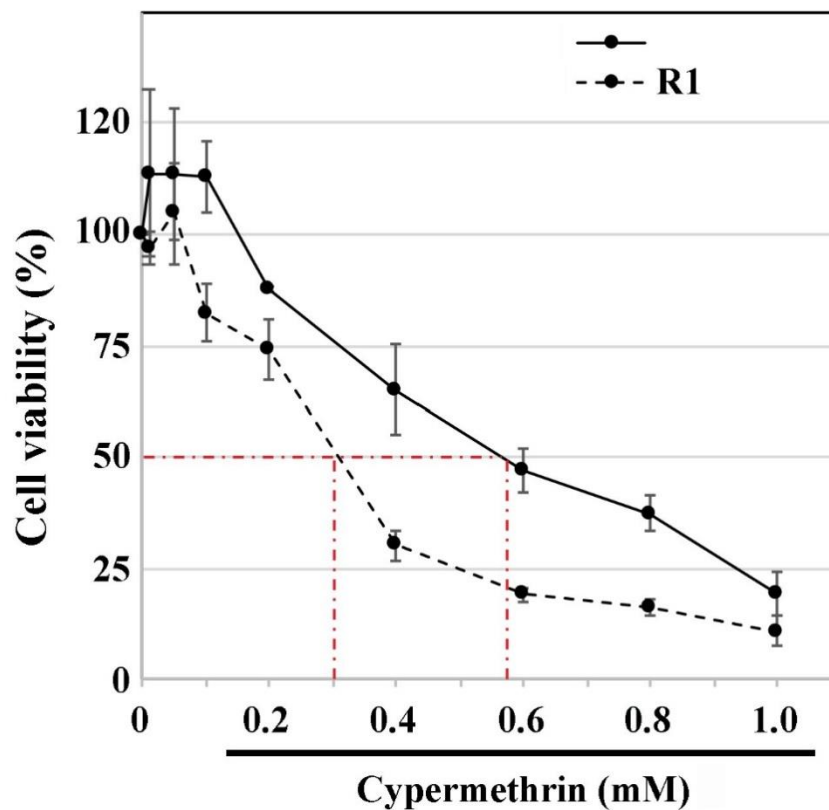

Figure 26. Dose/response curve to CYP of 3T3NIH and R1 after 72 h exposure. Data represent the mean ± SD of 3 independent experiments.

5.3.1 Cell growth dynamics

3T3NIH and R1 cell lines displayed different growth dynamics. In 3T3NIH, the number of exposed cells significantly decreased (p=0.024) compared to CTR within 8 h of culture (Figure 27). Then, CTR and treated

cells grew at the same rate (no difference, *p*=0.133, in the slope of the lines, Figure 27) with very similar population doubling (PD) time (22.78h and 27.70h, respectively). A PD time in agreement with previous published data (http://www.nih3t3.com/) for untreated 3T3NIH cells. Significant (p<0.003) decrease of R1 cells number was observed up to 24 h following 0.3 mM CYP exposure (Figure 27). Then, exposed cells started to grow, although at significantly lower rate compared to CTR, as evidenced by the significant reduction (p=0.008) of the regression slope (Figure 27); in other words, the PD time significantly increased from 16.21h (CTR cells) to 19.52h (exposed cells) (Tamm et al., 2013).
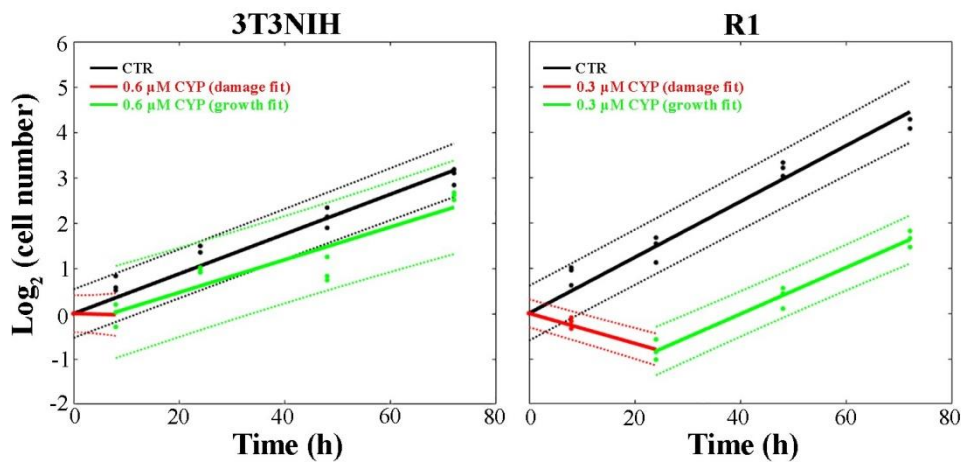
Figure 27. Fitted growth curves of CTR and CYP-exposed cells of 3T3NIH and R1 lines. Circles represent the experimental data; dotted lines are the upper and lower percentage bounds (95%).

To understand whether the decrease in cell number was due to apoptosis and/or alterations in the progression through the cell cycle stages, the Annexin V assay and the nuclear DNA content fluorometric evaluation were used, respectively.

5.3.2   Cell death

Figure 28 reports the fraction of 3T3NIH and R1 cells positive to Annexin V (AnV[+] early apoptotic marker), Annexin V and propidium iodide (AnV[+]/PI[+], late apoptotic marker), or propidium iodide (PI[+], cell death marker) after CYP exposure, expressed as fold change relative to CTR set at

1. After 8h exposure, AnV$^+$ and AnV$^+$/PI$^+$ 3T3NIHcells increased (1.5 and 1.7-fold, respectively, $p<0.001$) while PI$^+$ 3T3NIHcells decreased (0.6-fold, $p<0.05$) compared to CTR (Figure 2A). After 24 h, a further increase ($p<0.05$) up to 2.2- and 2.1-fold for AnV$^+$ and AnV$^+$/PI$^+$ cells, respectively, was observed, whereas PI$^+$ cells were not significantly different ($p>0.05$) when compared to CTR. A peak (2.2-fold increase, $p<0.05$) of cell death was observed after 48 h, whereas at 72h exposed cells completely recovered, showing the same degree of early or late apoptosis as that of CTR ($p>0.05$) (Figure 28A). AnV$^+$ and AnV$^+$/PI$^+$ R1 cells significantly increased after both 12 (3.2- and 2.4-fold, respectively; $p<0.05$) and 24 h (1.6- and 2.2-fold, respectively; $p<0.05$) exposure, when comparted to the CTR population (Figure 28B). At 48 h, only apoptotic PI$^+$ cells were detected, with a 1.4-fold-increase ($p<0.05$). A second relevant wave of apoptosis was recorded after 72h exposure with a 7.7-fold and a 5.3-fold increase of AnV$^+$ and AnV$^+$/PI$^+$ cells (Figure 28B).
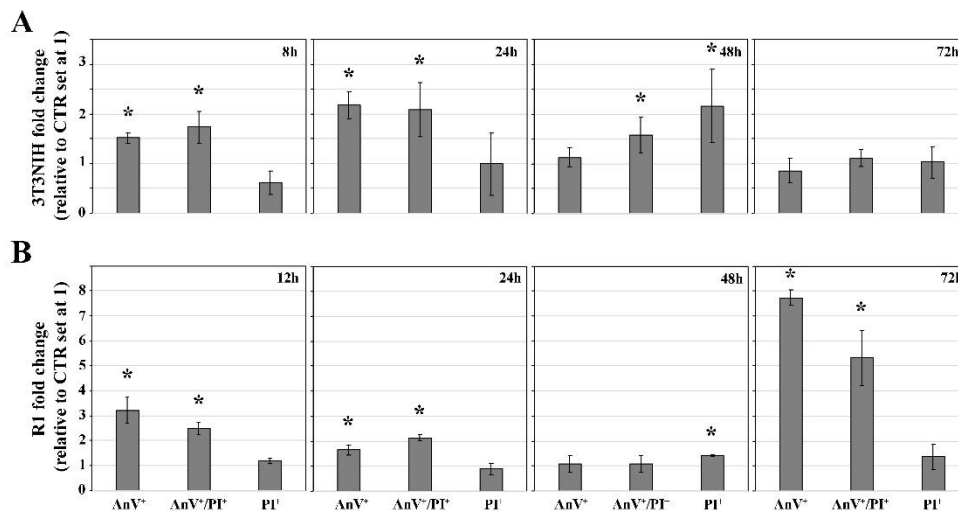
Figure 28. Annexin V positive (AnV$^+$), Annexin V and propidium iodide positive (AnV$^+$/PI$^+$) and propidium iodide positive (PI$^+$) cells in 3T3NIH (**A**) and R1 (**B**) cell lines, detected 8 (3T3NIH), 12 (R1), 24, 48 or 74h after CYP exposure. *$p<0.001$.

5.3.3 Cell cycle progression

To evaluate whether CYP exposure influences the distribution of cells in the different phases of the cell cycle, DNA content was detected using a one-parametric analysis of PI-stained nuclei of both cell lines. Unexposed 3T3NIH cells are at about 67% in G0/G1 phase, about 14% in S phase and about 18% in G2/M phase (Table 12) (Tai et al., 2012). While after 8 and 24 h 0.6 mM CYP exposure, the distribution of cells in the different phases of the cell cycle remains unaltered compared to CTR (Table 12), at 48 h, the frequency of cells in G0/G1 increased ($p<0.001$) and the frequency of cells in S and in G2-phase significantly decreased ($p<0.001$) (Table 12), suggesting an activation of a G0/G1 block of the cell cycle. The distribution of cells in the three phases returns comparable to CTR population after 72h exposure. For R1 CTR cells, the 32% distribution in G0/G1, 54% in S and 14% in G2/M phases recorded confirms previous findings of our and other groups (Rebuzzini et al., 2007, 2008). When exposed to CYP, the frequency of R1 cells distributed within the three phases of the cell cycle did not change up to 24 h (Table 12). At 48 and 72 h, the frequency of cells in G0/G1 phase significantly decreased ($p<0.001$), in association with a significant increase of cells in G2/M phase (Table 12), suggesting an activation of a G2/M cell cycle block at both time points.

Table 12. Cell cycle phase distribution of 3T3NIH and R1 cells during 72 h exposure to 0.6 and 0.3mM doses of CYP, respectively. * $p<0.001$ when compared to CTR.

|	Samples	Hours	Frequency of cells (mean±SD)		
			G0/G1	S	G2/M
3T3NIH	CTR	8	65.0±4.0	15.9±1.9	19±2.7
	CYP		62.3±1.5	17.1±0.6	20.6±2.2
	CTR	24	67.1±1.7	14.3±1.1	18.6±1.4
	CYP		67.9±3.2	15.1±1.4	17.0±1.8
	CTR	48	68.6±1.4	14.0±0.6	17.4±0.8
	CYP		79.2±1.4*	11.1±0.8*	9.7±2.0*
	CTR	72	66.6±0.7	15.9±0.4	17.5±0.9
	CYP		68.1±1.3	15.2±0.7	16.6±1.4
R1	CTR	8	26.9±4.4	48.9±2.8	24.4±1.6
	CYP		29.7±1.1	47.6±1.0	22.7±0.7
	CTR	24	31.6±2.9	54.2±3.1	14.2±0.3
	CYP		31.5±0.5	53.3±0.7	15.2±0.3
	CTR	48	29.1±2.2	52.8±1.6	18.1±1.0
	CYP		25.7±0.6*	51.6±0.3	22.7±0.6*
	CTR	72	30.9±1.4	54.0±1.4	15.1±0.8
	CYP		24.3±1.3*	54.6±0.9	21.1±1.8*

Then, we determined whether and at which levels reactive oxygen species (ROS) are induced by CYP. Also, we evaluated whether an antioxidant cellular response is triggered, by analysing the expression of catalase (*Cat*), superoxide dismutases 1, 2 and 3 (*Sod1*, *Sod2* and *Sod3*) and glutathione peroxidases 1 and 4 (*Gpx1* and *Gpx4*) genes which code for major antioxidant proteins against ROS.

5.3.4   ROS production and redox-related gene expression response

Compared to CTR, exposed 3T3NIH cells display higher levels of ROS at 24h and 48h (1.3- and 1.2-fold, respectively; $p<0.05$) (Figure 29A), but not at 8h and 72 h. Of the six gene transcripts (*Cat*, *Sod1*, *Sod2*, *Sod3*, *Gpx1* and *Gpx4*) analysed, no differences between CTR and exposed cells were detected within 8 h, whereas after 24h cells displayed significant increase ($p<0.05$) of *Cat* expression and slight but significant decrease ($p<0.05$) of *Sod3*, *Gpx1* and

Sod2 transcripts. *Sod2* transcripts remained low in exposed cells after 48 h culture. At 72h, slight (*p*<0.05) *Cat* and *Gpx4* induction was detected (Figure 29B). Exposed R1 cells showed 1.2-fold increase (*p*<0.05) in ROS production beginning at 24h of culture. ROS production continues to increase after both 48 and 72 h (1.3 and 1.6-fold, respectively, *p*<0.05) (Figure 29A). At 48 h culture, exposed R1 cells showed an active response to ROS production with the induction (*p*<0.001) of *Cat*, *Sod1*, *Sod2*, and *Gpx4* expression and of *Gpx1* (*p*<0.05) at 72h (Figure 29B).
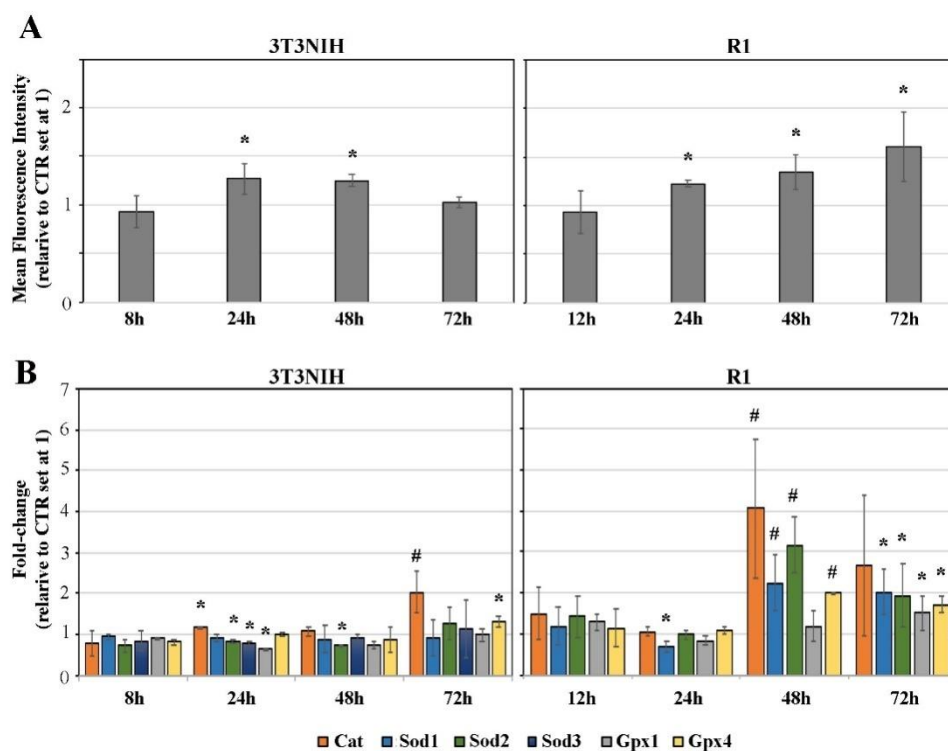
Figure 29. (**A**) Mean fluorescence intensity of in 3T3NIH and R1 cell populations at different time points in the presence of CYP; (**B**) Expression profile of *Catalase*, *Sod1*, *2* and *3* and of *Gpx1* and *4* ROS antioxidant genes, at different time points in the presence of CYP. The expression values of CTR samples were set at 1 for the calculation of the n-fold change. Values are expressed as mean ± SD. **p*<0.05, *#p*<0.001.

To determine if the detoxification mechanisms, known to be involved in the processes of elimination of environmental toxicants (Rushmore and Kong, 2002), were activated in response to CYP exposure, the expression profile of cytochromes P450 *Cyp1a1* and *Cyp1b1* (AHR-regulated of phase I) and *Nqo1*, *Gsta1* and *Ugt1a6* (AHR-regulated of phase II) enzymes was evaluated.

5.3.5 Phase I and phase II gene expression response

Compared to CTR, of the five genes analysed, three were up-regulated in 3T3NIH exposed cells: *Cyp1a1* ($p<0.05$) at 24h; *Ugt1a6* ($p<0.001$) from 24h, *Gsta1* ($p<0.001$) from 48h. The expression of the other two genes (*Cyp1b1* and *Nqo1*) remained unaltered ($p>0.01$) (Figure 29and Table 15). In exposed R1, of the two Phase I genes the level of *Cyp1a1* transcripts was similar to CTR at 12 and 72 h whereas it was lower ($p<0.05$) at both 24 and 48 h; *Cyp1b1* was down regulated ($p<0.05$) at 24 and 48h but up regulated ($p<0.001$) at 72 h of culture. *Ugt1a6* Phase II gene was initially down regulated ($p<0.05$), but up regulated ($p<0.001$) from 24h until the end of the culture period. Also up regulated ($p<0.001$) were *Gsta1* (from 48h) and *Nqo1* (at 72h) (Figure 30).
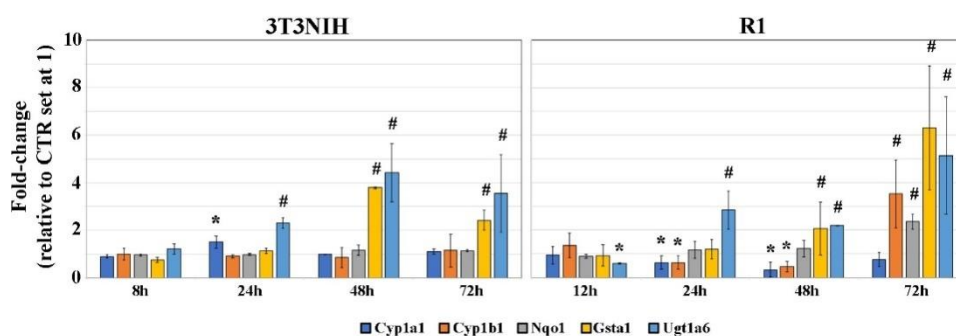
Figure 30. Expression profile of *Cyp1a1*, *Cyp1b1* (Phase I), *Nqo1*, *Gst1* and *Ugt1a6* (Phase II) detoxification genes, at different time points in the presence of CYP. The expression values of CTR samples were set at 1 for the calculation of the n-fold change. Values are expressed as mean ± SD. *$p<0.05$, #$p<0.001$.

5.4   Discussion

After exposure to their respective LD_{50} doses, R1 undifferentiated mESCs are highly damaged, compared to fibroblast 3T3NIH cells, showing a negative growth rate until 24 h exposure. When the R1 population overcame this phase, its growth rate and PD time were significantly lower compared to unexposed cells. To the contrary, 3T3NIH cells, soon after 8h exposure, reached the same growth rate and PD time of the CTR population. The reduction of R1 exposed cell population was due to the activation of CYP-induced apoptosis, after 8-24 h and at 72 h exposure, and cell cycle check points, at 48 and 72 h, likely a consequence of an increase of ROS production. In mESCs, ROS increase was accompanied by a significant up-regulation of mRNA transcripts of genes coding for the redox-enzymes. Conversely, 3T3NIH, entered apoptosis and arrested the cell cycle within 48h exposure, contrasting ROS more efficiently, and completely resolving CYP-induced damages within 72h, despite the persistence of the CYP in the medium. In parallel to apoptotic and cell cycle arrest processes activation, CYP also triggered the detoxification endogenous mechanisms. 3T3NIH cells fast induced the transcription of the cytochrome P450 *Cyp1a1* phase I gene, and *Gsta1* and *Ugt1a6* Phase II genes; in R1 cell lines, the expression of phase I *Cyp1a1* gene unexpectedly appeared to be reduced in exposed cells and *cyp1b1* is induced only at 72h exposure.

The results here reported confirmed previous observations of a major resistance to toxicants of differentiated cells (Cheung et al., 2009; Gerloff et al., 2013; Khwanraj et al., 2015) that, having a more mature metabolism, better tolerate the exposure to toxic molecules, when compared to undifferentiated cells. For example, differentiated SH-SY5Y neuroblastoma cells displayed higher tolerance to all-trans-retinoic acid (Cheung et al., 2009) or to inhibitor of mitochondrial complex (Khwanraj et al., 2015), when compared to their undifferentiated counterpart. Also, differentiated human intestinal Caco-2 cells were more resistant to some inorganic compounds (SiO_2, ZnO), than the respective undifferentiated population (Gerloff et al., 2013). CYP-induced apoptosis in R1 pluripotent stem cells might be associated, as reported in human undifferentiated SH-SY5Y cells, to a dysregulation of the pro-apoptotic proteins Bcl-2 and cytochrome c and of the anti-apoptotic protein Bax expression (AlKahtane et al., 2018; Raszewski et al., 2015). In R1 cells, the activation of the apoptotic response represented, soon after 12-24h exposure, a short-term response of the cells for the

elimination of highly damaged cells from the population. This early apoptotic event, also reported for other toxicants (Cervantes et al., 1994; Rebuzzini et al., 2012), guarantees the maintenance of the integrity of cell population and allows to eliminate those cells with a high mutational burden. The second wave of α-CYP-induced apoptosis, observed at 72h, might instead eliminate those cells with unrepairable damages that are found to be arrested in G2/M phase at 48 and 72h exposure. ROS production, accompanied by induction of redox-related genes, triggered apoptosis and cell cycle arrest, as reported in CYP-treated male mice, which, after ROS increased, showed up-regulation of the mRNA levels of SOD genes and Glutathione S-transferases (Jin et al., 2011b); similarly, human intestinal Caco-2 cells showed an increase in *Cat*, *Gpx* and *Sod* mRNAs upon exposure to other pyrethroid pesticides (Ilboudo et al., 2014). In parallel, CYP also triggered the detoxification endogenous mechanisms (Birben et al., 2012; Marouani et al., 2011; Omiecinski et al., 2011). The fast induction of cytochrome P450 *Cyp1a1* phase I and of Gsta1 and Ugt1a6 Phase II enzymes in 3T3NIH cells, allowed a rapid detoxification from CYP and the recovery of CTR phenotype in terms of cell growth. Our findings are in agreement with others reported for differentiated cell lines, when exposed either to CYP or other pesticides (Hodgson, 2012; Medina-Díaz et al., 2011), suggesting that in 3T3NIH differentiated cells the mechanism of detoxification was activated within 24 h of exposure, likely mediated by *Cyp1a1* gene induction. Differently, in R1 CYP-exposed cells, the expression of only *Cyp1b1* phase I gene was induced, as late as 72h exposure. These results might be explained assuming that i) the mechanism of detoxification of pyrethroids in undifferentiated stem cells is mediated by other members of cytochrome P450 family, such as *cyp1b1* (our results) or *Cyp9a10* (Hafeez et al., 2019), and not directly by *cyp1a1* or, alternatively, that ii) in undifferentiated stem cells, the activation of detoxification response mechanisms might be very slow and delayed in time (after 72 h exposure), since, immediately after CYP exposure, apoptosis and cell cycle arrest prevailed to eliminate damaged cells. The phase II *Nqo1*, *Gsta1* and *Ugt1a6* genes, which have a major role in the detoxification of many endobiotic and xenobiotic molecules including pesticides (Hodgson, 2012; Kiang et al., 2005), were induced and involved in CYP elimination also in undifferentiated R1 ESC cells. Alternatively, in undifferentiated R1 ESCs, iii) phase II Nqo1, Gsta1 and Ugt1a6 genes, which have a major role in the detoxification of many endobiotic and xenobiotic molecules including pesticides (Kiang et al., 2005; Hodgson, 2012), were directly induced within 24h exposure by Nuclear

factor erythroid 2-related factor 2 (Nrf2), a transcription factor that modulates antioxidant defence mechanism (He et al., 2015), as reported for other pollutant (Zhang et al., 2014), bypassing the activation of phase I genes.

In conclusion, the present study evidenced that exposure to the pyrethroid cypermethrin induces high toxic effects and cellular response in embryonic stem cells, a robust *in vitro* model of the very early stages of mammalian development. Our findings provide information that will be useful to improve our understanding of the effects of this widely diffused insecticide on early mammalian embryonic development and set the basis to investigate whether exposure to this chemical could affect the developmental potential of mESCs.

6 CONCLUSION

During my PhD work, I showed that ESCs - an in vitro model of the inner cell mass- and the cardiomyocytes obtained after 15 days of their in vitro differentiation are a valuable platform to study the effects of EDs (i.e., ATO, Aroclor 1254 and CYP) exposure.

In summary, the results obtained demonstrated that, on differentiated cardiomyocytes, ATO alters the contractile properties, the sarcomere structure, the expression and localization of connexins of cardiac syncytia. Aroclor 1254 interferes with the calcium-induced calcium-release mechanism (Ca2+ toolkit) of cardiomyocytes. On ESCs, CYP induces cell death and ROS production, interferes with cell growth and activates Phase II detoxification-response genes.

A further novelty of my work is the adaptation of the whole mount immunofluorescence technique to the organization of embryoid bodies. To this very complex cellular organization I applied bioinformatics tools to quantitatively evaluate, for the first time in a 3D context, morphological parameters useful to the understanding of the cellular response to EDs.

The results presented in this thesis work are preliminary, but necessary, to set the basis to further unravel the molecular mechanisms of toxicity induced following EDs exposure. Furthermore, they represent a starting point for understanding and deepening the hypothesis of a foetal origin of cardiac disease. To this purpose, it will be necessary, in the future, to investigate the presence of potential epigenetic modifications, which include changes in DNA methylation patterns, modification of histones and altered microRNAs expression levels that target the receptors or their signaling pathways. These epigenetic modifications, which can occur during perinatal life, might play key roles in the development of young adulthood diseases.

These studies were conducted on mouse cells but, in the future, it would be of extreme interest to translate these findings to humans. To this regard, the technology of induced pluripotent stem cells (iPSCs) and their differentiation in cardiomyocytes represents a useful model to verify whether exposure to EDs affects also human embryonic development and the functional and structural features of cardiomyocytes.

7 BIBLIOGRAPHY

Abernathy, C.O., Thomas, D.J., and Calderon, R.L. (2003). Health effects and risk assessment of arsenic. J. Nutr. *133*, 1536S-8S.

Agudo, A., Goñi, F., Etxeandia, A., Vives, A., Millán, E., López, R., Amiano, P., Ardanaz, E., Barricarte, A., Chirlaque, M.D., et al. (2009). Polychlorinated biphenyls in Spanish adults: determinants of serum concentrations. Environ. Res. *109*, 620–628.

Akelma, H., Kilic, E.T., Salik, F., Bicak, E.A., and Yektas, A. (2019). Pyrethroid intoxication: A rare case report and literature review. Nigerian Journal of Clinical Practice *22*, 442.

Alissa, E.M., and Ferns, G.A. (2011). Heavy metal poisoning and cardiovascular disease. J Toxicol*2011*, 870125.

AlKahtane, A.A., Alarifi, S., Al-Qahtani, A.A., Ali, D., Alomar, S.Y., Aleissia, M.S., and Alkahtani, S. (2018). Cytotoxicity and Genotoxicity of Cypermethrin in Hepatocarcinoma Cells: A Dose- and Time-Dependent Study. Dose Response *16*.

Aposhian, H.V., and Aposhian, M.M. (2006). Arsenic toxicology: five questions. Chem. Res. Toxicol. *19*, 1–15.

Ardeshir, A., Narayan, N.R., Méndez-Lagares, G., Lu, D., Rauch, M., Huang, Y., Van Rompay, K.K.A., Lynch, S.V., and Hartigan-O'Connor, D.J. (2014). Breast-fed and bottle-fed infant rhesus macaques develop distinct gut microbiotas and immune systems. Sci Transl Med *6*, 252ra120.

Arnold, S.J., and Robertson, E.J. (2009). Making a commitment: cell lineage allocation and axis patterning in the early mouse embryo. Nat. Rev. Mol. Cell Biol. *10*, 91–103.

Balakumar, P., and Kaur, J. (2009). Arsenic exposure and cardiovascular disorders: an overview. Cardiovasc. Toxicol. *9*, 169–176.

Balcombe, J.P., Barnard, N.D., and Sandusky, C. (2004). Laboratory Routines Cause Animal Stress. *43*, 10.

Barker, D.J. (1990). The foetaland infant origins of adult disease. BMJ *301*, 1111.

Barker, D.J., and Osmond, C. (1986). Infant mortality, childhood nutrition, and ischaemic heart disease in England and Wales. Lancet *1*, 1077–1081.

Barker, D.J.P., and Thornburg, K.L. (2013). The obstetric origins of health for a lifetime. Clin ObstetGynecol*56*, 511–519.

Barker, D.J., Winter, P.D., Osmond, C., Margetts, B., and Simmonds, S.J. (1989). Weight in infancy and death from ischaemic heart disease. Lancet *2*, 577–580.

Barker, D.J.P., Gelow, J., Thornburg, K., Osmond, C., Kajantie, E., and Eriksson, J.G. (2010). The early origins of chronic heart failure: impaired placental growth and initiation of insulin resistance in childhood. Eur. J. Heart Fail. *12*, 819–825.

Beldade, P., Mateus, A.R.A., and Keller, R.A. (2011). Evolution and molecular mechanisms of adaptive developmental plasticity. Molecular Ecology *20*, 1347–1363.

Bergman, Å., United Nations Environment Programme, and World Health Organization (2013). State of the science of endocrine disrupting chemicals - 2012 an assessment of the state of the science of endocrine disruptors (Geneva: WHO: UNEP).

Bhattacharjee, S., Fakhruddin, A.N.M., Chowdhury, M. a. Z., Rahman, M.A., and Alam, M.K. (2012). Monitoring of selected pesticides residue levels in water samples of paddy fields and removal of cypermethrin and chlorpyrifos residues from water using rice bran. Bull Environ ContamToxicol*89*, 348–353.

Birben, E., Sahiner, U.M., Sackesen, C., Erzurum, S., and Kalayci, O. (2012). Oxidative stress and antioxidant defense. World Allergy Organ J *5*, 9–19.

Bode, A.M., and Dong, Z. (2002). The paradox of arsenic: molecular mechanisms of cell transformation and chemotherapeutic effects. Crit. Rev. Oncol. Hematol. *42*, 5–24.

Bodwell, J.E., Kingsley, L.A., and Hamilton, J.W. (2004). Arsenic at very low concentrations alters glucocorticoid receptor (GR)-mediated gene activation but not GR-mediated gene repression: complex dose-response effects are

closely correlated with levels of activated GR and require a functional GR DNA binding domain. Chem. Res. Toxicol. *17*, 1064–1076.

Boheler, K.R., Czyz, J., Tweedie, D., Yang, H.-T., Anisimov, S.V., and Wobus, A.M. (2002). Differentiation of pluripotent embryonic stem cells into cardiomyocytes. Circ. Res. *91*, 189–201.

Bolker, J.A. (1995). Model systems in developmental biology. Bioessays*17*, 451–455.

Bondue, A., Lapouge, G., Paulissen, C., Semeraro, C., Iacovino, M., Kyba, M., and Blanpain, C. (2008). Mesp1 acts as a master regulator of multipotent cardiovascular progenitor specification. Cell Stem Cell *3*, 69–84.

Bradberry, S.M., Cage, S.A., Proudfoot, A.T., and Vale, J.A. (2005). Poisoning due to pyrethroids. Toxicol Rev *24*, 93–106.

Bradshaw, A.D. (2006). Unravelling phenotypic plasticity -- why should we bother? New Phytol. *170*, 644–648.

Brakefield, P.M., Gates, J., Keys, D., Kesbeke, F., Wijngaarden, P.J., Montelro, A., French, V., and Carroll, S.B. (1996). Development, plasticity and evolution of butterfly eyespot patterns. Nature *384*, 236–242.

Brand, T. (2003). Heart development: molecular insights into cardiac specification and early morphogenesis. Dev. Biol. *258*, 1–19.

Bremer, S., Cortvrindt, R., Daston, G., Eletti, B., Mantovani, A., Maranghi, F., Pelkonen, O., Ruhdel, I., and Spielmann, H. (2005). Reproductive and developmental toxicity. Altern Lab Anim*33 Suppl 1*, 183–209.

Brown, N., Spielmann, H., Bechter, R., Flint, O.P., Freeman, S.J., Jelinek, R.J., Koch, E., Nau, H., Newall, D.R., Palmer, A.K., et al. (1995). Screening chemicals for reproductive toxicity: The current alternatives. The report and recommendations of an ECVAM/ETS Workshop (ECVAM Workshop 12). ATLA Alternatives to Laboratory Animals *23*, 868–882.

Bry, L., Falk, P.G., Midtvedt, T., and Gordon, J.I. (1996). A model of host-microbial interactions in an open mammalian ecosystem. Science *273*, 1380–1383.

Buckingham, M., Meilhac, S., and Zaffran, S. (2005). Building the mammalian heart from two sources of myocardial cells. Nat. Rev. Genet. *6*, 826–835.

Burridge, P.W., Keller, G., Gold, J.D., and Wu, J.C. (2012). Production of de novo cardiomyocytes: human pluripotent stem cell differentiation and direct reprogramming. Cell Stem Cell *10*, 16–28.

Burton, G.J., Fowden, A.L., and Thornburg, K.L. (2016). Placental Origins of Chronic Disease. Physiol. Rev. *96*, 1509–1565.

Calafat, A.M., and Needham, L.L. (2007). Human Exposures and Body Burdens of Endocrine-Disrupting Chemicals. In Endocrine-Disrupting Chemicals, A.C. Gore, ed. (Totowa, NJ: Humana Press), pp. 253–268.

Carlin, D.J., Naujokas, M.F., Bradham, K.D., Cowden, J., Heacock, M., Henry, H.F., Lee, J.S., Thomas, D.J., Thompson, C., Tokar, E.J., et al. (2016). Arsenic and Environmental Health: State of the Science and Future Research Opportunities. Environ. Health Perspect. *124*, 890–899.

Cervantes, C., Ji, G., Ramírez, J.L., and Silver, S. (1994). Resistance to arsenic compounds in microorganisms. FEMS Microbiol. Rev. *15*, 355–367.

Chang, S.I., Jin, B., Youn, P., Park, C., Park, J.-D., and Ryu, D.-Y. (2007). Arsenic-induced toxicity and the protective role of ascorbic acid in mouse testis. Toxicol. Appl. Pharmacol. *218*, 196–203.

Chelu, M.G., Danila, C.I., Gilman, C.P., and Hamilton, S.L. (2004). Regulation of ryanodine receptors by FK506 binding proteins. Trends Cardiovasc. Med. *14*, 227–234.

Chen, M., and Zhang, L. (2011). Epigenetic mechanisms in developmental programming of adult disease. Drug Discov Today *16*, 1007–1018.

Chen, V.C., Stull, R., Joo, D., Cheng, X., and Keller, G. (2008). Notch signalingrespecifies the hemangioblast to a cardiac fate. Nat. Biotechnol. *26*, 1169–1178.

Chernoff, N., and Kavlock, R.J. (1982). An in vivo teratology screen utilizing pregnant mice. J Toxicol Environ Health *10*, 541–550.

Cheung, Y.-T., Lau, W.K.-W., Yu, M.-S., Lai, C.S.-W., Yeung, S.-C., So, K.-F., and Chang, R.C.-C. (2009). Effects of all-trans-retinoic acid on human SH-SY5Y neuroblastoma as in vitro model in neurotoxicity research. Neurotoxicology *30*, 127–135.

Choudhury, B.H., Das, B.K., and Chutia, P. (2013). Evaluation of pesticide residues in fish tissue samples collected from different markets of Jorhat district of Assam, India. *4*, 14.

Christoffels, V.M., Habets, P.E., Franco, D., Campione, M., de Jong, F., Lamers, W.H., Bao, Z.Z., Palmer, S., Biben, C., Harvey, R.P., et al. (2000). Chamber formation and morphogenesis in the developing mammalian heart. Dev. Biol. *223*, 266–278.

Concha, G., Vogler, G., Lezcano, D., Nermell, B., and Vahter, M. (1998). Exposure to inorganic arsenic metabolites during early human development. Toxicol. Sci. *44*, 185–190.

Costello, I., Pimeisl, I.-M., Dräger, S., Bikoff, E.K., Robertson, E.J., and Arnold, S.J. (2011). The T-box transcription factor Eomesodermin acts upstream of Mesp1 to specify cardiac mesoderm during mouse gastrulation. Nat. Cell Biol. *13*, 1084–1091.

Cota, B.M., and Allen, P.J. (2010). The developmental origins of health and disease hypothesis. PediatrNurs*36*, 157–167.

Cunny, H., and Hodgson, E. (2004). Toxicity Testing. In A Textbook of Modern Toxicology, (John Wiley & Sons, Ltd), pp. 351–397.

Dally, A. (1998). Thalidomide: was the tragedy preventable? Lancet *351*, 1197–1199.

David, R., Jarsch, V.B., Schwarz, F., Nathan, P., Gegg, M., Lickert, H., and Franz, W.-M. (2011). Induction of MesP1 by Brachyury(T) generates the common multipotent cardiovascular stem cell. Cardiovasc. Res. *92*, 115–122.

De Coster, S., and van Larebeke, N. (2012). Endocrine-Disrupting Chemicals: Associated Disorders and Mechanisms of Action. Journal of Environmental and Public Health *2012*, 1–52.

Debbab, M., Hajjaji, S.E., Aly, A.H., Dahchour, A., Azzouzi, M.E., and Zrineh, A. (2014). Cypermethrin Residues in Fresh Vegetables: Detection by HPLC and LC- ESIMS and their Effect on Antioxidant Activity. 8.

Diamanti-Kandarakis, E., Bourguignon, J.-P., Giudice, L.C., Hauser, R., Prins, G.S., Soto, A.M., Zoeller, R.T., and Gore, A.C. (2009). Endocrine-disrupting chemicals: an Endocrine Society scientific statement. Endocr. Rev. *30*, 293–342.

Dierickx, P., Doevendans, P.A., Geijsen, N., and van Laake, L.W. (2012). Embryonic Template-Based Generation and Purification of Pluripotent Stem Cell-Derived Cardiomyocytes for Heart Repair. J. of Cardiovasc. Trans. Res. *5*, 566–580.

Doetschman, T.C., Eistetter, H., Katz, M., Schmidt, W., and Kemler, R. (1985). The in vitro development of blastocyst-derived embryonic stem cell lines: formation of visceral yolk sac, blood islands and myocardium. J Embryol Exp Morphol*87*, 27–45.

Drolet, B., Simard, C., and Roden, D.M. (2004). Unusual effects of a QT-prolonging drug, arsenic trioxide, on cardiac potassium currents. Circulation *109*, 26–29.

Ducas, R.A., Seftel, M.D., Ducas, J., and Seifer, C. (2011). Monomorphic ventricular tachycardia caused by arsenic trioxide therapy for acute promyelocytic leukaemia. J R Coll Physicians Edinb*41*, 117–118.

Evans, M.J., and Kaufman, M.H. (1981). Establishment in culture of pluripotential cells from mouse embryos. Nature *292*, 154–156.

Fassina, L., Di Grazia, A., Naro, F., Monaco, L., De Angelis, M.G.C., and Magenes, G. (2011). Video evaluation of the kinematics and dynamics of the beating cardiac syncytium: an alternative to the Langendorff method. Int J Artif Organs *34*, 546–558.

Fässler, R., Rohwedel, J., Maltsev, V., Bloch, W., Lentini, S., Guan, K., Gullberg, D., Hescheler, J., Addicks, K., and Wobus, A.M. (1996). Differentiation and integrity of cardiac muscle cells are impaired in the absence of beta 1 integrin. J. Cell. Sci. *109 (Pt 13)*, 2989–2999.

Feo, M.L., Eljarrat, E., and Barceló, D. (2011). Performance of gas chromatography/tandem mass spectrometry in the analysis of pyrethroid insecticides in environmental and food samples. Rapid Communications in Mass Spectrometry *25*, 869–876.

Fisher, R.A. (1921). 014: On the "Probable Error" of a Coefficient of Correlation Deduced from a Small Sample.

Flecknell, P. (2002). Replacement, reduction and refinement. ALTEX *19*, 73–78.

Flint, O.P., and Orton, T.C. (1984). An in vitro assay for teratogens with cultures of rat embryo midbrain and limb bud cells. Toxicol. Appl. Pharmacol. *76*, 383–395.

Flora, S.J. (2009). Structural, chemical and biological aspects of antioxidants for strategies against metal and metalloid exposure. Oxid Med Cell Longev*2*, 191–206.

Fu, J.-D., Li, J., Tweedie, D., Yu, H.-M., Chen, L., Wang, R., Riordon, D.R., Brugh, S.A., Wang, S.-Q., Boheler, K.R., et al. (2006). Crucial role of the sarcoplasmic reticulum in the developmental regulation of Ca2+ transients and contraction in cardiomyocytes derived from embryonic stem cells. FASEB J. *20*, 181–183.

Garcia-Martinez, V., and Schoenwolf, G.C. (1993). Primitive-streak origin of the cardiovascular system in avian embryos. Dev. Biol. *159*, 706–719.

Genschow, E., Spielmann, H., Scholz, G., Seiler, A., Brown, N., Piersma, A., Brady, M., Clemann, N., Huuskonen, H., Paillard, F., et al. (2002). The ECVAM international validation study on in vitro embryotoxicity tests: results of the definitive phase and evaluation of prediction models. European Centre for the Validation of Alternative Methods. Altern Lab Anim*30*, 151–176.

Genschow, E., Spielmann, H., Scholz, G., Pohl, I., Seiler, A., Clemann, N., Bremer, S., and Becker, K. (2004). Validation of the embryonic stem cell test in the International ECVAM Validation Study on three in vitro embryotoxicity tests. Alternatives to Laboratory Animals: ATLA *32*, 209–244.

Gerloff, K., Pereira, D.I.A., Faria, N., Boots, A.W., Kolling, J., Förster, I., Albrecht, C., Powell, J.J., and Schins, R.P.F. (2013). Influence of simulated gastro-intestinal conditions on particle-induced cytotoxicity and interleukin-8 regulation in differentiated and undifferentiated Caco-2 cells. Nanotoxicology *7*, 353–366.

Gilbert, S.F. (2001). Ecological developmental biology: developmental biology meets the real world. Dev. Biol. *233*, 1–12.

Gilbert, S.F. (2002). The genome in its ecological context: philosophical perspectives on interspecies epigenesis. Ann. N. Y. Acad. Sci. *981*, 202–218.

Gilbert, S.F. (2005). Mechanisms for the environmental regulation of gene expression: ecological aspects of animal development. J. Biosci. *30*, 65–74.

Gilbert, S.F. (2012). Ecological developmental biology: environmental signals for normal animal development. Evol. Dev. *14*, 20–28.

Gilbert, S.F. (2016). Developmental Plasticity and Developmental Symbiosis: The Return of Eco-Devo. Curr. Top. Dev. Biol. *116*, 415–433.

Gilden, R.C. (2010). Pesticides use in hospitals: health protection, health hazards, and viable alternatives. NursAdm Q *34*, 320–326.

Giray, B., Gürbay, A., and Hincal, F. (2001). Cypermethrin-induced oxidative stress in rat brain and liver is prevented by vitamin E or allopurinol. Toxicol. Lett. *118*, 139–146.

Gore, A.C., Chappell, V.A., Fenton, S.E., Flaws, J.A., Nadal, A., Prins, G.S., Toppari, J., and Zoeller, R.T. (2015). EDC-2: The Endocrine Society's Second Scientific Statement on Endocrine-Disrupting Chemicals. Endocr. Rev. *36*, E1–E150.

Graf, U., Casanova, E.A., and Cinelli, P. (2011). The Role of the Leukemia Inhibitory Factor (LIF) - Pathway in Derivation and Maintenance of Murine Pluripotent Stem Cells. Genes (Basel) *2*, 280–297.

Gregg, N.M. (1991). Congenital cataract following German measles in the mother. 1941. Epidemiol. Infect. *107*, iii–xiv; discussion xiii-xiv.

Grimm, F.A., Hu, D., Kania-Korwel, I., Lehmler, H.-J., Ludewig, G., Hornbuckle, K.C., Duffel, M.W., Bergman, Å., and Robertson, L.W. (2015). Metabolism and metabolites of polychlorinated biphenyls. Crit. Rev. Toxicol. *45*, 245–272.

Hafeez, M., Liu, S., Jan, S., Shi, L., Fernández-Grandon, G.M., Gulzar, A., Ali, B., Rehman, M., and Wang, M. (2019). Knock-Down of Gossypol-Inducing Cytochrome P450 Genes Reduced Deltamethrin Sensitivity in Spodopteraexigua (Hübner). Int J Mol Sci *20*.

Halem, D. van, Bakker, S.A., Amy, G.L., and Dijk, J.C. van (2009). Arsenic in drinking water: a worldwide water quality concern for water supply companies. Drinking Water Engineering and Science *2*, 29–34.

Hales, C.N., and Barker, D.J. (2001). The thrifty phenotype hypothesis. Br. Med. Bull. *60*, 5–20.

Hartung, T. (2008). Thoughts on limitations of animal models. Parkinsonism Relat. Disord. *14 Suppl 2*, S81-83.

He, J.-L., Zhou, Z.-W., Yin, J.-J., He, C.-Q., Zhou, S.-F., and Yu, Y. (2015). Schisandra chinensis regulates drug metabolizing enzymes and drug transporters via activation of Nrf2-mediated signaling pathway. Drug Des DevelTher*9*, 127–146.

Hescheler, J., Fleischmann, B.K., Lentini, S., Maltsev, V.A., Rohwedel, J., Wobus, A.M., and Addicks, K. (1997). Embryonic stem cells: a model to study structural and functional properties in cardiomyogenesis. Cardiovasc. Res. *36*, 149–162.

Hocine, L., Merzouk, H., Merzouk, S.A., Ghorzi, H., Youbi, M., and Narce, M. (2016). The effects of alpha-cypermethrin exposure on biochemical and redox parameters in pregnant rats and their newborns. PesticBiochemPhysiol*134*, 49–54.

Hodgson, E. (2012). Metabolic Interactions of Environmental Toxicants in Humans. In Progress in Molecular Biology and Translational Science, (Elsevier), pp. 349–372.

Hoffman, J.A., and Merrill, B.J. (2007). New and renewed perspectives on embryonic stem cell pluripotency. Front. Biosci. *12*, 3321–3332.

Huang, F., Liu, Q., Xie, S., Xu, J., Huang, B., Wu, Y., and Xia, D. (2016). Cypermethrin Induces Macrophages Death through Cell Cycle Arrest and Oxidative Stress-Mediated JNK/ERK Signaling Regulated Apoptosis. Int J Mol Sci *17*.

Huen, K., Bradman, A., Harley, K., Yousefi, P., Boyd Barr, D., Eskenazi, B., and Holland, N. (2012). Organophosphate pesticide levels in blood and urine of women and newborns living in an agricultural community. Environ. Res. *117*, 8–16.

Hughes, M.F., Beck, B.D., Chen, Y., Lewis, A.S., and Thomas, D.J. (2011). Arsenic exposure and toxicology: a historical perspective. Toxicol. Sci. *123*, 305–332.

Hussain, A., Das Sarma, S., Babu, S., Pal, D., and Das Sarma, J. (2018). Interaction of arsenic with gap junction protein connexin 43 alters gap junctional

intercellular communication. BiochimBiophys Acta Mol Cell Res *1865*, 1423–1436.

Ilboudo, H., Bras-Gonçalves, R., Camara, M., Flori, L., Camara, O., Sakande, H., Leno, M., Petitdidier, E., Jamonneau, V., and Bucheton, B. (2014). Unravelling Human Trypanotolerance: IL8 is Associated with Infection Control whereas IL10 and TNFα Are Associated with Subsequent Disease Development. PLOS Pathogens *10*, e1004469.

Inglefield, J.R., Mundy, W.R., and Shafer, T.J. (2001). Inositol 1,4,5-triphosphate receptor-sensitive $Ca(2^+)$ release, store-operated $Ca(2^+)$ entry, and cAMP responsive element binding protein phosphorylation in developing cortical cells following exposure to polychlorinated biphenyls. J. Pharmacol. Exp. Ther. *297*, 762–773.

Itskovitz-Eldor, J., Schuldiner, M., Karsenti, D., Eden, A., Yanuka, O., Amit, M., Soreq, H., and Benvenisty, N. (2000). Differentiation of human embryonic stem cells into embryoid bodies compromising the three embryonic germ layers. Mol. Med. *6*, 88–95.

Izdebska, M., Klimaszewska-Wiśniewska, A., Lewandowski, D., Marcin Nowak, J., Gagat, M., and Grzanka, A. (2014). Arsenic trioxide preferentially induces nonapoptotic cell deaths as well as actin cytoskeleton rearrangement in the CHO AA8 cell line. PostepyHig Med Dosw (Online) *68*, 1492–1500.

Jin, Y., Wang, L., Ruan, M., Liu, J., Yang, Y., Zhou, C., Xu, B., and Fu, Z. (2011a). Cypermethrin exposure during puberty induces oxidative stress and endocrine disruption in male mice. Chemosphere *84*, 124–130.

Jin, Y., Zheng, S., Pu, Y., Shu, L., Sun, L., Liu, W., and Fu, Z. (2011b). Cypermethrin has the potential to induce hepatic oxidative stress, DNA damage and apoptosis in adult zebrafish (Danio rerio). Chemosphere *82*, 398–404.

Jirtle, R.L., and Skinner, M.K. (2007). Environmental epigenomics and disease susceptibility. Nat. Rev. Genet. *8*, 253–262.

Jomova, K., and Valko, M. (2011). Advances in metal-induced oxidative stress and human disease. Toxicology *283*, 65–87.

Jukam, D., Shariati, S.A.M., and Skotheim, J.M. (2017). Zygotic Genome Activation in Vertebrates. Dev. Cell *42*, 316–332.

Kabir, E.R., Rahman, M.S., and Rahman, I. (2015). A review on endocrine disruptors and their possible impacts on human health. Environ. Toxicol. Pharmacol. *40*, 241–258.

Kaltreider, R.C., Davis, A.M., Lariviere, J.P., and Hamilton, J.W. (2001). Arsenic alters the function of the glucocorticoid receptor as a transcription factor. Environ. Health Perspect. *109*, 245–251.

Kandárová, H., and Letašiová, S. (2011). Alternative methods in toxicology: pre-validated and validated methods. InterdiscipToxicol*4*, 107–113.

Kang, J.-H., Park, I.-S., Oh, W.-Y., Lim, H.-K., Wang, S.-Y., Lee, S.Y., Choi, K.H., Kim, J., Jung, S.-Y., Suh, C.K., et al. (2004). Inhibition of aroclor 1254-induced depletion of stored calcium prevents the cell death in catecholaminergic cells. Toxicology *200*, 93–101.

Kavlock, R.J., Daston, G.P., DeRosa, C., Fenner-Crisp, P., Gray, L.E., Kaattari, S., Lucier, G., Luster, M., Mac, M.J., Maczka, C., et al. (1996). Research needs for the risk assessment of health and environmental effects of endocrine disruptors: a report of the U.S. EPA-sponsored workshop. Environ. Health Perspect. *104 Suppl 4*, 715–740.

Keller, G. (2005). Embryonic stem cell differentiation: emergence of a new era in biology and medicine. Genes Dev. *19*, 1129–1155.

Kelly, R.G., and Buckingham, M.E. (2002). The anterior heart-forming field: voyage to the arterial pole of the heart. Trends Genet. *18*, 210–216.

Kezios, K.L., Liu, X., Cirillio, P.M., Kalantzi, O.I., Wang, Y., Petreas, M.X., Park, J.-S., Bradwin, G., Cohn, B.A., and Factor-Litvak, P. (2012). Prenatal polychlorinated biphenyl exposure is associated with decreased gestational length but not birth weight: archived samples from the Child Health and Development Studies pregnancy cohort. Environ Health *11*, 49.

Khwanraj, K., Phruksaniyom, C., Madlah, S., and Dharmasaroja, P. (2015). Differential Expression of Tyrosine Hydroxylase Protein and Apoptosis-Related Genes in Differentiated and Undifferentiated SH-SY5Y Neuroblastoma Cells Treated with MPP+. Neurol Res Int *2015*.

Kiang, T.K.L., Ensom, M.H.H., and Chang, T.K.H. (2005). UDP-glucuronosyltransferases and clinical drug-drug interactions. Pharmacol. Ther. *106*, 97–132.

Kim, T.-W., Che, J.-H., and Yun, J.-W. (2019). Use of stem cells as alternative methods to animal experimentation in predictive toxicology. Regul. Toxicol. Pharmacol. *105*, 15–29.

Kitchin, K.T. (2001). Recent advances in arsenic carcinogenesis: modes of action, animal model systems, and methylated arsenic metabolites. Toxicol. Appl. Pharmacol. *172*, 249–261.

Kleinjans, J., Botsivali, M., Kogevinas, M., Merlo, D.F., and NewGeneris consortium (2015). Foetalexposure to dietary carcinogens and risk of childhood cancer: what the NewGeneris project tells us. BMJ *351*, h4501.

Kodavanti, P.R.S. (2006). Neurotoxicity of persistent organic pollutants: possible mode(s) of action and further considerations. Dose Response *3*, 273–305.

Kodavanti, P.R., Derr-Yellin, E.C., Mundy, W.R., Shafer, T.J., Herr, D.W., Barone, S., Choksi, N.Y., MacPhail, R.C., and Tilson, H.A. (1998). Repeated exposure of adult rats to Aroclor 1254 causes brain region-specific changes in intracellular Ca2+ buffering and protein kinase C activity in the absence of changes in tyrosine hydroxylase. Toxicol. Appl. Pharmacol. *153*, 186–198.

Koopman-Esseboom, C., Morse, D.C., Weisglas-Kuperus, N., Lutkeschipholt, I.J., Van der Paauw, C.G., Tuinstra, L.G., Brouwer, A., and Sauer, P.J. (1994). Effects of dioxins and polychlorinated biphenyls on thyroid hormone status of pregnant women and their infants. Pediatr. Res. *36*, 468–473.

Koot, Y.E.M., Teklenburg, G., Salker, M.S., Brosens, J.J., and Macklon, N.S. (2012). Molecular aspects of implantation failure. Biochim. Biophys. Acta *1822*, 1943–1950.

Kopljar, I., De Bondt, A., Vinken, P., Teisman, A., Damiano, B., Goeminne, N., Van den Wyngaert, I., Gallacher, D.J., and Lu, H.R. (2017). Chronic drug-induced effects on contractile motion properties and cardiac biomarkers in human induced pluripotent stem cell-derived cardiomyocytes. Br. J. Pharmacol. *174*, 3766–3779.

Kuo, P.-L., Lee, H., Bray, M.-A., Geisse, N.A., Huang, Y.-T., Adams, W.J., Sheehy, S.P., and Parker, K.K. (2012). Myocyte shape regulates lateral registry of sarcomeres and contractility. Am. J. Pathol. *181*, 2030–2037.

La Merrill, M.A., Sethi, S., Benard, L., Moshier, E., Haraldsson, B., and Buettner, C. (2016). Perinatal DDT Exposure Induces Hypertension and Cardiac Hypertrophy in Adult Mice. Environ. Health Perspect. *124*, 1722–1727.

Langley, G. The Validity of Animal Experiments in Medical Research. 6.

Langley-Evans, S.C., and McMullen, S. (2010). Developmental origins of adult disease. Med PrincPract*19*, 87–98.

Lesiak, A., Zhu, M., Chen, H., Appleyard, S.M., Impey, S., Lein, P.J., and Wayman, G.A. (2014). The Environmental Neurotoxicant PCB 95 Promotes Synaptogenesis via Ryanodine Receptor-Dependent miR132 Upregulation. J. Neurosci. *34*, 717–725.

Levkovitz, R., Zaretsky, U., Gordon, Z., Jaffa, A.J., and Elad, D. (2013). In vitro simulation of placental transport: part I. Biological model of the placental barrier. Placenta *34*, 699–707.

Lubrano, C., Genovesi, G., Specchia, P., Costantini, D., Mariani, S., Petrangeli, E., Lenzi, A., and Gnessi, L. (2013). Obesity and metabolic comorbidities: environmental diseases? Oxid Med Cell Longev*2013*, 640673.

Lyytinen, A., Brakefield, P.M., Lindström, L., and Mappes, J. (2004). Does predation maintain eyespot plasticity in Bicyclusanynana? Proc. Biol. Sci. *271*, 279–283.

Manfo, F.P.T., Moundipa, P.F., Déchaud, H., Tchana, A.N., Nantia, E.A., Zabot, M.-T., and Pugeat, M. (2012). Effect of agropesticides use on male reproductive function: a study on farmers in Djutitsa (Cameroon). Environ. Toxicol. *27*, 423–432.

Marettova, E., Maretta, M., and Legáth, J. (2017). Effect of pyrethroids on female genital system. Review. Anim. Reprod. Sci. *184*, 132–138.

Marouani, N., Tebourbi, O., Mokni, M., Yacoubi, M.T., Sakly, M., Benkhalifa, M., and Ben Rhouma, K. (2011). Embryotoxicity and fetotoxicity following intraperitoneal administrations of hexavalent chromium to pregnant rats. Zygote *19*, 229–235.

Martin, A.F. (1981). Turnover of cardiac troponin subunits. Kinetic evidence for a precursor pool of troponin-I. J. Biol. Chem. *256*, 964–968.

Matthews, R.A. (2008). Medical progress depends on animal models - doesn't it? J R Soc Med *101*, 95–98.

McFall-Ngai, M., Heath-Heckman, E.A.C., Gillette, A.A., Peyer, S.M., and Harvie, E.A. (2012). The secret languages of coevolved symbioses: insights from the Euprymnascolopes-Vibrio fischeri symbiosis. Semin. Immunol. *24*, 3–8.

McMillen, I.C., and Robinson, J.S. (2005). Developmental origins of the metabolic syndrome: prediction, plasticity, and programming. Physiol. Rev. *85*, 571–633.

McMullen, S., and Mostyn, A. (2009a). Animal models for the study of the developmental origins of health and disease. Proc Nutr Soc *68*, 306–320.

McMullen, S., and Mostyn, A. (2009b). Animal models for the study of the developmental origins of health and disease. Proc Nutr Soc *68*, 306–320.

Medina-Díaz, I.M., Rubio-Ortíz, M., Martínez-Guzmán, M.C., Dávalos-Ibarra, R.L., Rojas- García, A.E., Robledo-Marenco, M.L., Barrón-Vivanco, B.S., Girón-Pérez, M.I., and Elizondo, G. (2011). Organophosphate pesticides increase the expression of alpha glutathione S-transferase in HepG2 cells. Toxicology in Vitro *25*, 2074–2079.

Meilhac, S.M., Lescroart, F., Blanpain, C., and Buckingham, M.E. (2014). Cardiac cell lineages that form the heart. Cold Spring HarbPerspect Med *4*, a013888.

Monneret, C. (2017). What is an endocrine disruptor? C. R. Biol. *340*, 403–405.

Monteiro, A., Chen, B., Ramos, D.M., Oliver, J.C., Tong, X., Guo, M., Wang, W.-K., Fazzino, L., and Kamal, F. (2013). Distal-Less Regulates Eyespot Patterns and Melanization in Bicyclus Butterflies. Journal of Experimental Zoology Part B: Molecular and Developmental Evolution *320*, 321–331.

Monti, M. (2016). Gamete and Embryo-FoetalOrigins of Adult Diseases. Eur J Histochem*60*.

Mummery, C.L., Zhang, J., Ng, E.S., Elliott, D.A., Elefanty, A.G., and Kamp, T.J. (2012). Differentiation of human embryonic stem cells and induced pluripotent stem cells to cardiomyocytes: a methods overview. Circ. Res. *111*, 344–358.

Mundy, W.R., Shafer, T.J., Tilson, H.A., and Kodavanti, P.R. (1999). Extracellular calcium is required for the polychlorinated biphenyl-induced increase of

intracellular free calcium levels in cerebellar granule cell culture. Toxicology *136*, 27–39.

Murphy, S.K., and Jirtle, R.L. (2003). Imprinting evolution and the price of silence. Bioessays*25*, 577–588.

Muthumani, M., and Prabu, S.M. (2014). Silibinin potentially attenuates arsenic-induced oxidative stress mediated cardiotoxicity and dyslipidemia in rats. Cardiovasc. Toxicol. *14*, 83–97.

Myöhänen, K., and Vähäkangas, K. (2012). Foetal exposure to food and environmental carcinogens in human beings. Basic Clin. Pharmacol. Toxicol. *110*, 101–112.

Nakanishi, T., Seguchi, M., and Takao, A. (1988). Development of the myocardial contractile system. Experientia*44*, 936–944.

Nantia Akono, E., KadaSanda, A., ManfoTsague, F.P., ChoumessiTchewonpi, A., Kewir, T.S., Tashi, S., and Travert, C. (2019). Momordica Foetida (Cucurbitaceae) Extract Alleviates Parastar (Insecticide) -Induced Toxicity on Pancreatic and Duodenal α-amylase Activity in Male Rats. Journal of Chemical Health Risks *9*, 97–105.

Naujokas, M.F., Anderson, B., Ahsan, H., Aposhian, H.V., Graziano, J.H., Thompson, C., and Suk, W.A. (2013). The broad scope of health effects from chronic arsenic exposure: update on a worldwide public health problem. Environ. HealthPerspect. *121*, 295–302.

Neri, T., Merico, V., Fiordaliso, F., Salio, M., Rebuzzini, P., Sacchi, L., Bellazzi, R., Redi, C.A., Zuccotti, M., and Garagna, S. (2011). The differentiation of cardiomyocytes from mouse embryonic stem cells is altered by dioxin. Toxicol. Lett. *202*, 226–236.

Newbold, R.R., Padilla-Banks, E., and Jefferson, W.N. (2006). Adverse effects of the model environmental estrogendiethylstilbestrol are transmitted to subsequent generations. Endocrinology *147*, S11-17.

Newbold, R.R., Padilla-Banks, E., Snyder, R.J., Phillips, T.M., and Jefferson, W.N. (2007). Developmental Exposure to Endocrine Disruptors and the Obesity Epidemic. ReprodToxicol*23*, 290–296.

Nomura, S., and Takano-Yamamoto, T. (2000). Molecular events caused by mechanical stress in bone. Matrix Biol. *19*, 91–96.

Noseda, M., Peterkin, T., Simões, F.C., Patient, R., and Schneider, M.D. (2011). Cardiopoietic factors: extracellular signals for cardiac lineage commitment. Circ. Res. *108*, 129–152.

Nugent, B.M., and Bale, T.L. (2015). The omniscient placenta: Metabolic and epigenetic regulation of foetal programming. Front Neuroendocrinol*39*, 28–37.

Ogasawara, A., Arakawa, T., Kaneda, T., Takuma, T., Sato, T., Kaneko, H., Kumegawa, M., and Hakeda, Y. (2001). Fluid Shear Stress-induced Cyclooxygenase-2 Expression Is Mediated by C/EBP β, cAMP-response Element-binding Protein, and AP-1 in Osteoblastic MC3T3-E1 Cells. J. Biol. Chem. *276*, 7048–7054.

Olson, E.N. (2001). Development. The path to the heart and the road not taken. Science *291*, 2327–2328.

Olsson, I.A.S., Silva, S.P. da, Townend, D., and Sandøe, P. (2016). Protecting Animals and Enabling Research in the European Union: An Overview of Development and Implementation of Directive 2010/63/EU. ILAR J *57*, 347–357.

Olszak, T., An, D., Zeissig, S., Vera, M.P., Richter, J., Franke, A., Glickman, J.N., Siebert, R., Baron, R.M., Kasper, D.L., et al. (2012). Microbial exposure during early life has persistent effects on natural killer T cell function. Science *336*, 489–493.

Omiecinski, C.J., Vanden Heuvel, J.P., Perdew, G.H., and Peters, J.M. (2011). Xenobiotic metabolism, disposition, and regulation by receptors: from biochemical phenomenon to predictors of major toxicities. Toxicol. Sci. *120 Suppl 1*, S49-75.

Paige, S.L., Plonowska, K., Xu, A., and Wu, S.M. (2015). Molecular regulation of cardiomyocyte differentiation. Circ. Res. *116*, 341–353.

Paravani, E.V., Simoniello, M.F., Poletta, G.L., Zolessi, F.R., and Casco, V.H. (2018). Cypermethrin: Oxidative stress and genotoxicity in retinal cells of the adult zebrafish. Mutat Res Genet Toxicol Environ Mutagen *826*, 25–32.

Paravani, E.V., Simoniello, M.F., Poletta, G.L., and Casco, V.H. (2019). Cypermethrin induction of DNA damage and oxidative stress in zebrafish gill cells. Ecotoxicol. Environ. Saf. *173*, 1–7.

Patandin, S., Koopman-Esseboom, C., de Ridder, M.A., Weisglas-Kuperus, N., and Sauer, P.J. (1998). Effects of environmental exposure to polychlorinated biphenyls and dioxins on birth size and growth in Dutch children. Pediatr. Res. *44*, 538–545.

Pavesi, A., Adriani, G., Rasponi, M., Zervantonakis, I.K., Fiore, G.B., and Kamm, R.D. (2015). Controlled electromechanical cell stimulation on-a-chip. Sci Rep *5*, 11800.

Pegg, W., and Michalak, M. (1987). Differentiation of sarcoplasmic reticulum during cardiac myogenesis. Am. J. Physiol. *252*, H22-31.

Pessah, I.N., Cherednichenko, G., and Lein, P.J. (2010). Minding the calcium store: Ryanodine receptor activation as a convergent mechanism of PCB toxicity. Pharmacol. Ther. *125*, 260–285.

Piersma, A.H., Genschow, E., Verhoef, A., Spanjersberg, M.Q.I., Brown, N.A., Brady, M., Burns, A., Clemann, N., Seiler, A., and Spielmann, H. (2004). Validation of the postimplantation rat whole-embryo culture test in the international ECVAM validation study on three in vitro embryotoxicity tests. Altern Lab Anim*32*, 275–307.

Ponikowski, P., Anker, S.D., AlHabib, K.F., Cowie, M.R., Force, T.L., Hu, S., Jaarsma, T., Krum, H., Rastogi, V., Rohde, L.E., et al. (2014). Heart failure: preventing disease and death worldwide. ESC Heart Fail *1*, 4–25.

Porte, C., Janer, G., Lorusso, L.C., Ortiz-Zarragoitia, M., Cajaraville, M.P., Fossi, M.C., and Canesi, L. (2006). Endocrine disruptors in marine organisms: approaches and perspectives. Comp. Biochem. Physiol. C Toxicol. Pharmacol. *143*, 303–315.

Potter, J.D. (1974). The content of troponin, tropomyosin, actin, and myosin in rabbit skeletal muscle myofibrils. Archives of Biochemistry and Biophysics *162*, 436–441.

Puttabyatappa, M., Cardoso, R.C., and Padmanabhan, V. (2016). Effect of maternal PCOS and PCOS-like phenotype on the offspring's health. Mol Cell Endocrinol *435*, 29–39.

Quansah, R., Armah, F.A., Essumang, D.K., Luginaah, I., Clarke, E., Marfoh, K., Cobbina, S.J., Nketiah-Amponsah, E., Namujju, P.B., Obiri, S., et al. (2015). Association of arsenic with adverse pregnancy outcomes/infant mortality: a

systematic review and meta-analysis. Environ. Health Perspect. *123*, 412–421.

Raghu, K.G., Yadav, G.K., Singh, R., Prathapan, A., Sharma, S., and Bhadauria, S. (2009). Evaluation of adverse cardiac effects induced by arsenic trioxide, a potent anti-APL drug. J. Environ. Pathol. Toxicol. Oncol. *28*, 241–252.

Ranganatha, N., and Kuppast, I.J. (2012). A review on alternatives to animal testing methods in drug development. International Journal of Pharmacy and Pharmaceutical Sciences *4*, 28–32.

Raszewski, G., Lemieszek, M.K., Łukawski, K., Juszczak, M., and Rzeski, W. (2015). Chlorpyrifos and Cypermethrin Induce Apoptosis in Human Neuroblastoma Cell Line SH-SY5Y. Basic & Clinical Pharmacology & Toxicology *116*, 158–167.

Ratnaike, R.N. (2003). Acute and chronic arsenic toxicity. Postgrad Med J *79*, 391–396.

Rawls, J.F., Samuel, B.S., and Gordon, J.I. (2004). Gnotobiotic zebrafish reveal evolutionarily conserved responses to the gut microbiota. Proc. Natl. Acad. Sci. U.S.A. *101*, 4596–4601.

Rebuzzini, P., Martinelli, P., Blasco, M., Giulotto, E., and Mondello, C. (2007). Inhibition of gene amplification in telomerase deficient immortalized mouse embryonic fibroblasts. Carcinogenesis*28*, 553–559.

Rebuzzini, P., Neri, T., Mazzini, G., Zuccotti, M., Redi, C.A., and Garagna, S. (2008). Karyotype analysis of the euploid cell population of a mouse embryonic stem cell line revealed a high incidence of chromosome abnormalities that varied during culture. Cytogenet. Genome Res. *121*, 18–24.

Rebuzzini, P., Pignalosa, D., Mazzini, G., Di Liberto, R., Coppola, A., Terranova, N., Magni, P., Redi, C.A., Zuccotti, M., and Garagna, S. (2012). Mouse embryonic stem cells that survive γ-rays exposure maintain pluripotent differentiation potential and genome stability. J. Cell. Physiol. *227*, 1242–1249.

Rebuzzini, P., Fassina, L., Mulas, F., Bellazzi, R., Redi, C.A., Di Liberto, R., Magenes, G., Adjaye, J., Zuccotti, M., and Garagna, S. (2013). Mouse embryonic stem cells irradiated with γ-rays differentiate into cardiomyocytes

but with altered contractile properties. Mutation Research/Genetic Toxicology and Environmental Mutagenesis *756*, 37–45.

Rebuzzini, P., Cebral, E., Fassina, L., Alberto Redi, C., Zuccotti, M., and Garagna, S. (2015). Arsenic trioxide alters the differentiation of mouse embryonic stem cell into cardiomyocytes. Sci Rep *5*, 14993.

Reddy, A.V.B., Moniruzzaman, M., and Aminabhavi, T.M. (2019). Polychlorinated biphenyls (PCBs) in the environment: Recent updates on sampling, pretreatment, cleanup technologies and their analysis. Chemical Engineering Journal *358*, 1186–1207.

Rhee, K.-J., Sethupathi, P., Driks, A., Lanning, D.K., and Knight, K.L. (2004). Role of commensal bacteria in development of gut-associated lymphoid tissues and preimmune antibody repertoire. J. Immunol. *172*, 1118–1124.

Ross, G. (2004). The public health implications of polychlorinated biphenyls (PCBs) in the environment. Ecotoxicol. Environ. Saf. *59*, 275–291.

Rossman, T.G. (2003). Mechanism of arsenic carcinogenesis: an integrated approach. Mutat. Res. *533*, 37–65.

Rubinstein, A.L. (2006). Zebrafish assays for drug toxicity screening. Expert Opinion on Drug Metabolism & Toxicology *2*, 231–240.

Rushmore, T.H., and Kong, A.-N.T. (2002). Pharmacogenomics, regulation and signalling pathways of phase I and II drug metabolizing enzymes. Curr. Drug Metab. *3*, 481–490.

Russell, W.M.S., and Burch, R.L. (1959). The principles of humane experimental technique (London: Methuen).

Saillenfait, A.-M., Ndiaye, D., and Sabaté, J.-P. (2015). Pyrethroids: exposure and health effects--an update. Int J Hyg Environ Health *218*, 281–292.

Samsó, M., Feng, W., Pessah, I.N., and Allen, P.D. (2009). Coordinated movement of cytoplasmic and transmembrane domains of RyR1 upon gating. PLoS Biol. *7*, e85.

Schlichting, C., and Pigliucci, M. (1998). Phenotypic Evolution: A Reaction Norm Perspective (Sinauer).

Schmalhausen, I.I. (1949). Factors of evolution: the theory of stabilizing selection (Oxford, England: Blakiston).

Sedan, O., Dolnikov, K., Zeevi-Levin, N., Fleishmann, N., Spiegel, I., Berdichevski, S., Amit, M., Itskovitz-Eldor, J., and Binah, O. (2010). Human embryonic stem cell-derived cardiomyocytes can mobilize 1,4,5-inositol trisphosphate-operated [Ca2+]i stores: the functionality of angiotensin-II/endothelin-1 signaling pathways. Ann. N. Y. Acad. Sci. *1188*, 68–77.

Segers, V.F.M., and Lee, R.T. (2008). Stem-cell therapy for cardiac disease. Nature *451*, 937–942.

Shanks, N., Greek, R., and Greek, J. (2009). Are animal models predictive for humans? Philos Ethics Humanit Med *4*, 2.

Sharma, R., Derr-Yellin, E.C., House, D.E., and Kodavanti, P.R. (2000). Age-dependent effects of Aroclor 1254R on calcium uptake by subcellular organelles in selected brain regions of rats. Toxicology *156*, 13–25.

Shen, Z.-X., Shi, Z.-Z., Fang, J., Gu, B.-W., Li, J.-M., Zhu, Y.-M., Shi, J.-Y., Zheng, P.-Z., Yan, H., Liu, Y.-F., et al. (2004). All-trans retinoic acid/As2O3 combination yields a high quality remission and survival in newly diagnosed acute promyelocytic leukemia. Proc. Natl. Acad. Sci. U.S.A. *101*, 5328–5335.

Shi, Y., Katsev, S., Cai, C., and Evans, S. (2000). BMP Signaling Is Required for Heart Formation in Vertebrates. Developmental Biology *224*, 226–237.

Silveira, P.P., Portella, A.K., Goldani, M.Z., and Barbieri, M.A. (2007). Developmental origins of health and disease (DOHaD). J Pediatr (Rio J) *83*, 494–504.

Smith, A.H., and Steinmaus, C.M. (2011). Arsenic in drinking water. BMJ *342*, d2248.

Soderlund, D.M. (2012). Molecular mechanisms of pyrethroid insecticide neurotoxicity: recent advances. Arch Toxicol*86*, 165–181.

Später, D., Hansson, E.M., Zangi, L., and Chien, K.R. (2014). How to make a cardiomyocyte. Development *141*, 4418–4431.

Spielmann, H., Pohl, I., Doring, B., Liebsch, M., and Moldenhauer, F. (1997). The embryonic stem cell test (EST), an in vitro embryotoxicity test using two permanent mouse cell lines: 3T3 fibroblasts and embryonic stem cells. In

Vitro Toxicology: Journal of Molecular and Cellular Toxicology *10*, 119–127.

Stappenbeck, T.S., Hooper, L.V., and Gordon, J.I. (2002). Developmental regulation of intestinal angiogenesis by indigenous microbes via Paneth cells. Proc. Natl. Acad. Sci. U.S.A. *99*, 15451–15455.

States J. Christopher, Barchowsky Aaron, Cartwright Iain L., Reichard John F., Futscher Bernard W., and Lantz R. Clark (2011). Arsenic Toxicology: Translating between Experimental Models and Human Pathology. Environmental Health Perspectives *119*, 1356–1363.

Stearns, S., de Jong, G., and Newman, B. (1991). The effects of phenotypic plasticity on genetic correlations. Trends Ecol. Evol. (Amst.) *6*, 122–126.

Steinberg, S.F. (2013). Oxidative stress and sarcomeric proteins. Circ. Res. *112*, 393–405.

Sukardi, H., Chng, H.T., Chan, E.C.Y., Gong, Z., and Lam, S.H. (2011). Zebrafish for drug toxicity screening: bridging the in vitro cell-based models and in vivo mammalian models. Expert Opin Drug MetabToxicol*7*, 579–589.

Sullivan, M.C., Hawes, K., Winchester, S.B., and Miller, R.J. (2008). Developmental Origins Theory from Prematurity to Adult Disease. Journal of Obstetric, Gynecologic, & Neonatal Nursing *37*, 158–164.

Sultan, S.E. (2003). Commentary: The promise of ecological developmental biology. J. Exp. Zool. B Mol. Dev. Evol. *296*, 1–7.

Sumi, D., Sasaki, T., Miyataka, H., and Himeno, S. (2011). Rat H9c2 cardiac myocytes are sensitive to arsenite due to a modest activation of transcription factor Nrf2. Arch Toxicol*85*, 1509–1516.

Sutcliffe, M.D., Tan, P.M., Fernandez-Perez, A., Nam, Y.-J., Munshi, N.V., and Saucerman, J.J. (2018). High content analysis identifies unique morphological features of reprogrammed cardiomyocytes. Sci Rep *8*, 1258.

Tai, M.-H., Weng, C.-H., Mon, D.-P., Hu, C.-Y., and Wu, M.-H. (2012). Ultraviolet C irradiation induces different expression of cyclooxygenase 2 in NIH 3T3 cells and A431 cells: the roles of COX-2 are different in various cell lines. Int J Mol Sci *13*, 4351–4366.

Tam, P.P.L., and Loebel, D.A.F. (2007). Gene function in mouse embryogenesis: get set for gastrulation. Nat. Rev. Genet. *8*, 368–381.

Tamm, C., PijuanGalitó, S., and Annerén, C. (2013). A comparative study of protocols for mouse embryonic stem cell culturing. PLoS ONE *8*, e81156.

Tang, W., and Ho, S. (2007). Epigenetic reprogramming and imprinting in origins of disease. Rev EndocrMetabDisord*8*, 173–182.

Tang, W., Wang, D., Wang, J., Wu, Z., Li, L., Huang, M., Xu, S., and Yan, D. (2018). Pyrethroid pesticide residues in the global environment: An overview. Chemosphere *191*, 990–1007.

Tapio, S., and Grosche, B. (2006). Arsenic in the aetiology of cancer. Mutat. Res. *612*, 215–246.

Tarrade, A., Panchenko, P., Junien, C., and Gabory, A. (2015). Placental contribution to nutritional programming of health and diseases: epigenetics and sexual dimorphism. J. Exp. Biol. *218*, 50–58.

Thiele, D.K., and Anderson, C.M. (2016). Developmental Origins of Health and Disease: A Challenge for Nurses. J PediatrNurs*31*, 42–46.

Thompson, B.R., and Metzger, J.M. (2014). Cell biology of sarcomeric protein engineering: disease modeling and therapeutic potential. Anat Rec (Hoboken) *297*, 1663–1669.

Thomson, J.A., Itskovitz-Eldor, J., Shapiro, S.S., Waknitz, M.A., Swiergiel, J.J., Marshall, V.S., and Jones, J.M. (1998). Embryonic stem cell lines derived from human blastocysts. Science *282*, 1145–1147.

Tilson, H.A., Jacobson, J.L., and Rogan, W.J. (1990). Polychlorinated biphenyls and the developing nervous system: cross-species comparisons. NeurotoxicolTeratol*12*, 239–248.

Tseng, C.-H. (2008). Cardiovascular disease in arsenic-exposed subjects living in the arseniasis-hyperendemic areas in Taiwan. Atherosclerosis *199*, 12–18.

Uner, N., Oruç, E.O., Canli, M., and Sevgiler, Y. (2001). Effects of cypermethrin on antioxidant enzyme activities and lipid peroxidation in liver and kidney of the freshwater fish, Oreochromis niloticus and Cyprinus carpio (L.). Bull Environ ContamToxicol*67*, 657–664.

Van Maele-Fabry, G., Lantin, A.-C., Hoet, P., and Lison, D. (2010). Childhood leukaemia and parental occupational exposure to pesticides: a systematic review and meta-analysis. Cancer Causes Control *21*, 787–809.

Van Vliet, P., Wu, S.M., Zaffran, S., and Pucéat, M. (2012). Early cardiac development: a view from stem cells to embryos. Cardiovasc. Res. *96*, 352–362.

Verma, V., Purnamawati, K., Manasi, null, and Shim, W. (2013). Steering signal transduction pathway towards cardiac lineage from human pluripotent stem cells: a review. Cell. Signal. *25*, 1096–1107.

Viatchenko-Karpinski, S., Fleischmann, B.K., Liu, Q., Sauer, H., Gryshchenko, O., Ji, G.J., and Hescheler, J. (1999). Intracellular Ca2+ oscillations drive spontaneous contractions in cardiomyocytes during early development. PNAS *96*, 8259–8264.

Voie, O.A., and Fonnum, F. (1998). Ortho substituted polychlorinated biphenyls elevate intracellular $[Ca(2^+)]$ in human granulocytes. Environ. Toxicol. Pharmacol. *5*, 105–112.

Walters, M.J., Wayman, G.A., and Christian, J.L. (2001). Bone morphogenetic protein function is required for terminal differentiation of the heart but not for early expression of cardiac marker genes. Mech. Dev. *100*, 263–273.

Wang, Z.-Y., and Chen, Z. (2008). Acute promyelocytic leukemia: from highly fatal to highly curable. Blood *111*, 2505–2515.

Watanabe, C., Inaoka, T., Matsui, T., Ishigaki, K., Murayama, N., and Ohtsuka, R. (2003). Effects of arsenic on younger generations. J Environ Sci Health A Tox Hazard Subst Environ Eng*38*, 129–139.

Wayman, G.A., Yang, D., Bose, D.D., Lesiak, A., Ledoux, V., Bruun, D., Pessah, I.N., and Lein, P.J. (2012). PCB-95 Promotes Dendritic Growth via Ryanodine Receptor–Dependent Mechanisms. Environ Health Perspect*120*, 997–1002.

Wesemann, D.R., Portuguese, A.J., Meyers, R.M., Gallagher, M.P., Cluff-Jones, K., Magee, J.M., Panchakshari, R.A., Rodig, S.J., Kepler, T.B., and Alt, F.W. (2013). Microbial colonization influences early B-lineage development in the gut lamina propria. Nature *501*, 112–115.

West-Eberhard, M.J. (2003). Developmental Plasticity and Evolution (Oxford, New York: Oxford University Press).

Westfall, M.V., Pasyk, K.A., Yule, D.I., Samuelson, L.C., and Metzger, J.M. (1997). Ultrastructure and cell-cell coupling of cardiac myocytes differentiating in embryonic stem cell cultures. Cell Motil. Cytoskeleton *36*, 43–54.

Wobus, A.M., and Boheler, K.R. (2005). Embryonic stem cells: prospects for developmental biology and cell therapy. Physiol. Rev. *85*, 635–678.

Wobus, A.M., Wallukat, G., and Hescheler, J. (1991). Pluripotent mouse embryonic stem cells are able to differentiate into cardiomyocytes expressing chronotropic responses to adrenergic and cholinergic agents and Ca2+ channel blockers. Differentiation *48*, 173–182.

Wong, P.W., Garcia, E.F., and Pessah, I.N. (2001). ortho-substituted PCB95 alters intracellular calcium signalling and causes cellular acidification in PC12 cells by an immunophilin-dependent mechanism. J. Neurochem. *76*, 450–463.

Yang, D., Kim, K.H., Phimister, A., Bachstetter, A.D., Ward, T.R., Stackman, R.W., Mervis, R.F., Wisniewski, A.B., Klein, S.L., Kodavanti, P.R.S., et al. (2009). Developmental exposure to polychlorinated biphenyls interferes with experience-dependent dendritic plasticity and ryanodine receptor expression in weanling rats. Environ. Health Perspect. *117*, 426–435.

Yang, H.-T., Tweedie, D., Wang, S., Guia, A., Vinogradova, T., Bogdanov, K., Allen, P.D., Stern, M.D., Lakatta, E.G., and Boheler, K.R. (2002). The ryanodine receptor modulates the spontaneous beating rate of cardiomyocytes during development. Proc. Natl. Acad. Sci. U.S.A. *99*, 9225–9230.

Yoo, M., Lim, Y.-H., Kim, T., Lee, D., and Hong, Y.-C. (2016). Association between urinary 3-phenoxybenzoic acid and body mass index in Korean adults: 1st Korean National Environmental Health Survey. Ann Occup Environ Med *28*.

Zakariyah, A., Rajgara, R., Shelton, M., Blais, A., Skerjanc, I.S., and Burgon, P.G. (2019). Combinatorial Utilization of Murine Embryonic Stem Cells and In Vivo Models to Study Human Congenital Heart Disease. Curr Protoc Stem Cell Biol*48*, e75.

Zhang, W., Liu, Y., Ge, M., Jing, J., Chen, Y., Jiang, H., Yu, H., Li, N., and Zhang, Z. (2014). Protective effect of resveratrol on arsenic trioxide-induced nephrotoxicity in rats. Nutr Res Pract*8*, 220–226.

Zhao, G.-R., Zhang, H.-M., Ye, T.-X., Xiang, Z.-J., Yuan, Y.-J., Guo, Z.-X., and Zhao, L.-B. (2008a). Characterization of the radical scavenging and antioxidant activities of danshensu and salvianolic acid B. Food Chem. Toxicol. *46*, 73–81.

Zhao, X., Feng, T., Chen, H., Shan, H., Zhang, Y., Lu, Y., and Yang, B. (2008b). Arsenic trioxide-induced apoptosis in H9c2 cardiomyocytes: implications in cardiotoxicity. Basic Clin. Pharmacol. Toxicol. *102*, 419–425.

Zhou, Y.-J., Huang, H.-R., Zhou, J., and Wang, L.-Q. (2018). Beta-cypermethrin exposure affects female reproduction by enhancing oxidative stress in mice uterine tissue. Regul. Toxicol. Pharmacol. *98*, 284–290.

Zhu, N., Yi-Li, and Zhang, F.-S. (2011). Catalytic dechlorination of polychlorinated biphenyls in subcritical water by Ni/Fe nanoparticles. Chemical Engineering Journal *171*, 919–925.

Zhu, N.-M., Wang, C.-F., and Zhang, F.-S. (2012). An integrated two-stage process for effective dechlorination of polychlorinated biphenyls in subcritical water in the presence of hydrogen donors. Chemical Engineering Journal *197*, 135–142.

Zoeller, R.T., Bergman, Å., Becher, G., Bjerregaard, P., Bornman, R., Brandt, I., Iguchi, T., Jobling, S., Kidd, K.A., Kortenkamp, A., et al. (2014). A path forward in the debate over health impacts of endocrine disrupting chemicals. Environ Health *13*, 118.

(1993). Guidelines for drinking-water quality (Geneva: World Health Organization).

(2001). National Primary Drinking Water Regulations; Arsenic and Clarifications to Compliance and New Source Contaminants Monitoring.

(2015). National Institute of Environmental Health Sciences (NIEHS).

8 SITOGRAPHY

https://www.austincc.edu/apreview/PhysText/Muscle.html

https://www.abcam.com/protocols/whole-mount-staining-protocol

https://imagej.nih.gov/ij/

9 LIST OF MANUSCRIPTS

Rebuzzini, P., Zuccolo, E., **Civello, C**., Fassina, L., Arechaga, J., Izquierdo, A., Faris, P., Zuccotti, M., Moccia, F., Garagna, S. 2018. Polychlorinated biphenyls reduce the kinematics contractile properties of embryonic stem cells-derived cardiomyocytes by disrupting their intracellular Ca^{2+} dynamics.Sci Rep.*17;8(1)*:17909.

SCIENTIFIC REP🞱RTS

Polychlorinated biphenyls reduce the kinematics contractile properties of embryonic stem cells-derived cardiomyocytes by disrupting their intracellular Ca²⁺ dynamics

Paola Rebuzzini[1,2], Estella Zuccolo[3], Cinzia Civello[1], Lorenzo Fassina[2,4], Juan Arechaga[5], Amaia Izquierdo[5], Pawan Faris[3,6], Maurizio Zuccotti[1,2], Francesco Moccia[3] & Silvia Garagna[1,2]

Persistent organic pollutants are a group of chemicals that include polychlorinated biphenyls (PCBs). PCBs exposure during adult life increases incidence and severity of cardiomyopathies, whereas *in utero* exposure determines congenital heart defects. Being fat-soluble, PCBs are passed to newborns through maternal milk, impairing heart functionality in the adult. It is still unknown how PCBs impair cardiac contraction at cellular/molecular levels. Here, we study the molecular mechanisms by which PCBs cause the observed heart contraction defects, analysing the alterations of Ca²⁺ toolkit components that regulate contraction. We investigated the effect that Aroclor 1254 (Aroclor), a mixture of PCBs, has on perinatal-like cardiomyocytes derived from mouse embryonic stem cells. Cardiomyocytes, exposed to 1 or 2 μg/ml Aroclor for 24 h, were analyzed for their kinematics contractile properties and intracellular Ca²⁺ dynamics. We observed that Aroclor impairs cardiomyocytes contractile properties by inhibiting spontaneous Ca²⁺ oscillations. It disrupts intracellular Ca²⁺ homeostasis by reducing the sarcoplasmic reticulum Ca²⁺ content and by inhibiting voltage-gated Ca²⁺ entry. These findings contribute to the understanding of the molecular underpinnings of PCBs-induced cardiovascular alterations, which are emerging as an additional life-threatening hurdle associated to PCBs pollution. Therefore, PCBs-dependent alteration of intracellular Ca²⁺ dynamics is the most likely trigger of developmental cardiac functional alteration.

Persistent organic pollutants are a variegated group of chemicals that include polychlorinated biphenyls (PCBs), the latter compounds containing a high number of chlorine atoms. PCBs have been widely used in electrical and electronic industries (production of plastics, adhesives, paints, carbonless copying paper, newsprint and caulking compounds[1,2]), since when, in 1979, their production and use were internationally banned. However, due to their high chemical stability, PCBs are still persisting and have wide diffusion into the environment.

Growing amounts of data link their bioaccumulation through the diet with their high toxicity; more specifically, several studies have evidenced that PCBs exposure during adult life leads to an increase in the incidence and severity of cardiomyopathies[3–7]. PCBs exposure alters the expression of GATA-4, Nkx-2.5, MEF-2c,

[1]Laboratorio di Biologia dello Sviluppo, Dipartimento di Biologia e Biotecnologie, Università degli Studi di Pavia, Pavia, Italy. [2]Centre for Health Technologies (C.H.T.), Università degli Studi di Pavia, Pavia, Italy. [3]Laboratorio di Fisiologia Generale, Dipartimento di Biologia e Biotecnologie, Università degli Studi di Pavia, Pavia, Italy. [4]Dipartimento di Ingegneria Industriale e dell'Informazione, Università degli Studi di Pavia, Pavia, Italy. [5]Laboratory of Stem Cells, Development and Cancer, Department of Cell Biology and Histology, Faculty of Medicine and Nursing, Universidad del País Vasco, Vizcaya, Spain. [6]Department of Biology, College of Science, Salahaddin University, Erbil, Kurdistan-Region of Iraq, Iraq. Correspondence and requests for materials should be addressed to P.R. (email: paola.rebuzzini@unipv.it) or M.Z. (email: maurizio.zuccotti@unipv.it) or S.G. (email: silvia.garagna@unipv.it)

OCT-1 cardiac nuclear transcription factors and other heart-specific genes (atrial and brain natriuretic peptide, alpha- and beta-myosin heavy chain, alpha-cardiac and alpha-skeletal actin) in adult primary rat cardiomyocytes[8]. In guinea pig ventricular myocytes, PCB 19 exposure decreases contractile force, action potential duration and amplitude, and intracellular Ca^{2+} transients through inhibition of L-type voltage-gated Ca^{2+} channels (VGCCs)[9]. Also, in other adult cardiac cellular models, PCBs alter the expression and/or activity of several components of the intracellular Ca^{2+} signalling machinery[10], such as type 2 ryanodine receptors (RyR2)[11] and the Sarco-Endoplasmic-Reticulum Ca^{2+}-ATPase (SERCA)[12].

PCBs prenatal exposure through placenta determines congenital heart defects[13,14] not attributable to inherited genetic mutations[5]. To this regard, exposed avian embryos display extensive cardiac dilation, thinner ventricle walls and reduced responsiveness to chronotropic stimuli[15], whereas zebrafish embryos show heart defects, reduction of the heart beating rate and irregular and weak contractions[16]. Reduced heart size and functional deficits have been described in mouse foetuses, as well as cardiac hypertrophy in offsprings, the latter showing increased sensitivity to cardiovascular insults in adulthood[5].

Importantly, being fat-soluble, PCBs accumulate in fat tissues and are passed to newborns through maternal milk[17], increasing the myocardial wall thickness and inducing cardiac hypertrophy, thus impairing heart functionality in the adult[18]. Whilst the detrimental effects on the perinatal heart anatomy are evident, unknown are the PCBs effects at the cellular and molecular levels. Our study aims at dissecting the key physiological processes behind the observed heart contraction defects, by analyzing in perinatal cardiomyocytes the calcium-induced calcium-release mechanism (Ca^{2+} toolkit) that finely regulates contraction.

Perinatal-like cardiomyocytes (hereafter named cardiomyocytes) were obtained from the *in vitro* differentiation of mouse embryonic stem cells (mESCs). Functionally, these cardiomyocytes form compact beating syncytia and exhibit electrophysiological features of excitation-contraction coupling described for isolated perinatal cardiac cells[19–21].

Following differentiation, cardiomyocytes were exposed for 24h to Aroclor 1254 (Aroclor), a mixture of more than 80 PCBs isomers and congeners with high number of chlorine atoms (54%)[2], at doses in the range of environmental contamination (1 and 2 µg/ml), then their kinematics contractile properties and the intracellular Ca^{2+} homeostasis were evaluated.

Results

Aroclor reduces the kinematics and dynamics properties (contractile properties) of beating syncytia. For the evaluation of the effects of Aroclor on the contractile properties of beating syncytia, we measured their kinematics and dynamics features on AVI videos, recorded from CTR samples and after 24h exposure to 1 or 2 µg/ml Aroclor. The chronotropic (beat frequency [Hz]), inotropic (contraction force [pixel/s^2] and contractility, i.e. the maximum contraction velocity, [pixel/s]) and ergotropic (consumption of ATP for kinetic energy [pixel^2/s^2]) features were mathematically calculated from the movement of the beating syncytia[22].

After exposure to 1 µg/ml Aroclor, both beat frequency and kinetic energy showed a 1.2-fold reduction ($p < 0.05$), whereas inotropic parameters remain unaltered ($p > 0.05$) when compared to CTR (Fig. 1A,D). A more adverse effect was observed when syncytia were exposed to 2 µg/ml, since all four parameters were significantly reduced ($p < 0.05$). Specifically, when compared to CTR, a 1.4-, 1.2-, 1.4-, 1.8-fold decrease of beat frequency, contractility, contraction force and kinetic energy, respectively, was observed (Fig. 1 and videos supplementary materials).

Aroclor reduces spontaneous intracellular Ca^{2+} oscillations. Aroclor, as previously shown for other PCBs[23,24], may induce alterations in the cardiomyocyte contraction properties through a derangement of the intracellular Ca^{2+} signalling machinery. Importantly, the contractile properties of beating syncytia depend on spontaneous Ca^{2+} oscillations, which arise even in the absence of electrical stimulation. These spontaneous Ca^{2+} spikes are generated by rhythmic Ca^{2+} release from sarcoplasmic reticulum (SR) through RyR2, which in turn evokes a Na^+/Ca^{2+} exchanger-mediated membrane depolarization and activates VGCCs[25,26].

When loading beating syncytia with the Ca^{2+}-sensitive fluorochrome Fura-2/AM, we observed, compared to CTR unexposed cells, a significant ($p < 0.05$) decrease in both amplitude (Fig. 2A,B) and frequency of spontaneous Ca^{2+} transients (Fig. 2A,C) in cardiomyocytes exposed to 1 or 2 µg/ml Aroclor. These results show that Aroclor may reduce cardiomyocyte contraction properties by interfering with the intracellular Ca^{2+} handling machinery in beating syncytia.

Aroclor does not alter the molecular machinery underlying spontaneous Ca^{2+} activity. In CTR samples, tetracaine (100 µM), a selective RyR inhibitor[27], caused a prompt inhibition of the intracellular Ca^{2+} spikes (Fig. 3A), thereby confirming the crucial role played by RyR2 in shaping the Ca^{2+} signal[25,26]. Similar to previous studies[25], removal of external Ca^{2+} ($0Ca^{2+}$) did not induce the abrupt interruption of the Ca^{2+} transients, but resulted in the progressive decline of their amplitude, determining complete arrest of Ca^{2+} activity after about 5 min (Fig. 3B). This finding is consistent with the notion that Ca^{2+} entry is triggered by spontaneous Ca^{2+} oscillations to refill the SR Ca^{2+} pool[26]. Conversely, the blockade of InsP$_3$Rs with 2-APB (50 µM) failed to affect the ongoing Ca^{2+} transients (Fig. 3C). Overall, these findings confirm that RyR2-dependent rhythmical Ca^{2+} release underlies the onset of the spontaneous Ca^{2+} oscillations, whereas voltage-dependent Ca^{2+} entry maintains them over time.

The same results were obtained when the beating syncytia were exposed to 1 (Fig. 3D–F) or 2 µg/ml (Fig. 3G–I) Aroclor. Therefore, RyR2 and VGCCs interact to shape the spontaneous Ca^{2+} oscillations also in Aroclor-exposed syncytia.

Earlier work showed that angiotensin II and endothelin 1 are able to modulate spontaneous Ca^{2+} oscillations in beating syncytia by inducing InsP$_3$-induced Ca^{2+} release from the SR[28]. In agreement with these
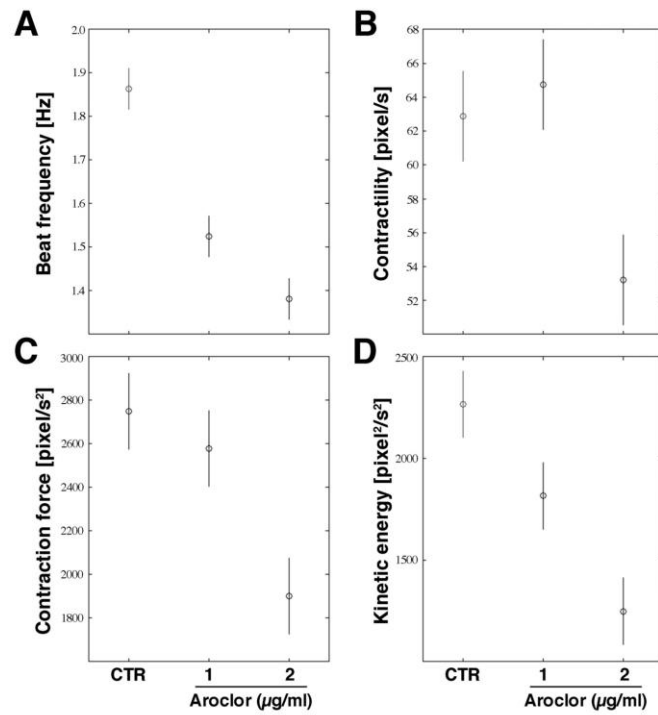
Figure 1. Kinematics contractile properties of cardiac beating syncytia. (**A**) Beat frequency [Hz]. (**B**) Contractility (maximum contraction velocity) [pixel/s]. (**C**) Contraction force [pixel/s²]. (**D**) Kinetic energy [pixel²/s²]. Horizontal bars represent the 95% confidence intervals for the differences between means according to the Least Significant Difference statistical test.
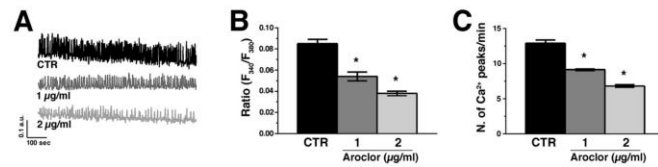
Figure 2. Ca²⁺ oscillations in cardiac beating syncytia. (**A**) Representative tracing of spontaneous Ca²⁺ spikes recorded in CTR or in the presence of either 1 or 2 μg/mL Aroclor. (**B**) Mean ± SE of the amplitude of the Ca²⁺ peaks recorded under the designated treatments. (**C**) Mean ± SE of the frequency of spontaneous Ca²⁺ spikes. *$p < 0.05$.

116
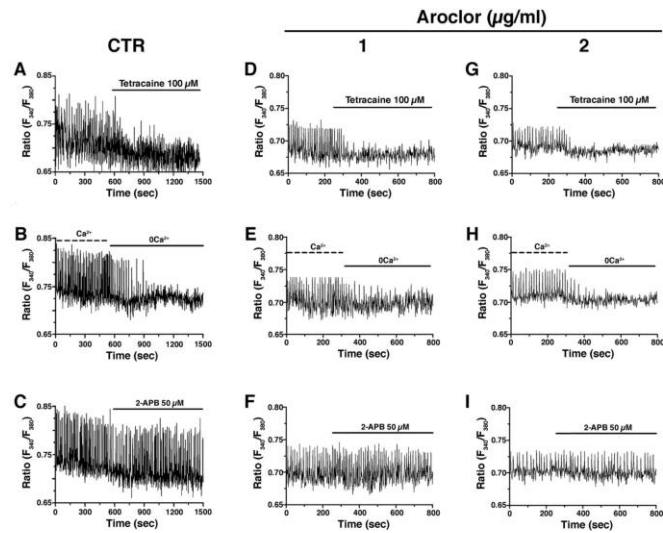
Figure 3. Intracellular Ca^{2+} spikes in CTR and 1 or 2 μg/ml-exposed cardiac beating syncytia. (**A**),(**D**) and (**G**) Tetracaine (100 μM) caused a prompt inhibition of the intracellular Ca^{2+} spikes; (**B**),(**E**) and (**H**) Extracellular Ca^{2+} removal (0Ca^{2+}) did not induce the abrupt interruption of the Ca^{2+} transients, but resulted in the progressive decline in the amplitude of the Ca^{2+} transients; (**C**),(**F**) and (**I**) Superfusion of 2-APB (50 μM) did not affect spontaneous Ca^{2+} spikes.

observations, the application of angiotensin II (1 μM) during ongoing oscillations caused a transient enlargement of the first Ca^{2+} spike, followed by a short-lasting reduction in the amplitude of the subsequent Ca^{2+} oscillations (Supplementary Figure 1SA). Conversely, when beating syncytia were exposed to 1 (Supplementary Figure 1SB) or 2 μg/ml (Supplementary Figure 1SC) Aroclor, angiotensin II (1 μM) caused a large Ca^{2+} spike whose decay to the baseline was overlapped by RyR2-dependent spontaneous Ca^{2+} oscillations. Of note, the Ca^{2+} response to angiotensin II was higher in the presence of 2 μM Aroclor. These observations suggest that the $InsP_3$-sensitive Ca^{2+} pool is increased in the presence of Aroclor, which further rules out the contribution of $InsP_3Rs$ to the spontaneous Ca^{2+} oscillations (see Discussion).

Next, we determined how Aroclor interferes with the single components of the Ca^{2+} toolkit involved in the oscillatory signal, reducing spontaneous intracellular Ca^{2+} oscillations.

Aroclor affects the intracellular Ca^{2+} oscillations reducing the SR Ca^{2+} content. The acute addition of Aroclor in the 0Ca^{2+} medium did not induce any detectable variation in $[Ca^{2+}]_i$ at both 1 (Fig. 4A) or 2 μg/ml (not shown). Instead, 24 h exposure to Aroclor caused a significant ($p < 0.05$) reduction in basal $[Ca^{2+}]_i$ (Fig. 4B). Therefore, we turned our attention to the Ca^{2+}-permeable pathways underlying the spontaneous Ca^{2+} oscillations, i.e., RyR2 and VGCCs. Caffeine (20 mM), a selective RyR agonist, triggered a Ca^{2+} response in CTR samples, while it failed in the presence of Aroclor at both concentrations (Fig. 5A,B). To further assess the effect of Aroclor on SR Ca^{2+} content, we used cyclopiazonic acid (CPA), known to inhibit SERCA activity thereby causing the progressive efflux of intraluminal Ca^{2+} through unidentified leakage channels[29,30]. This manoeuvre leads to the rapid depletion of the SR Ca^{2+} pool under 0Ca^{2+} conditions and, therefore, causes a transient increase in $[Ca^{2+}]_i$. The $[Ca^{2+}]_i$ indeed returns to the original baseline due to the concerted interaction of the Na^+/Ca^{2+} exchanger (NCX), plasma-membrane Ca^{2+}-ATPase (PMCA) and mitochondria. CPA-induced intracellular Ca^{2+} mobilization is a well-known index of SR Ca^{2+} content and is widely employed to compare SR Ca^{2+} content between control and treated cells[29–31]. In our experiments, exposure to Aroclor caused a significant reduction in CPA-induced Ca^{2+} release under 0Ca^{2+} conditions (Fig. 5C,D), which hints at a remarkable reduction in SR Ca^{2+} levels.

117
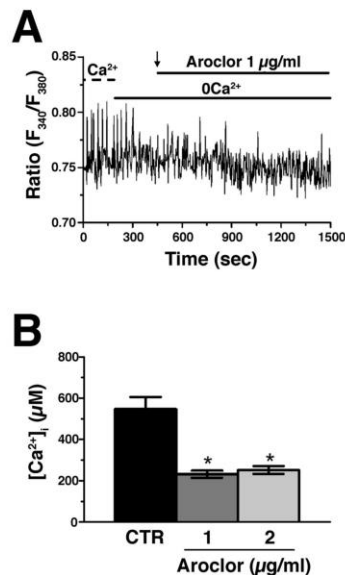
Figure 4. Acute effect of Aroclor on cardiac beating syncytia. (**A**) The acute addition of Aroclor (1 μg/mL, black arrow at 400 s) did not cause intracellular Ca^{2+} mobilization under $0Ca^{2+}$ conditions. (**B**) Mean ± SE of resting $[Ca^{2+}]_i$ in cardiac syncytia exposed to either 1 or 2 μg/mL Aroclor for 24 h. *$p < 0.05$.

Finally, we monitored voltage-dependent Ca^{2+} entry by depolarizing cardiomyocytes with high-KCl solution. We found that high-KCl-induced Ca^{2+} entry was significantly ($p < 0.05$) reduced in the presence of each dose of Aroclor (Fig. 5E,F).

Overall, these data strongly suggest that Aroclor reduces the SR Ca^{2+} content, thereby impairing RyR2-dependent Ca^{2+} release, decreases the resting $[Ca^{2+}]_i$ and inhibits voltage-dependent Ca^{2+} inflow in cardiomyocytes. As a consequence, the spontaneous Ca^{2+} oscillations that drive cardiac contraction are inhibited, which contributes to explain Aroclor-dependent cardiac functional alterations.

Aroclor modifies the expression of genes involved in Ca^{2+} toolkit. To assess whether Aroclor-induced inhibition of spontaneous Ca^{2+} oscillations is associated with changes in the expression profile of Ca^{2+} toolkit genes, we analyzed *Atp2a2* (coding for SERCA2A, cardiac isoform of the Ca^{2+}-ATPase that sequesters Ca^{2+} back into the SR), *Ryr2* (cardiac muscle SR RyR isoform), *Cacna1c* (α subunit of L-type VGCCs) and *Itpr2* (cardiac muscle SR InsP$_3$R isoform). The exposure to both Aroclor concentrations did not significantly alter the quantitative expression of *Atp2a2* gene ($p > 0.05$). Conversely, the expression of *Ryr2* and *Itpr2* significantly increased (1.7- and 1.9-fold, respectively), whereas the expression of *Cacna1c* significantly decreased (0.7-fold) only in syncytia exposed to 2 μg/ml (Fig. 6).

Discussion

Our study demonstrates that Aroclor exerts its detrimental effects on the beating properties of perinatal-like cardiomyocytes, acting on the intracellular Ca^{2+} machinery. Rhythmic beating in foetal and neonatal cardiomyocytes depends on spontaneous events of RyRs-mediated Ca^{2+} release from the SR, which may in turn evoke small depolarizations that trigger L-type VGCCs-driven action potentials[25,26]. The spontaneous intracellular Ca^{2+} oscillations represent the main source of Ca^{2+} for the contractile machinery during cardiac development[26,32]. It has long been known that PCB toxicity is consequent to the alteration of the intracellular Ca^{2+} machinery[10,33].

Consistent with these earlier observations, Aroclor heavily impairs spontaneous intracellular Ca^{2+} oscillations of cardiomyocytes, affecting both their frequency and amplitude. The signalling machinery underlying the rhythmic Ca^{2+} signal was not affected by the treatment, as, both in the absence and in the presence of Aroclor 1254, the intracellular Ca^{2+} oscillations were mainly driven by RyRs and supported by extracellular Ca^{2+} entry.

118
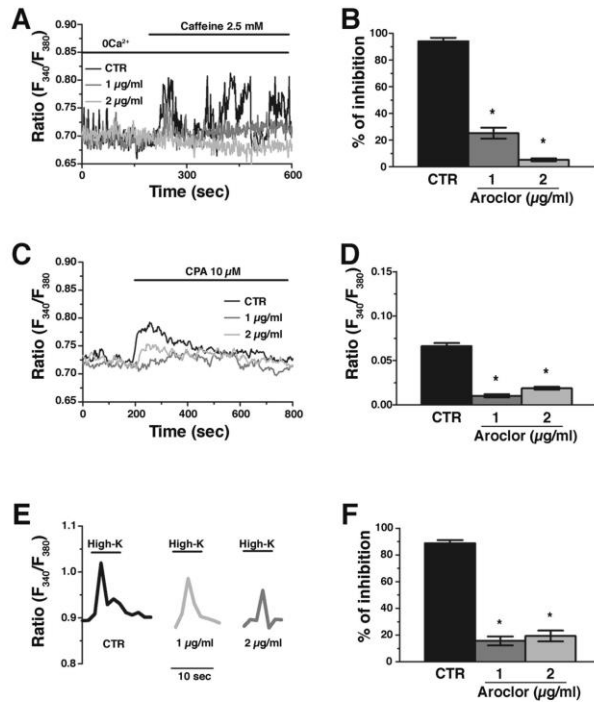
Figure 5. Ca²⁺ entry and RyRs-dependent Ca²⁺ release in 1 or 2 µg/ml-exposed cardiac beating syncytia. (**A**) Representative Ca²⁺ tracings of the Ca²⁺ response to caffeine (2.5 mM) in the absence or in the presence of either 1 or 2 µg/mL Aroclor. Extracellular Ca²⁺ was removed (0Ca²⁺) to prevent any contaminating effect from Ca²⁺ entry. (**B**) Mean ± SE of the percentage of Aroclor-induced inhibition of caffeine-induced Ca²⁺ transients. (**C**) Representative Ca²⁺ tracings of the Ca²⁺ response to cyclopiazonic acid (10 µM; CPA) in the absence or in the presence of either 1 or 2 µg/mL Aroclor. Extracellular Ca²⁺ was removed (0Ca²⁺) to prevent any contaminating effect from Ca²⁺ entry. (**D**) Mean ± SE of the percentage of Aroclor-induced inhibition of CPA-induced Ca²⁺ transients. (**E**) Representative tracings of the Ca²⁺ signals induced by sustained depolarization caused by high KCl (High-K) in the extracellular solution in the absence or in the presence of either 1 or 2 µg/mL Aroclor. (**F**) Mean±SE of the percentage of Aroclor-induced inhibition of High-K-induced Ca²⁺ transients. *$p < 0.05$.
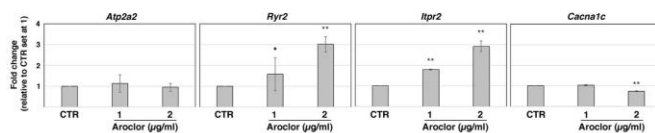
Figure 6. Gene expression analysis of cardiac beating syncytia. Expression profiles of *Atp2a2*, *Ryr2*, *Itpr2* and *Cacna1c*. The expression values of CTR samples were set at 1 for the calculation of the *n*-fold change. Values are expressed as mean ± SD. *$p < 0.05$; **$p < 0.001$.

119

We observed that, both in the absence or in the presence of Aroclor, the repetitive Ca^{2+} spikes were abruptly inhibited by tetracaine, thereby confirming that RyRs drive the spontaneous Ca^{2+} oscillations, and the removal of extracellular Ca^{2+} did not cause a prompt interruption of the Ca^{2+} spikes, as expected if they were mainly sustained by intracellular Ca^{2+} mobilization. Also, the pharmacological blockade of InsP$_3$Rs with 2-APB, a powerful and reliable blocker of such receptors[34,35], never affected the spontaneous Ca^{2+} oscillations, thereby ruling out InsP$_3$Rs from the mechanisms that drive the beating activity under our conditions. Of note, the stimulation of InsP$_3$Rs with angiotensin II caused a larger increase in $[Ca^{2+}]_i$ in beating syncytia exposed to Aroclor, while CTR cardiomyocytes only showed a modest enlargement of the first Ca^{2+} spike arising after agonist addition followed by a transient reduction in the amplitude of the following Ca^{2+} oscillations. These data strongly suggest that: 1) InsP$_3$Rs do not play a prominent role in inducing the spontaneous Ca^{2+} spikes, as the InsP$_3$-sensitive SR Ca^{2+} pool is up-regulated by Aroclor exposure, while the amplitude and frequency of Ca^{2+} oscillations are reduced; and 2) InsP$_3$Rs are, however, able to modulate RyRs-dependent Ca^{2+} release, as the transient depletion of the InsP$_3$-sensitive SR Ca^{2+} pool leads to a short-lasting decrease in the amplitude of Ca^{2+} spikes in CTR cardiomyocytes. The increase in *Itpr2* expression could explain the largest Ca^{2+} signal induced by angiotensin II in the presence of Aroclor. Consistently, 2 µg/ml Aroclor induces a dose-dependent elevation in both *Itpr2* transcripts and in the peak Ca^{2+} response to angiotensin II.

These data indicate that RyRs and VGCCs work to shape the spontaneous Ca^{2+} oscillations also in Aroclor-exposed syncytia and suggest that the signaling machinery underlying the spontaneous Ca^{2+} signal was not affected by the treatment. Thus, we moved our attention to single components of the Ca^{2+} toolkit involved in the oscillatory signal to evaluate whether and how Aroclor interferes with them. We determined that Aroclor exposure induced a significant reduction in basal $[Ca^{2+}]_i$ and in SR Ca^{2+} levels in cardiomyocytes, which was reflected in a dramatic decrease in the caffeine-releasable Ca^{2+} pool. Additionally, Aroclor heavily inhibited voltage-dependent Ca^{2+} entry, as measured in response to high-KCl extracellular solution. Therefore, Aroclor affects both the components of the Ca^{2+} toolkit which deliver Ca^{2+} to the cytosol during the spiking activity. Similar results were obtained in neuronal cells, in which it was demonstrated that Aroclor 1254 induced a depletion of SR Ca^{2+} store through the activation of InsP$_3$Rs[36,37].

The acute addition of Aroclor did not trigger any detectable increase in $[Ca^{2+}]_i$, suggesting that Aroclor is not able to cause a massive and rapid release of intraluminally stored Ca^{2+} which is the most intuitive mechanism to explain the depletion of the SR Ca^{2+} pool underpinning the rhythmic Ca^{2+} release (as discussed in more detail below). This result differs compared to that observed in rodent neurons[38–40] and PC12 cells[41], in which PCB-95 and Aroclor 1254 stimulate RyRs-dependent intracellular Ca^{2+} release. It has been demonstrated that PCB congeners sensitize RyRs by binding to one or more components of the RyR macromolecular complex, which could therefore act as receptors[10,42,43]. We speculate that in perinatal cardiomyocytes, characterized by an immature SR[44,45], the lack of expression of components of the adult RyR macromolecular complex may explain why Aroclor fails to increase $[Ca^{2+}]_i$. As Aroclor did not evoke an acute Ca^{2+} response, we reasoned that effects observed after 24h-exposure could be explained by an interference with the Ca^{2+} handling machinery.

Real Time PCR analysis demonstrated that both 1 or 2 µg/ml Aroclor induced a significant increase of the expression of *Ryr2*, as reported also in previous studies on rat cerebellum cells[46]. The upregulation of *Ryr2* transcript expression is predicted to increase, rather than decreasing, the release of Ca^{2+} from SR to the cytoplasm and thus increases the spiking activity of beating syncytia. However, it has been reported that Aroclor 1254 at 6–9 µM inhibits SR Ca^{2+} uptake, interfering with SERCA activity[47,48], and at 10–13 µM severely compromises the SERCA-mediated uptake of Ca^{2+} by SR microsomes[48]. The Aroclor concentrations that we used, i.e. 1 and 2 µg/ml, fall within this range and, therefore, might be able to interfere with SERCA-mediated Ca^{2+} sequestration. This mechanism could explain the fall in SR Ca^{2+} levels and, consequently, in the caffeine-releasable Ca^{2+} pool that we observed in the presence of both 1 and 2 µg/ml Aroclor. Additionally, as SR Ca^{2+} continuously leaks out in the cytosol to maintain the $[Ca^{2+}]_i$[49], this model would also explain the drop in resting Ca^{2+} levels caused by Aroclor-treated in the beating syncytia. Future investigations are required to confirm this hypothesis and to understand how Aroclor 1254 interacts with SERCA2A. Our data, however, rule out the down-regulation of *Atp2a2* expression, that codes for SERCA2A, as the transcript levels of this gene are not altered after 24 h Aroclor exposure. The mechanism whereby Aroclor inhibits SERCA activity is yet to be elucidated[47,48]. However, in cardiomyocytes, SERCA activity is severely reduced by cytosolic and mitochondria-derived reactive oxygen species (ROS), which therefore lead to a dramatic reduction in SR Ca^{2+} concentration[50,51]. Interestingly, a recent work showed that ROS production through the mitochondrial pathway started to increase after 1 h of Aroclor exposure in the human lung cancer cell line A549[52]. This mechanism could explain why the inhibitory effect of Aroclor is not acute and requires a prolonged incubation also in the beating syncytia.

In addition to reducing SR Ca^{2+} levels, we found that Aroclor attenuated voltage-dependent Ca^{2+} entry, which is necessary to maintain the spontaneous Ca^{2+} oscillations over time, at both 1 and 2 µg/ml. Real Time PCR disclosed that only 2 µg/ml Aroclor 1254 decreased the expression of *Cacna1c*, which encodes for the α subunit of L-type VGCCs. While this mechanism is likely to play a major role in reducing voltage-dependent Ca^{2+} entry at the higher dose, it does not explain the inhibitory effect observed at 1 µg/ml. However, earlier reports revealed that PCBs are able to increase Ca^{2+} permeability across the plasma membrane in several cell types, causing a long-lasting influx of Ca^{2+} through unidentified Ca^{2+}-permeable channels[53] or through store-operated Ca^{2+} channels[54]. Also, Aroclor 1254 activates the Ca^{2+}-permeable *N*-methyl-D-aspartate receptors[55], inhibits the non-selective cation channel TRP Vanilloid 6 (TRPV6)[56] and stimulates Cl⁻-permeable γ-aminobutyric acid (GABA)$_A$ receptors[55,57] in newborn rat neocortical neurons. All together, these findings clearly demonstrate that PCB congeners, including Aroclor 1254, have the potential to modulate plasma membrane channels, although it remains to be elucidated whether this interaction is direct or mediated by auxiliary partners. We hypothesize that, besides reducing *Cacna1c* expression, Aroclor 1254 inhibits L-type VGCCs through a non-yet identified mechanism in cardiomyocytes.

In conclusion, for the first time, we demonstrate that perinatal cardiac syncytia exposed to Aroclor 1254 undergo a dramatic functional alteration of the kinematics contractile properties, due to the disruption of the intracellular Ca^{2+} machinery. These findings contribute to the understanding of the molecular underpinnings of PCBs-induced cardiovascular alterations, which are emerging as an additional life-threatening hurdle associated to PCB pollution. Therefore, PCBs-dependent alteration of intracellular Ca^{2+} machinery is the most likely trigger of developmental cardiac functional alterations.

Methods

Cell lines. R1 mESC line (kindly provided by Dr. Nagy from Samuel Lunenfeld Research Institute, Mount Sinai Hospital, Toronto, Ontario, Canada) and STO cell line (ATCC, CRL-2225) were cultivated as previously described[58]. Briefly, R1 was cultivated in Knockout DMEM added with 15% ESC Qualified FBS, 2 mM L-glutamine, 1X non-essential amino acids, 0.5% penicillin/streptomycin (all from Thermo Fisher Scientific), 0.1 mM β-mercaptoethanol (Sigma) and 500 U/ml ESGRO-LIF (Merck Millipore, Italy). The STO cell line was maintained in DMEM (Sigma) supplemented with 10% foetal bovine serum, 4 mM L-glutamine, 1X non-essential amino acids, 0.5% penicillin–streptomycin solution (all from Thermo Fisher Scientific), 0.1 mM β-mercaptoethanol (Sigma) and 0.2 mg/mL geneticin (Sigma). ESCs were routinely passaged enzymatically every 2/3 days with trypsin/EDTA 0.05%, alternating a passage on STO feeder cells with two passages on gelatin-coated p55 dish, and maintained in an incubator at 37 °C with 5% CO_2 in air.

Differentiation of mESCs into perinatal-like cardiomyocytes and Aroclor treatment. mESCs were induced to differentiate through the formation of embryoid bodies (EBs) *in vitro* by removing the Leukemia Inhibitory Factor (LIF) from culture medium (differentiation medium), using the hanging drop method[59,60]. For EBs formation, about seventy 20 µl droplets of differentiation medium containing 10^3 mESCs were plated on the lid of p55 Petri dishes. On day 3 of culture, the developing EBs were transferred on 0.1% agarose-coated tissue dishes (Corning) and from day 5, about 5–8 EBs were plated in single 1.9 cm^2 well and cultivated up to 15 days.

Aroclor 1254 (Pancreac Nova Chimica) was dissolved in 100% dimethyl sulfoxide (DMSO; Sigma) to a concentration of 20 mg/ml. This solution was added to the differentiation medium on day 15 to a final concentration of 1 or 2 µg/ml. As control (CTR) samples, cells were exposed to 0.01% DMSO. Cells were harvested 24 h after either Aroclor or DMSO exposure. This procedure was repeated for three independent experiments.

Contraction assay. On day 5 of differentiation, 25 EBs were plated onto 22 mm gelatin-coated Glass Bottom Dish (WillCo Wells) and cultured up to day 15. At day 15, cells were exposed to Aroclor and then transferred into the culture chamber of a Nikon BioStation IM at 37 °C and 5% CO_2 for video recording. For each of the three independent experiments, AVI videos of the beating syncytia were recorded from 10 randomly chosen CTR or Aroclor-exposed samples, using the Snagit software and further analyzed with the Video Spot Tracker (VST) program (http://cismm.cs.unc.edu/downloads). Then, videos were processed according to the image processing algorithm based on the Matlab programming language (The MathWorks, Inc., Natick, MA)[22,61].

Measurement of Ca^{2+} transients in mESCs-derived cardiomyocytes. Ca^{2+} dynamics in mESCs-derived cardiomyocytes were measured by using a conventional epifluorescence Ca^{2+} imaging system, as shown elsewhere[25,26]. At day 5 of differentiation, EBs were plated on 12 mm coverslips in 24-multiwell plates. At day 15 beating cardiac syncytia, exposed to DMSO, 1 or 2 µg/ml Aroclor for 24 h, were analyzed for Ca^{2+} transients. Cells were loaded with 0.5 µM Fura-2/AM (1 mM stock in DMSO; Thermo Fisher Scientific) for 20 min at 37 °C. Then, after washing with pre-warmed Ca^{2+}-containing Tyrode's solution (NaCl 154 mM, KCl 4 mM, $MgCl_2$ 1 mM, $CaCl_2$ 2 mM, HEPES 5 mM and Glucose 5.5 mM), the coverslips were fixed to the bottom of a Petri dish and the cells observed by an upright epifluorescence Axiolab microscope (Carl Zeiss, Oberkochen, Germany), equipped with a Zeiss 40× Achroplan objective (water-immersion, 2.0 mm working distance, 0.9 numerical aperture). Voltage-dependent Ca^{2+} entry was stimulated by replacing 40 mM NaCl with an equimolar amount of KCl (high-KCl solution). Intracellular Ca^{2+} release was monitored in the medium without Ca^{2+} (0 Ca^{2+}) and supplemented with 10 mM EGTA. Cells were excited alternately at 340 and 380 nm wavelengths and the emitted light was detected at 510 nm. A first neutral density filter (1 or 0.3 optical density) reduced the overall intensity of the excitation light and a second neutral density filter (optical density = 0.3) was coupled to the 380 nm filter to reach the intensity of the 340 nm wavelength. A round diaphragm was used to increase the contrast. Excitation filters were mounted on a filter wheel (Lambda 10, Sutter Instrument, Novato, CA, USA). Custom software, working in LINUX environment, was used to drive the camera (Extended-ISIS Camera, Photonic Science, Millham, UK), the filter wheel and to measure and plot on-line the fluorescence from 30–45 rectangular "regions of interest" (ROI) enclosing 30–60 areas within each of the beating syncytia. Each ROI was identified by a number. The ratio of fluorescence emitted at 340 and 380 nm was recorded as an indicator of the changes in intracellular Ca^{2+} concentration ($[Ca^{2+}]_i$). The experiments were performed at room temperature (22 °C). Ratio measurements were performed and plotted every 1.5 s for 900 s. The resting $[Ca^{2+}]_i$ was measured by exploiting the Grynkiewicz equation, as shown in Zuccolo *et al.*[30].

RNA extraction, reverse transcription and quantitative Real-Time PCR. On day 16, following 24 h Aroclor exposure, RNA was extracted using the GenElute Mammalian Total RNA Kit according to the manufacturer's instruction (Sigma) from about 200 EBs from each CTR and 1 or 2 µg/ml Aroclor-exposed samples. Three independent experiments were performed on a total of about 1800 EBs.

Reverse transcription was performed in a final volume of 20 µl reaction mixture with 1 µg of RNA, 1x PCR buffer, 5 mM $MgCl_2$, 4 mM of each dNTP, 0.625 M oligo d(T)$_{16}$, 1.875 M Random Hexamers, 20 U RNase Inhibitor, 50 U MuLV reverse transcriptase (all from Thermo Fisher Scientific). The conditions for the reverse transcription were as follows: 25 °C for 10 min, 42 °C for 15 min, 99 °C for 5 min. One twentieth of the resulting cDNA was amplified in duplicate by Real-Time PCR in 20 µl reaction mixture with 200 nM of each specific primer

121

(designed using Primer 3 software; see Table 1S) and the MESA GREEN qPCR MasterMix Plus for SYBR assay no ROX sample (Eurogentec) at 1X as final concentration. The amplification reaction, performed in a Rotorgene 6000 (Corbett Life Science), was with the following program: 95 °C for 5 min, followed by 40 cycles at 95 °C for 10 s, 60 °C for 15 s, 72 °C for 20 s. β-2-microglobulin gene expression was used for sample normalization[60]. The Rotorgene 6000 Series Software 1.7 was used for the comparative concentration analysis.

Statistics. PCR expression data are presented as means ± standard deviation (SD), while the syncytium contractile parameters are expressed as means ± 95% confidence interval for the differences between means. Data were analyzed by the one-way ANOVA and by the *post hoc* LSD test. As to Ca^{2+} imaging data, the frequency of spontaneous Ca^{2+} transients was evaluated by dividing the number of Ca^{2+} transients arising over the stabilization of intracellular Ca^{2+} dynamics (i.e. after 1–3 min from the beginning of the recording) by 60 s. The amplitude of intracellular Ca^{2+} release in response to CPA, which is commonly used to estimate SR Ca^{2+} content, or caffeine and the amplitude of high-KCl-induced Ca^{2+} entry was measured as the difference between the ratio at the peak of intracellular Ca^{2+} mobilization and the mean ratio of 1 min baseline before the peak. Pooled data are given as means ± standard error (SE) and statistical significance ($p < 0.05$) was evaluated by the Student's *t*-test for unpaired observations. Each Ca^{2+} trace is representative of 80–200 ROIs recorded from at least three embryoid bodies.

References

1. Ross, G. The public health implications of polychlorinated biphenyls (PCBs) in the environment. *Ecotoxicol. Environ. Saf.* **59**, 275–91 (2004).
2. Safe, S. H. Polychlorinated biphenyls (PCBs): environmental impact, biochemical and toxic responses, and implications for risk assessment. *Crit. Rev. Toxicol.* **24**, 87–149 (1994).
3. Jokinen, M. P. *et al.* Increase in cardiovascular pathology in female Sprague-Dawley rats following chronic treatment with 2,3,7,8-tetrachlorodibenzo-p-dioxin and 3,3′,4,4′,5-pentachlorobiphenyl. *Cardiovasc. Toxicol.* **3**, 299–310 (2003).
4. Humblet, O., Birnbaum, L., Rimm, E., Mittleman, M. A. & Hauser, R. Dioxins and cardiovascular disease mortality. *Environ. Health Perspect.* **116**, 1443–8, https://doi.org/10.1289/ehp.11579 (2008).
5. Kopf, P. G. & Walker, M. K. Overview of developmental heart defects by dioxins, PCBs, and pesticides. *J. Environ. Sci. Health C. Environ. Carcinog. Ecotoxicol. Rev.* **27**, 276–85, https://doi.org/10.1080/10590500903310195 (2009).
6. Goncharov, A., Bloom, M., Pavuk, M., Birman, I. & Carpenter, D. O. Blood pressure and hypertension in relation to levels of serum polychlorinated biphenyls in residents of Anniston, Alabama. *J. Hypertens.* **28**, 2053–60, https://doi.org/10.1097/HJH.0b013e32833c5f3e (2010).
7. Perkins, J. T., Petriello, M. C., Newsome, B. J. & Hennig, B. Polychlorinated biphenyls and links to cardiovascular disease. *Environ. Sci. Pollut. Res. Int.* **23**, 2160–72, https://doi.org/10.1007/s11356-015-4479-6 (2016).
8. Borlak, J. & Thum, T. PCBs alter gene expression of nuclear transcription factors and other heart-specific genes in cultures of primary cardiomyocytes: possible implications for cardiotoxicity. *Xenobiotica* **32**, 1173–83 (2002).
9. Jo, S. H., Choi, S. Y., Kim, K. T. & Lee, C. O. Effects of polychlorinated biphenyl 19 (2,2′,6-trichlorobiphenyl) on contraction, Ca2+ transient, and Ca2+ current of cardiac myocytes. *J. Cardiovasc. Pharmacol.* **38**, 11–20 (2001).
10. Pessah, I. N., Cherednichenko, G. & Lein, P. J. Minding the calcium store: Ryanodine receptor activation as a convergent mechanism of PCB toxicity. *Pharmacol. Ther.* **125**, 260–85, https://doi.org/10.1016/j.pharmthera.2009.10.009 (2010).
11. Wong, P. W. & Pessah, I. N. Ortho-substituted polychlorinated biphenyls alter calcium regulation by a ryanodine receptor-mediated mechanism: structural specificity toward skeletal- and cardiac-type microsomal calcium release channels. *Mol. Pharmacol.* **49**, 740–51 (1996).
12. Kodavanti, P. R., Ward, T. R., McKinney, J. D. & Tilson, H. A. Inhibition of microsomal and mitochondrial Ca2+ -sequestration in rat cerebellum by polychlorinated biphenyl mixtures and congeners. Structure-activity relationships. *Arch. Toxicol.* **70**, 150–7 (1996).
13. Tilson, H. A., Jacobson, J. L. & Rogan, W. J. Polychlorinated biphenyls and the developing nervous system: cross-species comparisons. *Neurotoxicol. Teratol.* **12**, 239–48 (1990).
14. Zhu, C. *et al.* Differential expression profile of MicroRNAs during differentiation of cardiomyocytes exposed to polychlorinated biphenyls. *Int. J. Mol. Sci.* **13**, 15955–66, https://doi.org/10.3390/ijms131215955 (2012).
15. Carro, T., Taneyhill, L. A. & Ann Ottinger, M. The effects of an environmentally relevant 58-congener polychlorinated biphenyl (PCB) mixture on cardiac development in the chick embryo. *Environ. Toxicol. Chem.* **32**, 1317–24, https://doi.org/10.1002/etc.2179 (2013).
16. Li, M. *et al.* Toxic effects of polychlorinated biphenyls on cardiac development in zebrafish. *Mol. Biol. Rep.* **41**, 7973–83, https://doi.org/10.1007/s11033-014-3692-6 (2014).
17. Agudo, A. *et al.* Polychlorinated biphenyls in Spanish adults: determinants of serum concentrations. *Environ. Res.* **109**, 620–8, https://doi.org/10.1016/j.envres.2009.03.009 (2009).
18. La Merrill, M. A. *et al.* Perinatal DDT Exposure Induces Hypertension and Cardiac Hypertrophy in Adult Mice. *Environ. Health Perspect.* **124**, 1722–1727 (2016).
19. Metzger, J. M., Samuelson, L. C., Rust, E. M. & Westfall, M. V. Embryonic stem cell cardiogenesis applications for cardiovascular research. *Trends Cardiovasc. Med.* **7**, 63–8, https://doi.org/10.1016/S1050-1738(96)00138-7 (1997).
20. Hescheler, J. *et al.* Establishment of ionic channels and signalling cascades in the embryonic stem cell-derived primitive endoderm and cardiovascular system. *Cells Tissues Organs* **165**, 153–64 (1999).
21. Boheler, K. R. *et al.* Differentiation of pluripotent embryonic stem cells into cardiomyocytes. *Circ. Res.* **91**, 189–201 (2002).
22. Fassina, L. *et al.* Video evaluation of the kinematics and dynamics of the beating cardiac syncytium: an alternative to the Langendorff method. *Int. J. Artif. Organs* **34**, 546–58, https://doi.org/10.5301/IJAO.2011.8510 (2011).
23. Dingemans, M. M. *et al.* Hydroxylation increases the neurotoxic potential of BDE-47 to affect exocytosis and calcium homeostasis in PC12 cells. *Environ. Health Perspect.* **116**, 637–43, https://doi.org/10.1289/ehp.11059 (2008).
24. Choi, S. Y. *et al.* Non-Dioxin-Like Polychlorinated Biphenyls Inhibit G-Protein Coupled Receptor-Mediated Ca2+ Signaling by Blocking Store-Operated Ca2+ Entry. *PLoS One* **11**, e0150921, https://doi.org/10.1371/journal.pone.0150921 (2016).
25. Viatchenko-Karpinski, S. *et al.* Intracellular Ca2 + oscillations drive spontaneous contractions in cardiomyocytes during early development. *Proc. Natl. Acad. Sci. USA* **96**, 8259–64 (1999).
26. Yang, H. T. *et al.* The ryanodine receptor modulates the spontaneous beating rate of cardiomyocytes during development. *Proc. Natl. Acad. Sci. USA* **99**, 9225–30 (2002).
27. Malara, A. *et al.* The Plant Hormone Abscisic Acid Is a Prosurvival Factor in Human and Murine Megakaryocytes. *J. Biol. Chem.* **292**, 3239–51, https://doi.org/10.1074/jbc.M116.751693 (2017).

28. Sedan, O. *et al.* Human embryonic stem cell-derived cardiomyocytes can mobilize 1,4,5-inositol trisphosphate-operated [Ca2+]i stores: the functionality of angiotensin-II/endothelin-1 signaling pathways. *Ann. N. Y. Acad. Sci.* **1188**, 68–77, https://doi.org/10.1111/j.1749-6632.2009.05085.x (2010).

29. Lodola, F. *et al.* Store-operated Ca2+ entry is remodelled and controls *in vitro* angiogenesis in endothelial progenitor cells isolated from tumoral patients. *PLoS One* **7**, e42541, https://doi.org/10.1371/journal.pone.0042541 (2012).

30. Zuccolo, E. *et al.* Constitutive Store-Operated Ca(2+) Entry Leads to Enhanced Nitric Oxide Production and Proliferation in Infantile Hemangioma-Derived Endothelial Colony-Forming Cells. *Stem Cells Dev.* **25**, 301–19, https://doi.org/10.1089/scd.2015.0240 (2016).

31. Pierro, C., Cook, S. J., Foets, T. C., Bootman, M. D. & Roderick, H. L. Oncogenic K-Ras suppresses IP$_3$-dependent Ca^{2+} release through remodelling of the isoform composition of IP$_3$Rs and ER luminal Ca^{2+} levels in colorectal cancer cell lines. *J. Cell. Sci.* **127**, 1607–19, https://doi.org/10.1242/jcs.141408 (2014).

32. Fu, J. D. *et al.* Crucial role of the sarcoplasmic reticulum in the developmental regulation of Ca2+ transients and contraction in cardiomyocytes derived from embryonic stem cells. *FASEB J.* **20**, 181–3 (2006).

33. Kodavanti, P. R. Neurotoxicity of persistent organic pollutants: possible mode(s) of action and further considerations. *Dose Response* **3**, 273–305, https://doi.org/10.2203/dose-response.003.03.002 (2006).

34. Dragoni, S. *et al.* Vascular endothelial growth factor stimulates endothelial colony forming cells proliferation and tubulogenesis by inducing oscillations in intracellular Ca2+ concentration. *Stem Cells.* **29**, 1898–1907, https://doi.org/10.1002/stem.734 (2011).

35. Mikoshiba, K. Role of IP3 receptor signaling in cell functions and diseases. *Adv. Biol. Regul.* **57**, 217–227, https://doi.org/10.1016/j.jbior.2014.10.001 (2015).

36. Inglefield, J. R., Mundy, W. R. & Shafer, T. J. Inositol 1,4,5-triphosphate receptor-sensitive Ca(2+) release, store-operated Ca(2+) entry, and cAMP responsive element binding protein phosphorylation in developing cortical cells following exposure to polychlorinated biphenyls. *J. Pharmacol. Exp. Ther.* **297**, 762–73 (2001).

37. Kang, J. H. *et al.* Inhibition of aroclor 1254-induced depletion of stored calcium prevents the cell death in catecholaminergic cells. *Toxicology* **200**, 93–101 (2004).

38. Lesiak, A. *et al.* The environmental neurotoxicant PCB 95 promotes synaptogenesis via ryanodine receptor-dependent miR132 upregulation. *J. Neurosci.* **34**, 717–25, https://doi.org/10.1523/JNEUROSCI.2884-13.2014 (2014).

39. Wayman, G. A. *et al.* PCB-95 modulates the calcium-dependent signaling pathway responsible for activity-dependent dendritic growth. *Environ. Health Perspect.* **120**, 1003–9, https://doi.org/10.1289/ehp.1104833 (2012a).

40. Wayman, G. A. *et al.* PCB-95 promotes dendritic growth via ryanodine receptor-dependent mechanisms. *Environ. Health Perspect.* **120**, 997–1002, https://doi.org/10.1289/ehp.1104832 (2012b).

41. Wong, P. W., Garcia, E. F. & Pessah, I. N. Ortho-substituted PCB95 alters intracellular calcium signaling and causes cellular acidification in PC12 cells by an immunophilin-dependent mechanism. *J. Neurochem.* **76**, 450–63 (2001).

42. Chelu, M. G., Danila, C. I., Gilman, C. P. & Hamilton, S. L. Regulation of ryanodine receptors by FK506 binding proteins. *Trends Cardiovasc. Med.* **14**, 227–34 (2004).

43. Samso, M., Feng, W., Pessah, I. N. & Allen, P. D. Coordinated movement of cytoplasmic and transmembrane domains of RyR1 upon gating. *PLoS Biol.* **7**, e85, https://doi.org/10.1371/journal.pbio.1000085 (2009).

44. Pegg, W. & Michalak, M. Differentiation of sarcoplasmic reticulum during cardiac myogenesis. *Am. J. Physiol.* **252**, H22–31 (1987).

45. Nakanishi, T., Seguchi, M. & Takao, A. Development of the myocardial contractile system. *Experientia* **44**, 936–44 (1988).

46. Yang, D. *et al.* Developmental exposure to polychlorinated biphenyls interferes with experience-dependent dendritic plasticity and ryanodine receptor expression in weanling rats. *Environ. Health Perspect.* **117**, 426–35 (2009).

47. Kodavanti, P. R. *et al.* Repeated exposure of adult rats to Aroclor 1254 causes brain region-specific changes in intracellular Ca^{2+} buffering and protein kinase C activity in the absence of changes in tyrosine hydroxylase. *Toxicol. Appl. Pharmacol.* **153**, 186–98 (1998).

48. Sharma, R., Derr-Yellin, E. C., House, D. E. & Kodavanti, P. R. Age-dependent effects of Aroclor 1254R on calcium uptake by subcellular organelles in selected brain regions of rats. *Toxicology* **156**, 13–25 (2000).

49. Takeshima, H., Venturi, E. & Sitsapesan, R. New and notable ion-channels in the sarcoplasmic/endoplasmic reticulum: do they support the process of intracellular Ca2+ release? *J. Physiol.* **593**, 3241–51, https://doi.org/10.1113/jphysiol.2014.281881 (2015).

50. Zima, A. V. & Blatter, L. A. Redox regulation of cardiac calcium channels and transporters. *Cardiovasc. Res.* **71**, 310–321 (2006).

51. Li, Q. *et al.* Mitochondria-derived ROS bursts disturb Ca^{2+} cycling and induce abnormal automaticity in guinea pig cardiomyocytes: a theoretical study. *Am. J. Physiol. Heart Circ. Physiol.* **308**, H623–636, https://doi.org/10.1152/ajpheart.00493.2014 (2015).

52. Zhong, Y. *et al.* Aroclor 1254 inhibits cell viability and induces apoptosis of human A549 lung cancer cells by modulating the intracellular Ca(2+) level and ROS production through the mitochondrial pathway. *J. Environ. Sci. Health A. Tox. Hazard. Subst. Environ. Eng.* **50**, 806–813, https://doi.org/10.1080/10934529.2015.1019797 (2015).

53. Mundy, W. R., Shafer, T. J., Tilson, H. A. & Kodavanti, P. R. Extracellular calcium is required for the polychlorinated biphenyl-induced increase of intracellular free calcium levels in cerebellar granule cell culture. *Toxicology* **136**, 27–39 (1999).

54. Voie, O. A. & Fonnum, F. Ortho substituted polychlorinated biphenyls elevate intracellular [Ca(2+)] in human granulocytes. *Environ. Toxicol. Pharmacol.* **5**, 105–12 (1998).

55. Inglefield, J. R. & Shafer, T. J. Polychlorinated biphenyl-stimulation of Ca(2+) oscillations in developing neocortical cells: a role for excitatory transmitters and L-type voltage-sensitive Ca(2+) channels. *J. Pharmacol. Exp. Ther.* **295**, 105–13 (2000a).

56. An, J. *et al.* The toxic effects of Aroclor 1254 exposure on the osteoblastic cell line MC3T3-E1 and its molecular mechanism. *Toxicology* **295**, 8–14, https://doi.org/10.1016/j.tox.2012.02.009 (2012).

57. Inglefield, J. R. & Shafer, T. J. Perturbation by the PCB mixture aroclor 1254 of GABA(A) receptor-mediated calcium and chloride responses during maturation *in vitro* of rat neocortical cells. *Toxicol. Appl. Pharmacol.* **164**, 184–95 (2000b).

58. Rebuzzini, P. *et al.* Mouse embryonic stem cells that surviv γ-rays exposure maintain pluripotent differentiation potential and genome stability. *J. Cell Physiol.* **227**, 1242–9, https://doi.org/10.1002/jcp.22908 (2012).

59. Neri, T. *et al.* The differentiation of cardiomyocytes from mouse embryonic stem cells is altered by dioxin. *Toxicol. Lett.* **202**, 226–36, https://doi.org/10.1016/j.toxlet.2011.02.008 (2011).

60. Rebuzzini, P. *et al.* Arsenic trioxide alters the differentiation of mouse embryonic stem cell into cardiomyocytes. *Sci. Rep.* **5**, 14993, https://doi.org/10.1038/srep14993 (2015).

61. Rebuzzini, P. *et al.* Mouse embryonic stem cells irradiated with γ-rays differentiate into cardiomyocytes but with altered contractile properties. *Mutat. Res.* **756**, 37–45, https://doi.org/10.1016/j.mrgentox.2013.06.007 (2013).

123

Author Contributions

P.R. has contributed with the conception and design, collection and assembly of data, data analysis and interpretation, manuscript writing; E.Z. has contributed with collection of data; C.C. has contributed with collection of data; L.F. has contributed with kinematics properties analysis and has written the algorithm of such analysis; J.A. has contributed with conception and design of experiments; A.I. has contributed with collection of data; P.F. has contributed with collection of data; M.Z. has contributed with conception and design, data analysis and interpretation, manuscript writing; F.M. has contributed with conception and design, data analysis and interpretation, manuscript writing; S.G. has contributed with conception and design, data analysis and interpretation, manuscript writing.

Additional Information

Supplementary information accompanies this paper at https://doi.org/10.1038/s41598-018-36333-z.

Competing Interests: The authors declare no competing interests.

Publisher's note: Springer Nature remains neutral with regard to jurisdictional claims in published maps and institutional affiliations.

124